Unraveling and Elucidating Two Dehydrogenation Pathways on NiOOH Electrocatalysts

By

Michael T. Bender

A dissertation submitted in partial fulfillment of the
requirements for the degree of

Doctor of Philosophy
(Chemistry)

at the
UNIVERSITY OF WISCONSIN-MADISON
2022

Date of final oral examination: 7/20/2022

The dissertation is approved by the following members of the Final Oral Committee:

Kyoung-Shin Choi, Professor, Chemistry
John Berry, Professor, Chemistry
Ive Hermans, Professor, Chemistry
Shannon Stahl, Professor, Chemistry

Abstract

Selective oxidation of alcohols, aldehydes, and amines to corresponding carboxylic acids and nitriles is of broad importance for applications in organic synthesis. In addition, these electrochemical conversions are considered viable anode reaction that can replace the oxygen evolution reaction as the anodic process paired with H_2 evolution or other reductive fuel production reactions in electrochemical and photoelectrochemical cells to simultaneously decrease the energy requirements and allow for production of valuable products at both electrodes. NiOOH is among the most promising electrocatalysts for selectively achieving these dehydrogenation reactions. Since the 1970's, oxidation of alcohols and amines on NiOOH has been understood to proceed through an indirect mechanism in which the applied potential is used to electrochemically oxidize $Ni(OH)_2$ to NiOOH which can then act as a chemical oxidizing agent to oxidize an alcohol or amine in solution through a rate limiting hydrogen atom transfer from the alpha position of the alcohol/amine to NiOOH. More recently, however, a few reports have emerged indicating that there is a sperate, potential dependent oxidation mechanism that occurs concurrently with this well known indirect oxidation pathway.

In the work presented in this dissertation, I confirm the existence of this second, potential dependent pathway for oxidation of alcohols, amines, and aldehydes on NiOOH. Then by taking advantage of an electrochemical procedure I developed to deconvolute the current through these two pathways, I reveal that the different functional groups have distinct preferences for the two pathways. Further experiments examine the effect of solution pH, organic species concentration, applied bias, and isotopic substitution of protium for deuterium on the rate of these two competing oxidation pathways. By synthesizing the insights from these experiments, a comprehensive mechanistic understanding of the two pathways can be achieved including an elucidation of their

respective active sites, key mechanistic steps, the factors controlling their rate, and the conditions that can lead to one pathway being favored over the other. These insights are then applied to achieve unprecedented insights into the mechanism of oxidation of 5-hydroxymethylfurfrual (HMF) to 2,5-furandicarboxylic acid (FDCA), which has been one of the most intensely studied biomass valorization reactions in recent years. Overall, this work provides an essential foundation for understanding the mechanism of various oxidative electrochemical dehydrogenation reactions on oxide and hydroxide-based catalytic electrodes.

Acknowledgements

As I reflect upon the completion of my time at graduate school, I can't help but be struck by how incredible the whole scientific enterprise is. The academic journey I have taken is only possible because generations of researchers before me have through careful and diligent work paved a path of knowledge about the natural world for others to follow. This path of knowledge is the fruit of a collaborative effort stretching across centuries and uniting people from all around the world in the common purpose of discovering and sharing truths about the world around us. That this can exist at all seems a great and beautiful thing and I'm proud to be part of it. I hope the work I've done up to this point and will do in the future can add a few more bricks to this path and pay forward the debt I owe to those who have come before by smoothing the way for future researchers to reach ever greater insights.

There are a great many people who have contributed in ways both big and small to my particular academic journey and who have my heartfelt thanks. First and foremost, I wish to thank my advisor, Prof. Kyoung-Shin Choi. From the very beginning it was clear how dedicated you are to fostering your students and allowing them to reach their full potential as scientists. I have learned a tremendous amount from you and have grown not only in specific scientific knowledge but also in my confidence as a scientist and my skill as both a researcher and communicator. You have been an excellent mentor and role model and I will always be grateful for all the time and effort you have invested in me and my development as a scientist.

To my committee, Profs. John Berry, Ive Hermans, and Shannon Stahl, I thank you for taking the time to offer me important guidance and feedback on my academic journey. To Ive and John, I am grateful both for your valuable feedback and questions during the previous grad school milestones and for your instruction as professors during my coursework. To Shannon, I am grateful

you have taken the time to serve on my final committee and am eager to hear what thoughts and questions you have at my defense.

To Prof. Sharon Hammes-Schiffer, Dr. Yan Choi Lam, and Dr. Robert Warburton, thank you for being excellent collaborators. The calculations you performed were invaluable in allowing the projects described in this dissertation to be successful and the conclusions I am able to present here are far stronger as a result of superb work you did.

To the members of the Choi group both past and present, thank you all for making the Choi group such a supportive and friendly environment to work in. It has been a delight to know and work with each of you and to learn from you all each week as you present the fruits of your own research journeys. To Dr. Dongho Lee, thank you for being an excellent mentor during my transition to graduate research and for your work and guidance helping me in my first projects. To Dr. DongKi Lee and Dr. Brandon Taitt, I'm delighted to have had the opportunity to work so closely with both of you during different stages of my graduate school career. I greatly value all the time we spent discussing our results and bouncing ideas back and forth and for the guidance and wisdom you shared with me. Finally, to Xin Yuan, thank you for all the discussions we've had over the last 4 years. I've learned a tremendous amount from you and the countless hours we've spent reasoning through fundamental concepts and puzzling over curious results have been among my most cherished in graduate school. I'm deeply grateful I've had the opportunity to work with you.

I also wish to extend my thanks to all the great teachers I've had over the years from grammar school on up. Without your instruction and dedication to education I would not be who I am today. In particular, I wish to thank my undergraduate research advisor, Prof. Joshua Farrell not only for giving me my first introduction into and guidance in conducting chemistry research,

but also for being an excellent professor in all the classes I took with you. The lessons you taught me both in terms of research and in my coursework were essential to allowing me to succeed in graduate school. I also wish to extend a special thank you to Mr. Steven Whittington, who taught my AP Chemistry class in high school. It was you who first sparked my love for chemistry and who set my feet on this path.

Finally, I wish to extend my heartfelt thanks to my family. To my siblings, Theresa and Thomas, thank you for making my childhood so wonderful and memorable. It's been a joy to grow up alongside you and to see all you've accomplished. I cherish the time we spend together and am delighted that I'll be able to share this moment with you. Finally, to my parents, who have loved and tirelessly supported me through every stage of my life no words can adequately express my gratitude. When I think of all the time, effort, and love you have gifted me with these past 29 years it takes my breath away. Thank you for being the best parents anyone could hope for. I couldn't be here without you and I love you both dearly.

List of Publications:

1. Yuan, X.; Lee, K.; **Bender, M. T.**; Schmidt, J.R.; Choi, K.-S. “Mechanistic Differences between Electrochemical Hydrogenation and Hydrogenolysis of 5-Hydroxymethylfurfural and Their pH Dependence” *ChemSusChem* **2022**.
2. **Bender, M. T.**; Choi, K.-S. “Electrochemical Dehydrogenation Pathways of Amines to Nitriles on NiOOH” *JACS Au* **2022**, *2*, 1169−1180.
3. **Bender, M. T.**; Choi, K.-S. “Electrochemical Oxidation of HMF via Hydrogen Atom Transfer and Hydride Transfer on NiOOH and the Impact of NiOOH Composition” *ChemSusChem.* 2022, *15*, e2022006.
4. **Bender, M. T.**; Warburton, R.; Hammes-Schiffer, S.; Choi, K.-S. “Understanding Hydrogen Atom and Hydride Transfer Processes during Electrochemical Alcohol and Aldehyde Oxidation” *ACS Catal.* **2021**, *11*, 15110−1524.
5. Lee, D. K.; Kubota, S. R.; Janes, A.; **Bender, M. T**.; Woo, J.; Schmidt, J. R.; Choi, K.-S. “The Impact of 5-Hydroxymethyl Furfural (HMF)-Metal Interactions on the Electrochemical Reduction Pathways of HMF on Various Metal Electrodes” *ChemSusChem*. **2021**, *14*, 4563−4572.
6. **Bender, M. T.**; Lam, Y.-C.; Hammes-Schiffer, S. ; Choi, K.-S. “Unraveling Two Pathways for Electrochemical Alcohol and Aldehyde Oxidation on NiOOH" *J. Am. Chem. Soc.* **2020**, *142*, 21538-21547.
7. **Bender, M. T.**; Yuan, X.; Choi, K.-S. “Alcohol oxidation as alternative anode reactions paired with (photo) electrochemical fuel production reactions" *Nat. Commun.* **2020**, *11*:4594.
8. Taitt, B. J.; **Bender, M. T.**; Choi, K.-S. “Impacts of the Regeneration Pathways of the Oxoammonium Cation on Electrochemical Nitroxyl Radical-Mediated Alcohol Oxidation" *ACS Catal.* **2020**, *10*, 265-275.
9. Wang, J.; Peurifoy, S.R.; **Bender, M. T.**; Ng, F.; Choi, K.-S.; Nuckolls, C.; Arnold, M.S. “Non-fullerene Acceptors for Harvesting Excitons from Semiconducting Carbon Nanotubes" J. Phys. Chem. C. **2019**, *123*, 21395-21402.

Table of Contents

Chapter 1: Introduction to Electrochemical Dehydrogenation Reactions on NiOOH electrodes

Portions of this chapter have been adapted from:

Bender, M. T.; Yuan, X.; Choi, K.-S. Alcohol oxidation as alternative anode reactions paired with (photo)electrochemical fuel production reactions. *Nat. Commun.* **2020**, 11, 4594. DOI: 10.1038/s41467-020-18461-1

1.1 Importance of electrochemical fuel and chemical production reactions.

There is a great need to develop renewable and environmentally benign routes to achieve both fuel production and synthesis of fine and commodity chemicals. On the reductive side, aqueous (photo)electrochemical reactions have received a great deal of attention as promising avenues through which green fuel production can be achieved with water reduction to H_2 gas, CO_2 reduction to carbon fuels, and N_2 reduction to NH_3 all receiving a great deal of research attention.[1,2] Aqueous (photo)electrochemical fuel production offers several attractive features including the ability to be conducted at ambient temperature and pressure, the use of water as the hydrogen source, and the ability to be driven by renewable energy sources (either directly by sunlight for photoelectrochemical reactions or by renewably generated electricity for electrochemical reactions). Additionally, (photo)electrochemical reduction of N_2 and CO_2 are achieved without prereducing water to H_2, eliminating steps involved in the storage, delivery, and use of H_2.

In (photo)electrochemical cells, production of the desired fuel at the cathode must be paired with an oxidation reaction at the anode. Traditionally, water oxidation through the oxygen evolution reaction (OER) has been used as this anode reaction. This choice has the advantage of being simple, as it does not necessitate the addition of any other species, and the O_2 produced is environmentally benign. OER, however, is kinetically slow and requires a large overpotential. This results in an increase in the operating voltage of the cell (when the cell current is fixed) or a decrease in the rate of fuel production (when the input voltage is fixed). Additionally, while O_2 is benign, it is not a highly valued product. As such, in recent years attention has been directed to finding more attractive oxidative reactions that form value-added products that can be paired with reduction reactions of interest. This is of great importance not only as a means of increasing the economic viability of (photo)electrochemical fuel production but also as way of synthesizing

industrially relevant oxidative products through a greener route than is provided by more traditional thermochemical methods.

1.2 Biomass valorization as an alternative anodic reaction.

Features that make a reaction an attractive alternative to OER include: (1) being thermodynamically or kinetically more favorable than OER, (2) production of a valuable product, (3) production of H^+ to maintain the overall solution pH (as all the aforementioned fuel production reactions consume H^+), and (4) abundance of the reactant and high demand for the product. A variety of reactions have been investigated in recent years as potential alternative anodic reactions that can be paired with fuel production, including oxidation of Cl^- to Cl_2 or HClO, oxidation of water to H_2O_2, and oxidation of various organic molecules to molecules of greater value.[3–9] Among these reactions, oxidative valorization of biomass derived intermediates to produce commodity chemicals is of particular interest because it possesses all of the aforementioned features required to be a promising alternative anode reaction. The biomass conversion reaction that has perhaps attracted the most research interest is the valorization of 5-hydroxymethylfurfural (HMF), a key intermediate produced from cellulosic biomass. This can be oxidized to a variety of products (**Scheme 1.1**), with 2,5-furandicarboxylic acid (FDCA), a potential replacement for the terephthalic acid used in polyethylene terephthalate (PET) plastics,[5] being the most widely pursed product, though 2,5-diformylfuran (DFF) is also highly desirable as it has important applications for the synthesis of pharmaceuticals, resins, various fine chemicals, and an antifungal agent.[10-13] In addition to HMF valorization, oxidation of glucose and glycerol, which can be produced abundantly from cellulosic biomass conversion and biodiesel production, respectively, to more value-added products such as glucaric acid, dihydroxyacetone, and formic acid is also of great interest.[6,7] We note that all the above biomass valorization reactions involve oxidation of alcohol

and aldehyde functional groups. Accordingly, materials that perform these reactions effectively have great potential as electrocatalysts for these alternative anodic reactions that can be paired with fuel production.

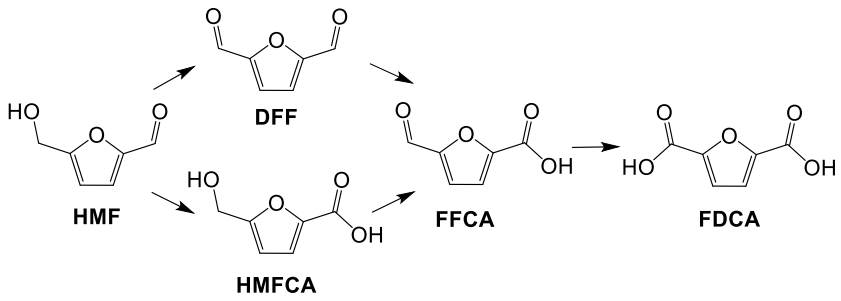

Scheme 1.1. Scheme depicting two possible routes for oxidation of HMF to FDCA.

1.3 Notable Alcohol Oxidation Electrocatalysts.

Several materials have been investigated for their ability to electrochemically oxidize biomass derived alcohols and aldehydes. One approach has been to use type of noble metals such as Pt and Au that have traditionally been employed in thermochemical biomass oxidations.[14] This has some advantages, such as early onsets for catalytic current and stability in acidic conditions, however, there are also some significant drawbacks including the high cost of materials, low current densities, and poor selectivity for full oxidation to carboxylic acids. For example, Au electrocatalysts can effectively oxidize the aldehyde in HMF to form 5-hydroxymethylfuran-2-carboxylic acid (HMFCA)[15] and Pt can oxidize alcohol in HMF to form 2,5-diformylfuran (DFF) in moderate selectivity,[16] but neither is effective at fully oxidizing HMF to form FDCA, which is the most sought-after product.

An alternative approach that addresses many of the issues with the noble metal electrodes is to use transition metal oxides to perform these oxidations (with oxide here including hydroxides and oxyhydroxides). While these electrocatalysts do require the application of more positive potentials before the onset of catalytic current for reasons that will be explained in section 1.4

below, they offer the distinct advantages of being far cheaper, being able to achieve greater current densities, and showing very high selectivity toward oxidation to carboxylic acids. A number of transition metal oxides have been found to be highly effective for these reactions, for example, Cu,[17] Co,[18] and Ni-based[8] ones have all been reported to convert HMF to FDCA with ≥95% selectivity and Faradic efficiency (FE). Of these, Ni-based electrocatalysts stand out as being both the most widely studied and generally the most active and a wide variety of as prepared Ni-based materials have been investigated for these conversions including nickel boride,[19] phosphide,[20] nitride,[21] sulfide,[9] and selenide.[22] Critically, however, x-ray photoelectron spectroscopy (XPS) data collected after these electrodes were used to conduct electrolysis experiments showed that in all cases the surface spontaneously converts to NiOOH under reaction conditions. A similar phenomenon has been observed for Co-based electrocatalysts (the second most widely studied class of materials for these conversions), with borides[23] and phosphides[24-25] being found to convert to CoOOH under reaction conditions.

1.4 Prior mechanistic understanding of dehydrogenation on MOOH electrocatalysts.

Given the highly promising performance they have shown for oxidation of biomass-derived alcohols and aldehydes, there is great value in understanding the mechanism through which MOOH electrocatalysts generally and NiOOH electrocatalysts specifically achieve these conversions. This is especially true given that biomass-derived starting molecules of interest such as HMF, glycerol, and glucose possess multiple functional groups that can be oxidized to form a variety of different products. Having a strong understanding of the reaction mechanism can therefore be invaluable in rationally identifying reaction conditions and catalyst modification strategies that will be effective in producing a desired product in high selectivity. Similarly, understanding how the alcohol/aldehyde oxidation mechanism compares to that of OER on these

electrocatalysts is important for rationally choosing catalyst compositions and reaction conditions that minimize the amount of current that goes to perform OER, which is always a concern that must be kept in mind given the aqueous reaction conditions and that MOOH electrocatalysts also tend to be highly active for OER.

While we are most interested in understanding the oxidation of biomass-derived compounds on these electrocatalysts, studying these reactions is challenging given that they have multiple functional groups that all undergo competitive oxidation. Therefore, before theses more complicated cases can be investigated, it is important to first develop an accurate understanding of the mechanism for general alcohol and aldehyde oxidation on MOOH electrocatalysts. The foundations for this understanding were established 50 years ago in a pair of papers by Fleishmann *et al*.[26,27] In them, cyclic voltammograms (CVs) and linear sweep voltammograms (LSVs) corresponding to oxidation of a series of alcohols and amines on Ni, Co, Cu, and Ag anodes were examined under alkaline conditions where an oxide/hydroxide layer would spontaneously form. In doing so, Fleishmann *et al*. made a few key observations. First, in all cases the onset of alcohol/amine oxidation coincided with the conversion of the lower valent metal oxide to a higher valent one (e.g. oxidation of $Ni(OH)_2$ to NiOOH) and the oxidation of the alcohol/amine resulted in an enhancement of the current for the oxidation peak corresponding to conversion of the lower valent oxide to the higher valent oxide. Moreover, the peak in the return sweep of the CVs corresponding to reduction of the higher valent oxide (e.g. NiOOH reduction back to $Ni(OH)_2$) was either absent or significantly diminished in the presence of the organic species. Based on this, they argued that the mechanism for alcohol/aldehyde oxidation was an indirect one in which the electrocatalyst must first be electrochemical oxidized to a higher valent oxide and that it is this higher valent oxide that is active for oxidation of the organic species.[27] This explains why in all

cases the current onset for organic oxidation coincides with the oxidation of the lower valent oxide and also why transition metal oxides consistently require much higher applied biases than the noble metals to initiate alcohol/aldehyde oxidation, as the noble metals do not share this requirement to form the higher valent oxide before becoming active for oxidation of organic species. Once the higher valent oxide forms, Fleishmann *et al*. argue that an organic species will adsorb on these sites and that the higher valent oxide will then act as a chemical oxidizing agent to oxidize the alcohol/amine adsorbed on it.[27] Drawing on the rate data they observed with their various metal oxides and on earlier work by Konaka *et al*. examining the reactivity of "nickel peroxide" as a chemical oxidizing agent,[28] Fleishmann *et al*. argue that this chemical oxidation reaction proceeds through a rate limiting hydrogen atom transfer of a hydrogen at the alpha position of the alcohol to the higher valent metal oxide, which is reduced in the process back to the lower valent state.[27] This lower valent oxide can then be re-oxidized by the applied bias to reform the active higher valent oxide. This process explains both the enhancement of the peak corresponding to oxidation of the lower oxide in the presence of organic species as well as the diminishment in the peak corresponding to reduction of the higher valent oxide as the chemical reaction with the organic species will continuously convert the higher valent oxide to the lower valent one. The steps involved in this indirect mechanism are summarized in **Scheme 1.2** using $Ni(OH)_2$/NiOOH as a model for the lower valent oxide/ higher valent oxide.

$$OH^- + Ni(OH)_2 \underset{\text{fast}}{\overset{-e^-}{\rightleftharpoons}} NiOOH + H_2O \quad (1)$$

$$RCH_2OH_{sol} \rightleftharpoons RCH_2OH_{ads} \quad (2)$$

$$(RCH_2OH)_{ads} + NiOOH \xrightarrow[\text{RDS}]{\text{HAT}} R\dot{C}HOH_{ads} + Ni(OH)_2 \quad (3)$$

$$R\dot{C}HOH_{ads} + 3NiOOH + H_2O \rightarrow\rightarrow\rightarrow RCOOH_{sol} + 3Ni(OH)_2 \quad (4)$$

Scheme 1.2. Mechanism proposed by Fleishmann et al. for the oxidation of alcohols and amines on MOOH catalysts (with NiOOH shown as an example electrocatalyst).

While the mechanism outlined above did receive some initial criticism,[29,30] it became widely accepted in the 50 years following its publication.[31-34] Moreover, while the initial work discussed only alcohol/amine oxidation, later papers extended the mechanism to also describe oxidation of aldehydes as they will first undergo hydration to form a 1,1-gemainal diol before being oxidized and thus can undergo the same mechanism.[33-36] More recently, however, a few works have noted the presence of a second, potential dependent current feature in LSVs collected for oxidation of various alcohols, aldehydes, and amines that occurs at more positive potentials than that for oxidation of the lower valent oxide(**Figure 1.1**).[8,37,38] Such a feature cannot be explained by the indirect mechanism proposed by Fleishmann *et al.* as the current through that mechanism should be evident as a characteristic enhancement in the peak associated with oxidation of $Ni(OH)_2$ to NiOOH because oxidation of the organic species consumes NiOOH and generates $Ni(OH)_2$ during the LSV, thereby requiring more current to fully oxidize $Ni(OH)_2$ to NiOOH. Because, however, in this mechanism the applied bias is only being used to generate the higher valent oxide and does not have any direct effect on the rate limiting HAT step, the current through this pathway should rapidly become potential independent and it cannot explain the second, potential dependent (PD) feature seen in **Figure 1.1** at more positive applied biases. This indicates that there is a second oxidation pathway active for oxidation of alcohols and aldehydes that occurs concurrently with the well-known indirect pathway proposed by Fleishmann *et al.*

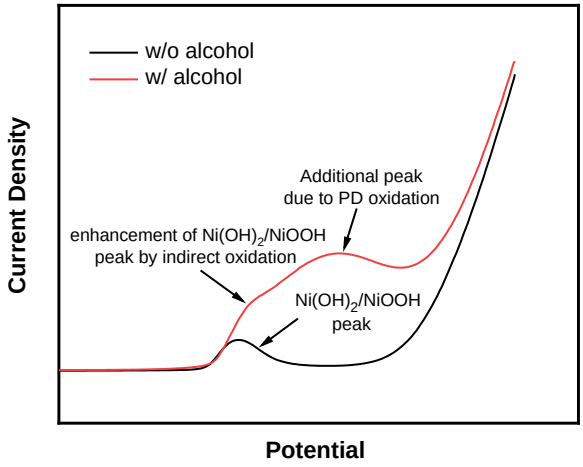

Figure 1.1. Schematic LSV showing the current profiles generated when using a $Ni(OH)_2$ working electrode without (black) and with (red) alcohol present in solution.

Though a few studies noted the existence of this second pathway, details about it such as its mechanism, how prevalent it is relative to the indirect pathway, and what factors influence its rate were not well understood. A few studies speculated that it might correspond to a direct oxidation pathway in which oxidation occurs on Ni^{3+} sites in NiOOH and that those sites remain as Ni^{3+} throughout the process;[8,37,38] however, no experiments were done to verify this hypothesis. Moreover, analysis of this second pathway was made challenging by the fact that it occurs concurrently with indirect oxidation and produces the same terminal carboxylic acid product. Accordingly, if a comprehensive understanding of alcohol and aldehyde oxidation on NiOOH electrocatalysts were to be achieved, a method to separate out and quantify the relative contributions of these two pathways would need to be developed, the mechanism for this second, PD pathway identified, and the factors affecting it and its competition with both indirect oxidation and OER elucidated. These are the primary topics I will explore in the following chapters of this dissertation.

1.5 Summary of dissertation Work.

As noted above, in order to understand the differences between PD and indirect oxidation it was necessary develop a method capable of deconvoluting and quantifying their respective contributions to the overall oxidation current. In chapter 2 I describe an electroanalytic technique I developed to achieve this and apply it to study the oxidation of a variety of aliphatic and aromatic alcohols and aldehydes and determine that the PD pathway is dominant for alcohol oxidation while the indirect pathway dominates for oxidation of aldehydes. Furthermore, drawing on a combination of experimental results and computational work performed in collaboration with Sharon Hammes-Schiffer's group, I propose that the PD pathway involves a potential driven hydride transfer ($2e^-$, $1H^+$) to Ni^{4+} sites as opposed to the hydrogen atom transfer ($1e^-$, $1H^+$) involved in the indirect pathway.

In Chapter 3, I expand on the insights laid out in Chapter 2 by examining the effect varying the pH and alcohol/aldehyde concentration has on oxidation through the two pathways. Using this data, I identify what conditions favor oxidation through the two pathways and why this is the case. Moreover, by pairing these results with kinetic isotope effect studies I also reveal which steps are critical for controlling the rates of the two pathways and how this can change depending on the reaction conditions.

While the discussion above has focused on alcohol/aldehyde oxidation, Fleishmann *et al.*'s initial work also proposed that oxidation of primary amines to nitriles occurs through the indirect pathway.[26,27] As nitriles are important synthetic intermediates with application in the synthesis of pharmaceuticals, fine chemicals, and agricultural chemicals, oxidation of primary amines to nitriles can also be viable anodic reactions to pair with cathodic fuel production to yield a value-added product at both electrodes.[39-41] Accordingly, understanding the mechanism of these reactions on NiOOH is also of great interest so in Chapter 4 I apply the same electroanalytic

techniques used in Chapters 2 and 3 to probe the conversion of primary amines to nitriles. This reveals that amines are also oxidized through both pathways and overall show similar reactivity to alcohols. This confirms that the indirect and PD pathway are not just relevant to alcohol/aldehyde oxidation but rather that they apply for a more broad set of dehydrogenation reactions.

Finally, in Chapter 5 I use the knowledge gleaned from studying the PD and indirect pathway for oxidation of a variety of simple alcohols and aldehydes to allow me to effectively examine the more complicated mechanistic question of HMF oxidation to FDCA. In that chapter, I lay out the relative contribution of both pathways to oxidation of HMF and its oxidative intermediates on the way to FDCA, reveal whether this reaction occurs preferentially through the DFF rout or HMFCA route (**Scheme 1.1)**, identify what steps limit the HMF oxidation rate, and examine how catalyst modifications to shift the potential of the $Ni(OH)_2$/NiOOH affects the rate of HMF oxidation through both pathways and the overall electrolysis performance.

Overall, the work contained in this dissertation forms an essential foundation for understanding dehydrogenation mechanisms on NiOOH electrocatalysts. It lays out an electroanalytical technique that can be used to probe these reactions, provides a comprehensive discussion and analysis of two pathways for oxidation of a variety of general alcohols and aldehydes, and demonstrates how this knowledge can be used both to understand the more complicated mechanisms of biomass oxidation reactions and to guide and gauge the impact of modifications to the electrocatalysts that perform these biomass valorization reactions. While the work contained in this dissertation is restricted to oxidations on NiOOH electrocatalysts, it is quite likely both the indirect and PD pathway are active for oxidation reactions on a broader set of MOOH catalysts. It is my hope that future work will explore how these insights can be used to understand dehydrogenation reactions on a broader class of electrocatalysts as well as examine

how they can be applied to rationally design electrocatalysts and reaction conditions to optimize a variety of oxidative biomass valorization reactions.

1.6 References

10. Voiry, D.; Shin, H. S.; Loh, K. P.; Chhowalla, M. Low-dimensional catalysts for hydrogen evolution and CO2 reduction. *Nat. Rev. Chem.* **2018**, *2*, 0105.
11. Cui, X.; Tang, C.; Zhang, Q. A review of electrocatalytic reduction of dinitrogen to ammonia under ambient conditions. *Adv. Energy Mater.* **2018**, *8*, 1800369.
12. Sayama, K. Production of high-value-added chemicals on oxide semiconductor photoanodes under visible light for solar chemical-conversion processes. *ACS Energy Lett.* **2018**, *3*, 1093–1101.
13. Xu, Y.; Zhang, B. Recent advances in electrochemical hydrogen production from water assisted by alternative oxidation reactions. *ChemElectroChem.* **2019**, *6*, 3214–3226.
14. Cha, H. G.; Choi, K.-S. Combined biomass valorization and hydrogen production in a photoelectrochemical cell. **2015**, *Nat. Chem. 7*, 328–333.
15. Liu, W.-J.; Xu, Z.; Zhao, D.; Pan, X.-Q.; Li, H.-C.; Hu, X.; Fan, Z.-Y.; Wang, W.-K.; Zhao, G.-H.; Jin, S.; Huber, G. W.; Yu, H.-Q. Efficient electrochemical production of glucaric acid and H2 via glucose electrolysis. *Nat. Commun.* **2020**, *11*, 1–11.
16. Han, X.; Sheng, H.; Yu, C.; Walker, T. W.; Huber, G. W.; Qiu, J.; Jin, S. Electrocatalytic oxidation of glycerol to formic acid by CuCo2O4 spinel oxide nanostructure catalysts. *ACS Catal.* **2020**, *10*, 6741–6752.
17. Taitt, B. J., Nam, D.-H. & Choi, K.-S. A comparative study of nickel, cobalt, and iron oxyhydroxide anodes for the electrochemical oxidation of 5-hydroxymethylfurfural to 2,5-furandicarboxylic acid. *ACS Catal.* **2019**, *9*, 660–670.
18. You, B., Liu, X., Jiang, N. & Sun, Y. A general strategy for decoupled hydrogen production from water splitting by integrating oxidative biomass valorization. *J. Am. Chem. Soc.* **2016**, *138*, 13639–13646.
19. Poeta, M. D.; Schell, W. A.; Dykstra, C. C.; Jones, S.; Tidwell, R. R.; Czarny, A.; Bajic, M.; Bajic, M.; Kumar, A.; Boykin, D.; Perfect, J. R. Structure-in vitro activity relationships of pentamidine analogues and dication-substituted bis-benzimidazoles as new antifungal agents. *Antimicrob. Agents Chemother.* **1998**, *42*, 2495–2502.

20. Xu, Y.; Jia, X.; Ma, J.; Gao, J.; Xia, F.; Li X.; Xu, J. Efficient synthesis of 2,5-dicyanofuran from biomass-derived 2,5-diformylfuran via an oximation–dehydration strategy. *ACS Sustainable Chem. Eng.* **2018**, *6*, 2888–2892.
21. Amarasekara, A. S.; Green, D.; Williams, L.D. Renewable resources based polymers: synthesis and characterization of 2,5-diformylfuran–urea resin *Eur. Polym. J.* **2009**, *45*, 595–598.
22. Hopkins, K. T.; Wilson, W. D.; Bender, B. C.; McCurdy, D. R.; Hall, J. E.; Tidwell, R. R.; Kumar, A.; Bajic, M.; Boykin, D. W. Extended aromatic furan amidino derivatives as anti-pneumocystis carinii agents. *J Med Chem.* **1998**, *41*, 3872–3878.
23. Zhang, Z.; Deng, K. Recent advances in the catalytic synthesis of 2,5-furandicarboxylic acid and its derivatives *ACS Catal.* **2015**, *5*, 6529–6544.
24. Chadderdon, D. J.; Xin, L.; Qi, J.; Qiu, Y.; Krishna, P.; More, K. L.; Li, W. Electrocatalytic oxidation of 5-hydroxymethylfurfural to 2,5-furandicarboxylic acid on supported Au and Pd bimetallic nanoparticles. *Green Chem.* **2014**, *16*, 3778–3786.
25. Cao, T. ; Wu, M.; Ordomsky, V. V.; Xin, X.; Wang, H.; Metivier, P.; Pera-Titus, M. Selective electrogenerative oxidation of 5-hydroxymethylfurfural to 2,5-furandialdehyde. *ChemSusChem*, **2017**, *10*, 4851–4854.
26. Nam, D. H.; Taitt, B. J.; Choi, K.-S. Copper-based catalytic anodes to produce 2,5-furandicarboxylic acid, a biomass-derived alternative to terephthalic acid. *ACS Catal.* **2018**, *8*, 1197–1206.
27. Zhou, Z.; Chen, C.; Gao, M.; Xia, B.; Zhang, J. In situ anchoring of a Co_3O_4 nanowire on nickel foam: an outstanding bifunctional catalyst for energy-saving simultaneous reactions. *Green Chem.*, **2019**, *21*, 6699–6706.
28. Zhang, P.; Sheng, X.; Chen, X.; Fang, Z.; Jiang, J.; Wang, M.; Li, F.; Fan, L.; Ren, Y.; Zhang, B.; Timmer, B. J. J.; Ahlquist, M. S. G.; Sun, L. Paired electrocatalytic oxygenation and hydrogenation of organic substrates with water as the oxygen and hydrogen source. *Angew. Chem., Int. Ed.* **2019**, *58*, 9155–9159.
29. You, B.; Jiang, N.; Liu X.; Sun, Y. Simultaneous H_2 generation and biomass upgrading in water by an efficient noble-metal-free bifunctional electrocatalyst. *Angew. Chem., Int. Ed.* **2016**, *55*, 9913–9917.
30. Zhang, N.; Zou, Y.; Tao, L.; Chen, W.; Zhou, L.; Liu, Z.; Zhou, B.; Huang, G.; Lin, H.; Wang, S. Electrochemical oxidation of 5-hydroxymethylfurfural on nickel nitride/carbon Nanosheets:

reaction pathway determined by in situ sum frequency generation vibrational spectroscopy *Angew. Chem., Int. Ed.* **2019**, *58*, 15895–15903.

31. Gao, L.; Liu, Z.; Ma, J.; Zhong, L.; Song, Z.; Xu, J.; Gan, S.; Han, D.; Niu, L. NiSe@NiOx core-shell nanowires as a non-precious electrocatalyst for upgrading 5-hydroxymethylfurfural into 2,5-furandicarboxylic acid. *Appl. Catal., B* **2020**, *261*, 118235.
32. Weidner, J.; Barwe, S.; Sliozberg, K.; Piontek, S.; Masa, J.; Apfel, U.-P.; W. P.; Schuhmann, W. Cobalt–metalloid alloys for electrochemical oxidation of 5-hydroxymethylfurfural as an alternative anode reaction in lieu of oxygen evolution during water splitting. *J. Org. Chem*., **2018**, *14*, 1436–1445.
33. Kang, M. J.; Yu, H. J.; Kim, H. S.; Cha, H. G. Deep eutectic solvent stabilised Co–P films for electrocatalytic oxidation of 5-hydroxymethylfurfural into 2,5-furandicarboxylic acid. *New J. Chem.* **2020**, *44*, 14239–14245.
34. Jiang, N.; You, B.; Boonstra, R.; Terrero-Rodriguez, I. M.; Sun, Y. Integrating electrocatalytic 5-hydroxymethylfurfural oxidation and hydrogen production via Co–P-derived electrocatalysts. *ACS Energy Lett.* **2016**, *1*, 386–390.
35. Fleischmann, M.; Korinek, K.; Pletcher, D. The oxidation of organic compounds at a nickel anode in alkaline solution *J. Electroanal. Chem. Interfacial Electrochem.* **1971**, *31*, 39−49.
36. Fleischmann, M.; Korinek, K.; Pletcher, D. The kinetics and mechanism of the oxidation of amines and alcohols at oxide-covered nickel, silver, copper, and cobalt electrodes. *J. Chem. Soc., Perkin Trans. 2* **1972**, *10*, 1396−1403.
37. Konaka, R.; Terabe, S.; Kurama, K. Mechanism of the oxidation reaction with nickel peroxide. *J. Org. Chem.* **1969**, *34*, 1334.
38. Vértes, G.; Horányi, G. Some problems of the kinetics of organic compounds at oxide-covered nickel electrodes. J. Electroanal. Chem. Interfacial Electrochem. 1974, 52, 47−53.
39. Robertson, P. M. On the oxidation of alcohols and amines at nickel oxide electrodes: mechanistic aspects. J. Electroanal. Chem. Interfacial Electrochem. 1980, 111, 97−104.
40. Schafer, H.-J. Oxidation of organic compounds at the nickel¨hydroxide electrode. Top. Curr. Chem. 1987, 142, 101−129.
41. Miao, Y.; Ouyang, L.; Zhou, S.; Xu, L.; Yang, Z.; Xiao, M.; Ouyang, R. Electrocatalysis and electroanalysis of nickel, its oxides, hydroxides and oxyhydroxides toward small molecules. Biosens. Bioelectron. 2014, 53, 428−439.

42. Lyalin, B. V.; Petrosyan, V. A. Oxidation of organic compounds on NiOOH electrode. Russ. J. Electrochem. 2010, 46, 1199−1214.
43. Francke, R.; Quell, T.; Wiebe, A.; Waldvogel, S. R. Oxygen-Containing Compounds. Organic Electochemistry: Revised and Expanded; CRC Press: Boca Raton, FL, 2016; Chapter 26.
44. Van Effen, R. M.; Evans, D. H. J. Electroanal. Chem., 107 (1980) 405-418
45. Kaulen, J.; Schäfer, H.-J. Oxidation of alcohols by electrochemically regenerated nickel oxide hydroxide. Selective oxidation of hydroxysteroids. Tetrahedron 1982, 38, 3299−3308.
46. Houache, M. S. E.; Hughes, K.; Ahmed, A.; Safari, R.; Liu, H.; Botton, G. A.; Baranova, E. A. Electrochemical valorization of glycerol on Ni-rich bimetallic NiPd nanoparticles: insight into product selectivity using in situ polarization modulation infrared-reflection absorption spectroscopy. ACS Sustainable Chem. Eng. 2019, 7, 14425−14434.
47. Kapałka, A.; Cally, A.; Neodo, S.; Comninellis, C.; Wachter, M.; Udert, K. M. Electrochemical behavior of ammonia at Ni/Ni(OH)2 electrode. *Electrochem. Commun.* **2010**, *12*, 18−21.
48. Yamaguchi, K.; Mizuno, N. Development of highly active heterogeneous oxidation catalysts based on the properties of metal hydroxides. *Top. Catal.* **2014**, *57*, 1196-1207.
49. Tseng, K.-N. T.; Szymczak, N. K. Dehydrogenative oxidation of primary amines to nitriles. *Synlett* **2014**, *25*, 2385–2389.
50. Schümperli, M. T.; Hammond, C.; Hermans, I. Developments in the aerobic oxidation of amines. *ACS Catal.* **2012**, *2*, 1108−1117.

Chapter 2: Unraveling Two Pathways for Electrochemical Alcohol and Aldehyde Oxidation on NiOOH

Portions of this chapter have been adapted from:

Bender, M. T.; Lam, Y. C.; Hammes-Schiffer, S.; Choi, K.-S. Unraveling two pathways for electrochemical alcohol and aldehyde oxidation on NiOOH. *J. Am. Chem. Soc.* **2020**, *142*, 21538−21547. DOI 10.1021/jacs.0c10924

2.1 Introduction

Electrochemical alcohol oxidation to produce molecules of greater value is an important reaction for energy and catalysis sciences.[1] In addition to its utility in organic synthesis, electrochemical alcohol oxidation is also considered a viable anode reaction that can replace water oxidation as the oxidative reaction paired with H_2 evolution or other reductive fuel production reactions in electrochemical and photoelectrochemical cells to increase their efficiency and utility.[2-5] Interestingly, one of the most promising catalysts for the selective oxidation of alcohols to their corresponding carboxylic acids is NiOOH,[5-10] a material that has also been extensively studied as an oxygen evolution catalyst.[1] Thus, developing in-depth mechanistic insight into alcohol oxidation on NiOOH is of great interest in advancing our understanding of NiOOH as an electrocatalyst.

The mechanism for electrochemical alcohol oxidation on NiOOH has been well established by Fleischmann *et al*. as shown in **Scheme 2.1**.[10,11] Under open circuit conditions, the resting state of NiOOH is $Ni(OH)_2$. Thus, the first step is the electrochemical oxidation of $Ni(OH)_2$ to NiOOH. The NiOOH then serves as a chemical oxidant and abstracts an α-hydrogen atom from the alcohol, which is rate limiting.[10,11] This step converts NiOOH back to $Ni(OH)_2$, and the role of the applied potential is to keep regenerating NiOOH from the $Ni(OH)_2$ produced by this chemical oxidation of alcohol. Since $Ni(OH)_2$/NiOOH serves as a solid-state mediator, and the applied potential is used only to regenerate the mediator, this mechanism is referred to as indirect oxidation in the literature.[7,8] As long as the applied potential is sufficiently positive to rapidly regenerate NiOOH, the rate of indirect alcohol oxidation is independent of the applied potential because the chemical oxidation of the alcohol by NiOOH is the rate determining step (RDS).[11]

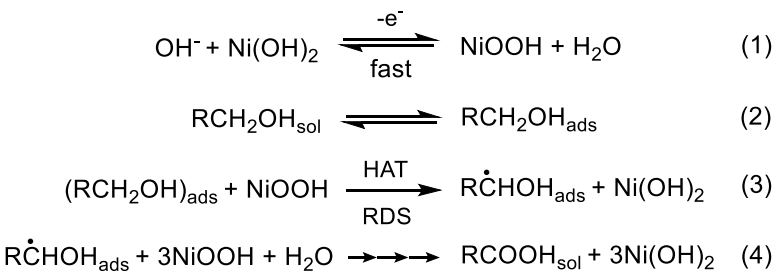

Scheme 2.1. Mechanism proposed by Fleischmann et al. for the indirect oxidation of alcohols at NiOOH electrodes in alkaline aqueous media.

While this mechanism has been well accepted for the past several decades,[9-19] there have been a few studies reporting electrocatalytic behaviors of NiOOH that cannot be explained by the indirect mechanism.[6,20-23] These papers commonly report the observation of potential-dependent (PD) alcohol oxidation at potentials more positive than the potential enabling indirect oxidation. In these studies, this PD oxidation was referred to as direct oxidation in contrast to the indirect oxidation mechanism proposed by Fleischmann *et al.*,[6,7,22,23] because these studies hypothesized that this PD oxidation may involve direct electrocatalysis in which Ni^{3+} sites remain as Ni^{3+} throughout the mechanism.[22,23] However, no evidence has been presented to support this hypothesis. In fact, other than its existence, not much is known about the PD oxidation mechanism on NiOOH.

The goal of the current study is to clearly elucidate the PD oxidation mechanism on NiOOH with a detailed understanding of its mechanistic difference from Fleischmann's potential-independent indirect oxidation. The challenge of studying the PD oxidation mechanism is that in the potential region where it is enabled, the contribution from indirect oxidation still remains. Thus, it is difficult to accurately deconvolute the rates of PD and indirect oxidation, a critical step if a mechanistic understanding of both processes is to be developed.

In this study, we report a three-step electrochemical procedure that can not only deconvolute the rates of indirect and PD oxidation but also identify the oxidation state of Ni involved with indirect and PD oxidation. We applied this procedure to a variety of aliphatic and aromatic alcohols and aldehydes to quantitatively study the rates of indirect and PD oxidation on NiOOH and to demonstrate the substrate-dependence of the two oxidation mechanisms. Furthermore, we combined experimental and computational studies to propose hydride transfer as a plausible dehydrogenation mechanism that is responsible for PD oxidation, in contrast to indirect oxidation that achieves dehydrogenation via hydrogen atom transfer (HAT). We also demonstrate that PD oxidation is enabled only when Ni^{4+} is formed. Our combined experimental and computational investigations provide a coherent and thorough understanding of the mechanistic differences between indirect and PD oxidation on NiOOH.

2.2 Results and Discussion

2.2.1 Qualitative Assessment Through LSVs.

The oxidation of various aliphatic and aromatic alcohols and aldehydes on NiOOH was investigated in this study. Aldehydes were included because aldehyde oxidation in aqueous electrolyte proceeds through a geminal diol and is thus a type of alcohol oxidation. Also, aldehydes are intermediates for the oxidation of alcohols to carboxylic acids. Thus, the comparative study of alcohol and aldehyde oxidation can provide useful and important insights.

Figure 2.1 shows linear sweep voltammograms (LSVs) of representative alcohols and aldehydes, which can be used to qualitatively assess the contribution of indirect and PD oxidation. These LSVs clearly show how the contributions of indirect and PD oxidation dramatically change depending on the molecular structure of the substrate.

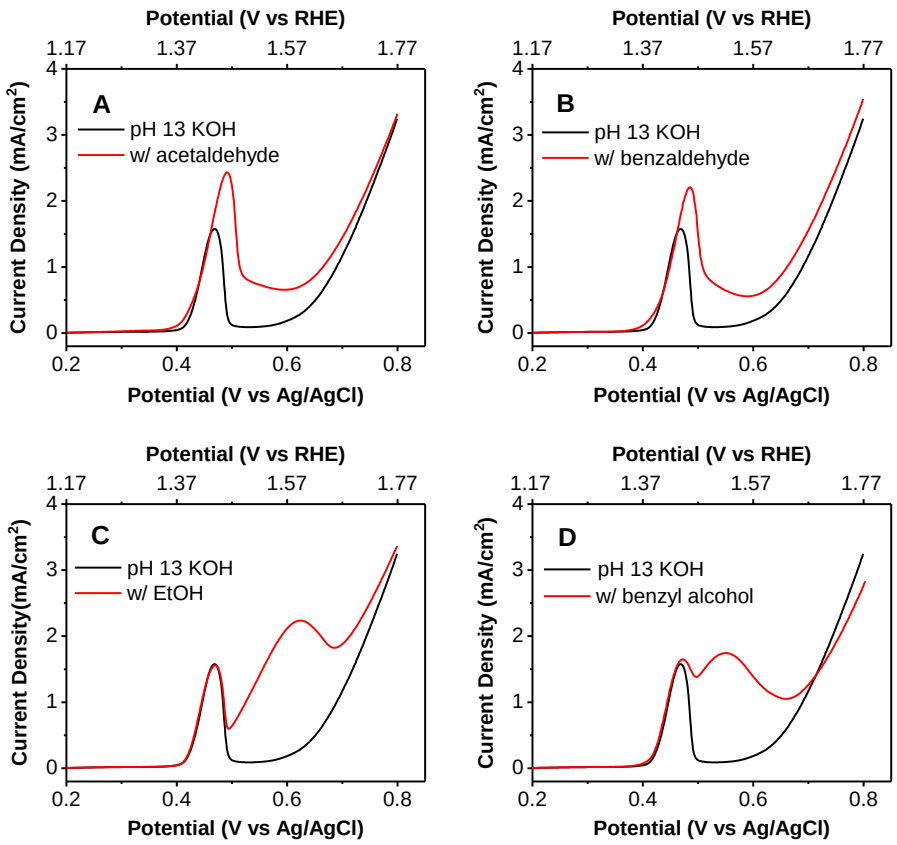

Figure 2.1. LSVs using a $Ni(OH)_2$ working electrode in a pH 13 solution without (black) and with (red) A) 10 mM acetaldehyde, B) 10 mM benzaldehyde, C) 10 mM EtOH and D) 10 mM benzyl alcohol (scan rate 10mV/s).

When no organic substrate is present (**Figure 2.1, black line**), a peak corresponding to the conversion of $Ni(OH)_2$ into NiOOH is observed with an onset at ~0.4V vs Ag/AgCl followed by an oxidative wave corresponding to water oxidation starting shortly before 0.6V vs Ag/AgCl. When acetaldehyde or benzaldehyde is present in solution (**Figure 2.1A-B, red line**), since NiOOH can be reduced back to $Ni(OH)_2$ by oxidizing the aldehydes during the potential sweep, more current is generated for the conversion of $Ni(OH)_2$ to NiOOH, resulting in an enhancement of the $Ni(OH)_2$/NiOOH peak. The enhancement of the $Ni(OH)_2$/NiOOH peak is thus directly

related to the rate of indirect oxidation of the aldehydes by NiOOH via the mechanism proposed by Fleischmann *et al.*[10,11]

Conversely, the LSVs for the oxidation of EtOH and benzyl alcohol (**Figure 2.1C-D, red line**) show no or only modest enhancement of the $Ni(OH)_2$/NiOOH peak and instead feature a new anodic peak at a more positive applied bias, which cannot be explained through Fleischmann's potential-independent indirect oxidation. This peak is instead associated with the PD oxidation mechanism, which has been referred to as direct oxidation in previous studies.[6,7,22,23] Of further note is that the prominence of the PD oxidation peak relative to the very modest enhancement of the $Ni(OH)_2$/NiOOH peak in the presence of either EtOH or benzyl alcohol suggests that, contrary to the findings of Fleischmann *et al.*,[10,11] for alcohol oxidation the PD pathway is actually dominant. Additionally, the observation that the LSV with benzyl alcohol shows a slight enhancement of the $Ni(OH)_2$/NiOOH peak while the one with EtOH does not suggests that the structural details of the substrate, such as aromaticity, may play a role in determining the relative prominence of the indirect vs the PD mechanism.

2.2.2 Description of Rate Deconvolution Procedure.

While the LSVs presented above reveal qualitative information about the preference of different substrates for the PD and indirect oxidation pathways, the overlap of currents corresponding to initial oxidation of $Ni(OH)_2$, the indirect process, the PD process, and water oxidation makes it difficult to quantitatively assess the rates of the two mechanisms. Additionally, the swept potential and unstirred solution present during an LSV are different from the conditions present during a constant potential electrolysis that might be used when trying to efficiently convert one of these substances to its carboxylic acid. To address these issues, we developed a 3-step electrochemical procedure to deconvolute and identify the rates of the PD and

indirect mechanisms under conditions that more closely match those of a constant potential electrolysis (**Scheme 2.2**). A general overview of the technique will be given here with additional details in the experimental section.

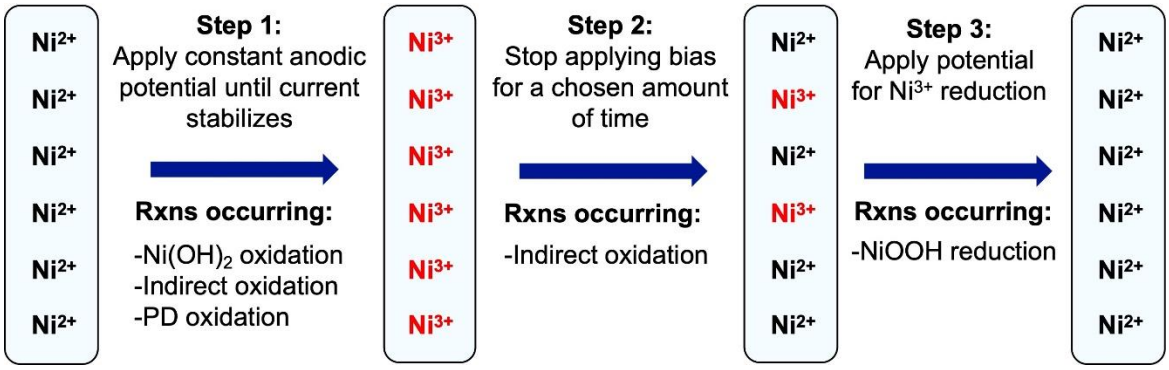

Scheme 2.2. A schematic representation of the 3-step rate deconvolution procedure. (For the sake of simplicity the oxidized Ni catalyst is depicted as having only Ni^{3+} sites; however, as will be shown below, depending on the applied potential Ni^{4+} sites can also form.)

The 3-step procedure is performed in a rapidly stirred alcohol/aldehyde solution with a $Ni(OH)_2$ working electrode (WE). In the first step a constant positive potential is applied long enough for the current to stabilize to a steady state value. During this step the $Ni(OH)_2$ electrode is converted into the oxidation state it would be in during a constant potential electrolysis at that applied potential, and both the indirect and PD processes are occurring. In the second step the applied potential is turned off, and the NiOOH electrode is left in the stirred solution under open circuit conditions for a specified length of time. During this time neither the PD process nor NiOOH regeneration can occur as both require applied bias, but the potential-independent indirect process will continue unabated, converting NiOOH back into $Ni(OH)_2$ as it acts as a chemical oxidizing agent reacting with the alcohol/aldehyde. In the third step a reducing potential is applied to convert the remaining NiOOH back to $Ni(OH)_2$. The magnitude of the charge passed during this

third step is equivalent to the number of coulombs needed to reduce all the higher valent Ni ions remaining after the second step back to Ni^{2+} to form $Ni(OH)_2$ (hereafter referred to as "charge stored" in the NiOOH). By repeating this 3-step process with different times stirring under open circuit conditions in step 2, a data series can be constructed showing the disappearance of positive charge from the NiOOH as a function of time left at open circuit during step 2 (**Figure 2.2**). For all the substrates tested here, a plot of 1/(charge stored) vs time is linear at relatively short times stirring at open circuit, indicating that over this time span the disappearance of charge proceeds as if it is "second order" in charge stored (**Figure S3**). This allows the rate of disappearance of charge from these films at time *t* to be calculated using a pseudo-second order rate law equation (eq. 1) where $Q_{film}(t)$ is the charge stored in the Ni film at time *t* and k_{obs} is the slope of the $1/(Q_{film})$ vs *t* plot.

$$-\frac{dQ_{film}(t)}{dt} = k_{obs}{Q_{film}}^2(t) \quad (1)$$

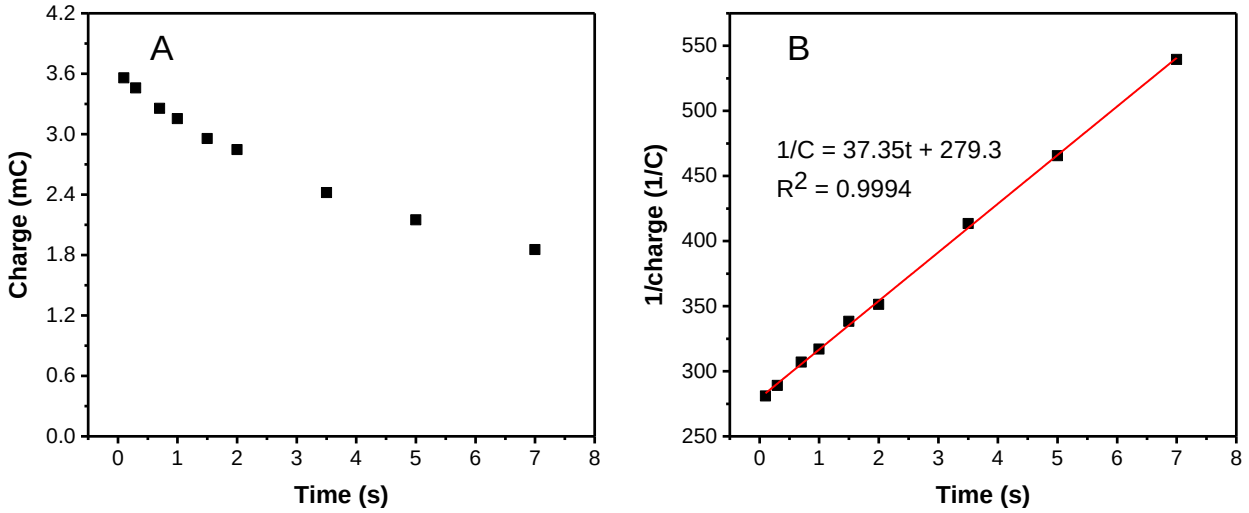

Figure 2.2 Depiction of A) Charge vs time and B) 1/Charge vs time for the amount of positive charge remaining in a NiOOH film after a given length of time sitting at open circuit condition in a stirred pH 13 10 mM furfural solution.

Moreover, since the charge is disappearing from the NiOOH film as a result of being used to oxidize alcohol/aldehyde through the indirect process, the instantaneous rate of disappearance of charge from the film is equal to the rate of the indirect process at that time (eq. 2).

$$-\frac{dQ_{\text{film}}(t)}{dt} = I_{\text{indirect}}(t) \quad (2)$$

We note that we are using I_{indirect}(t) in eq. 2 to refer to the rate of the indirect process even though there is no externally measurable current during step 2 (which is at open circuit) because the units of that rate are coulombs per second. Furthermore, we also note that the instantaneous rate of the indirect process at t = 0 s during step 2 has a special meaning as it corresponds to the steady state partial current for the indirect process at the potential applied in step 1 (I_{indirect}). Thus, once I_{indirect} is determined by solving eq. 1 for t = 0 s, the steady state partial current for the PD process (I_{PD}) at the potential applied during step 1 can be calculated from the total steady state current observed in step 1 (I_{tot}) using eq. 3 as long as the potential chosen for step 1 is before the onset of water oxidation.

$$I_{\text{tot}} = I_{\text{indirect}} + I_{\text{PD}} \quad (3)$$

Lastly, we note here that it is likely the "true" rate equation describing the relationship between stored charge and the rate of indirect oxidation is more complicated than the simple pseudo-second order equation expressed in eq. 1. For the purpose of deconvoluting I_{indirect} and I_{PD}, however, it is not necessary that this be the "true" rate equation to describe this reaction. Rather, we require only that it accurately reflects the change in charge stored in the nickel film over the timespan of interest, and for all the substrates studied here a simple pseudo-second order relationship does so successfully.

2.2.3 Evaluating the Rate of Indirect and PD Oxidation.

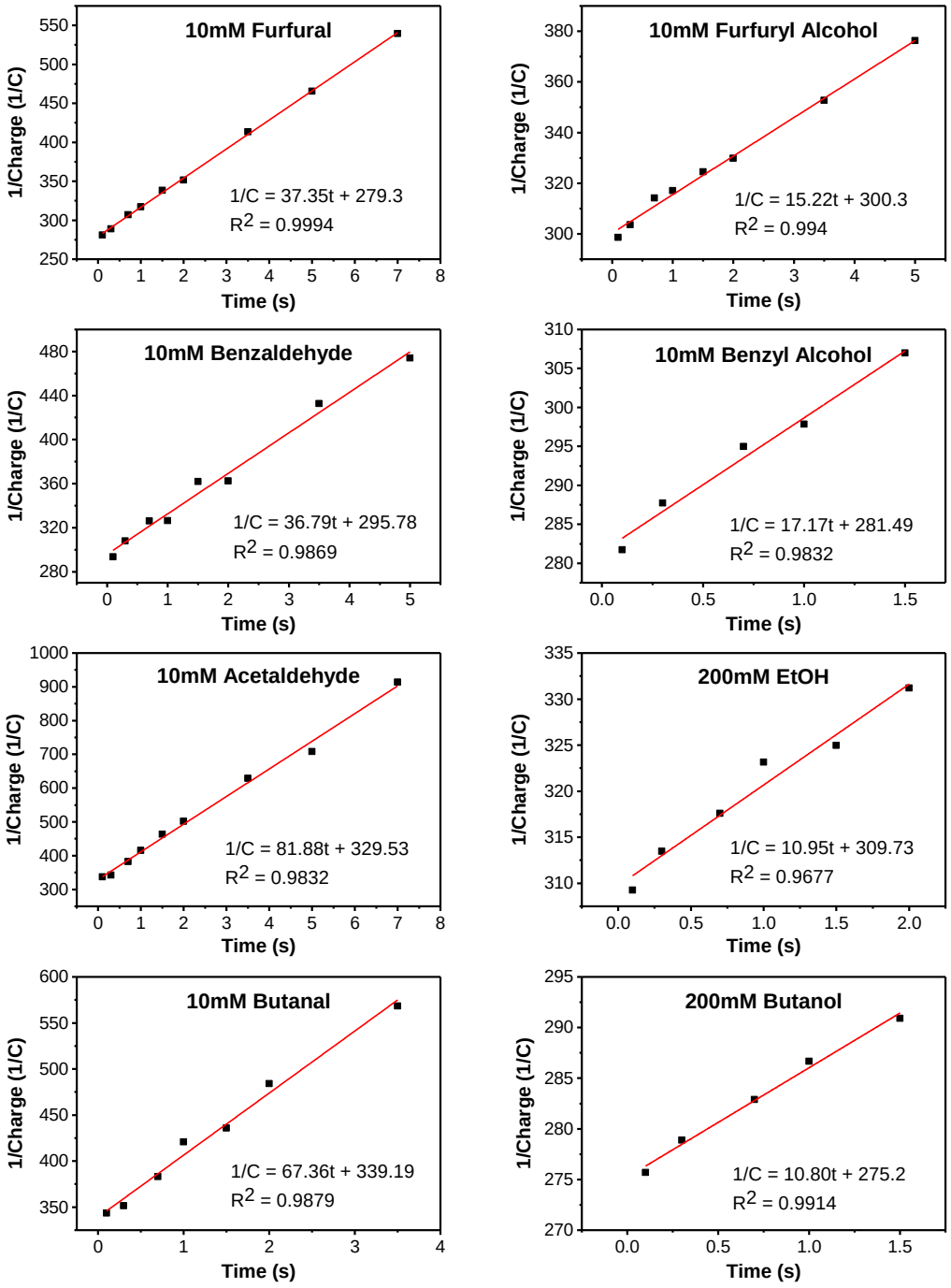

Figure S3. 1/Charge vs time plot for the amount of positive charge remaining in NiOOH films after given lengths of time sitting at open circuit condition in a stirred pH 13 alcohol or aldehyde solution.

The method described above was used to evaluate the rates of the indirect and PD process for oxidation of a variety of aromatic and aliphatic alcohols in pH 13 KOH at 0.55V vs Ag/AgCl. The resulting 1/charge vs time plots are shown in **Figure 2.3** and the deconvoluted indirect and PD currents are shown in **Figure 2.4**. We confirmed that under these conditions a high Faradaic efficiency toward oxidation of the alcohol/aldehyde to the corresponding aldehyde/carboxylic acid ($\leq$ 95%) is achieved for all the substrates tested. Oxidation of the aldehydes and aliphatic alcohols resulted in the corresponding carboxylic acid as the only detectible product while oxidation of the aromatic alcohols produced a mixture of the corresponding aldehyde and carboxylic acid. For the aliphatic alcohols 200 mM was used rather than 10 mM because at 10 mM the slow rate of the indirect process made it challenging to measure accurately.

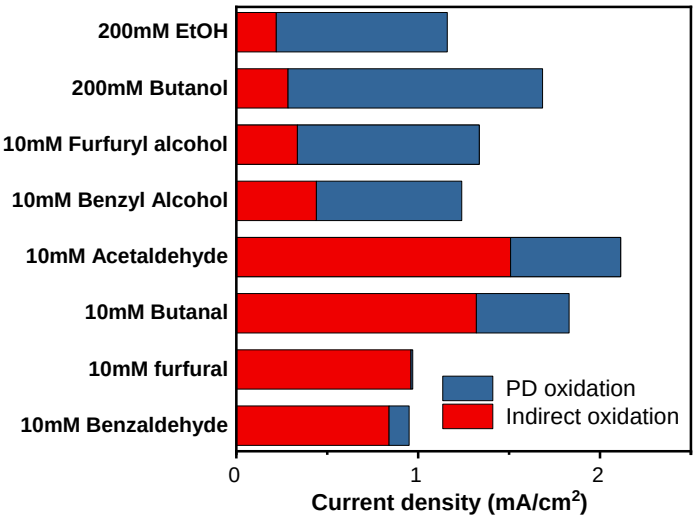

Figure 2.4. The component of the current due to indirect (red) and PD (blue) oxidation of alcohols and aldehdes at 0.55V vs Ag/AgCl and pH 13.

The data presented in **Figure 2.4** reveals alcohols and aldehydes have a distinct difference in their respective preferences for indirect and PD oxidation. As was suggested qualitatively by the LSVs, the rate deconvolution data shows that at 0.55 V vs Ag/AgCl PD oxidation is the

dominant process through which alcohols react. Conversely, aldehydes react preferentially through the indirect process and their partial current densities for the indirect process are considerably higher than those of their corresponding alcohols. To understand this increased preference of aldehydes toward the indirect process relative to their corresponding alcohols we need to first consider the tendency for aldehydes to convert into a geminal diol under alkaline conditions. For the aldehydes studied here, the equilibrium ratio of aldehyde to geminal diol molecules at pH 13 was estimated through nuclear magnetic resonance (NMR) spectroscopy by comparing the ratio of the integration of the aldehyde peak to that of the rest of the protons. This showed that for furfural 56% was converted into the diol while for benzaldehyde 65% was in the diol form. For the aliphatic aldehydes no aldehyde peak was visible so they were assumed to be nearly 100% diol. The fact that the aliphatic aldehydes readily undergo oxidation while being entirely converted into geminal diols suggests that for "aldehyde" oxidation the diol is the actual reactive form of the molecule, with the mechanism being comparable to that through which alcohols react. This in turn allows us to rationalize the increased preference of aldehydes toward the indirect process relative to their equivalent alcohols. This is because the second –OH group that diols have bound to the α-C would result in additional stabilization of the radical intermediate formed following the rate limiting HAT step of the indirect process (**Scheme 2.1, step 3**).

The data in **Figure 2.4** also confirms that aromaticity increases the relative proportion of oxidations that occur through the indirect pathway for both alcohols and aldehydes. This can also be attributed to additional stabilization of the radical intermediate formed during the indirect pathway as the radical formed on the α-C will be delocalized throughout the adjacent aromatic ring.

2.2.4 Average Ni Valence.

Next, we investigated what valence of Ni in NiOOH is associated with indirect and PD oxidation by modifying the rate deconvolution technique described above. We used solutions of 10 mM furfural (pH 13), 200 mM EtOH (pH 13) and pH 13 KOH without any organic substrate to study how the average Ni valence changes for indirect oxidation, PD oxidation, and water oxidation when we apply a gradually more positive potential to NiOOH. Furfural and EtOH were chosen because they have the highest proportion of oxidations occurring through the indirect and PD mechanisms, respectively.

In the modified procedure, the constant potential held in step 1 was varied and the time at open circuit in step 2 was fixed at 0.1 s across all measurements (see the Experimental section for further details). We selected 0.1 s for the time at open circuit because this was the shortest time for which we could obtain an accurate measure of the charge stored in the NiOOH film. The average amount of Ni present in a film was determined to be 23.6 ± 0.4 nmol by inductively coupled plasma mass spectrometry (ICP–MS). This quantity, along with the charge passed in step 3 of the rate deconvolution procedure, allowed the average Ni valence under steady state conditions at the potential applied in step 1, *E,* to be calculated according to eq. 4, where Q_E is the magnitude of the charge passed during step 3, n_{Ni} is the moles of Ni in the NiOOH film, and F is Faraday's constant.

$$\langle \text{Ni valence} \rangle = 2 + \frac{Q_{\text{E}}}{n_{Ni}F} \qquad (4)$$

The results of these experiments are shown in **Figure 2.5A** where the average Ni valence as a function of applied potential during indirect oxidation of furfural, PD oxidation of EtOH, and water oxidation are compared. **Figure 2.5B** shows the steady state current obtained while stirring at each applied potential. This shows that, in pH 13 KOH, as the potential is increased from 0.45 V vs Ag/AgCl the average Ni valence increases roughly linearly from +3.47 until plateauing at

about +3.8 at 0.625 V vs Ag/AgCl. This increase in average valence is due to an accumulation of Ni^{4+} sites in the film as potential is increased, and the plateau is due to an increasing rate of Ni^{4+} consumption as the rate of water oxidation increases. The Ni valence of NiOOH in a similar operating condition has previously been determined using quasi in-situ X-ray absorption spectroscopy (XAS), although only one potential was used for the measurement due to procedural complexity. The reported value of +3.7 as the Ni valence at 0.665 V vs Ag/AgCl in a pH 13 KOH solution agrees well with our measurement of +3.8 at 0.65 V vs Ag/AgCl in the same pH 13 KOH solution.[24] We note that our procedure, which is based on simple electrochemical techniques and a straightforward data workup, provides a convenient yet effective way to rapidly determine the average Ni valence in NiOOH at numerous different operating potentials and under various solution conditions without needing access to a synchrotron, a complex measurement setup, or data interpretation based on comparison with reference samples.

When 10 mM furfural is present, the average Ni valence drops to about +2.57 at 0.45V vs Ag/AgCl. This is because Ni^{3+} is consumed by furfural via indirect oxidation. **Figure 2.5A** also reveals that from 0.5 V onward the average valence increases at the same rate with furfural as without it until plateauing at 0.625 V vs Ag/AgCl at +3.63, indicating that the indirect oxidation of furfural does not significantly affect the accumulation of Ni^{4+}. This, coupled with the observation that the steady state current for furfural oxidation does not increase significantly from 0.5 V vs Ag/AgCl to 0.55 V vs Ag/AgCl and actually decreases at potentials above this (**Figure 2.5B**), indicates that either Ni^{4+} sites are not significantly more reactive toward the indirect process than Ni^{3+} sites or that furfural cannot effectively outcompete water oxidation intermediates for access to the Ni^{4+} sites. The latter would explain why the steady state current for furfural falls as the potential increases and more of the sites are converted to Ni^{4+}. Moreover, if, as will be

discussed below, the PD oxidation occurs at Ni^{4+} sites, this inability for furfural to outcompete water oxidation intermediates for adsorption on Ni^{4+} sites would explain the very low rate of oxidation of furfural through the PD mechanism.

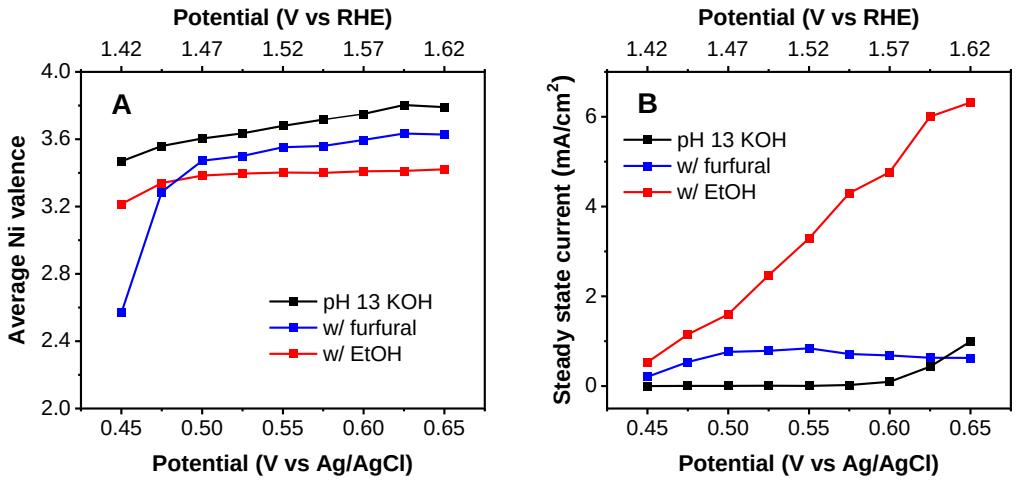

Figure 2.5. A) The average steady state Ni valence in a stirred pH 13 solution as a function of potential in the absence (black) and presence of 10 mM furfural (blue) and 200 mM EtOH (red). B) Steady state current in a pH 13 stirred solution in the absence (black) and presence of 10 mM furfural (blue) and 200 mM EtOH (red).

In contrast, when EtOH is present, the average Ni valence even at 0.45V vs Ag/AgCl is well above +3 and between 0.45 V and 0.5 V, where the rate of EtOH oxidation is still fairly modest, the increase in Ni valence in the 200 mM EtOH solution tracks closely with that in pH 13 KOH. In the EtOH solution, however, the average Ni valence reaches a plateau at ~+3.4 and does not significantly increase as the potential is further increased (**Figure 2.5A**), despite an increasing steady state oxidation current (**Figure 2.5B**). This plateau in the average Ni valence indicates that the presence of EtOH inhibits the accumulation of Ni^{4+} in the film, meaning PD oxidation of EtOH consumes Ni^{4+}. Moreover, this plateau suggests that at potentials above 0.525V vs Ag/AgCl regeneration of Ni^{4+} from the reduced catalyst limits the rate of catalyst turnover and that the

observed potential dependence of the PD oxidation rate (**Figure 2.5B**) may be due to a faster regeneration of Ni^{4+} at higher applied biases. The fact that PD oxidation also involves a change in oxidation state in NiOOH indicates that the name "direct oxidation" used in previous studies[6,7,22,23] is not actually an accurate description of PD oxidation. (The term "direct oxidation" was used in previous studies based on the assumption that the oxidation state of Ni remained as +3 throughout PD oxidation.[22,23]) The reason that PD oxidation is potential-dependent is not because Ni^{3+} remains as Ni^{3+} during oxidation but rather because generation of the site Ni^{4+} needed to perform PD oxidation is both potential and rate-affecting and because the applied bias is necessary to activate those Ni4+ sites toward the PD mechanism. This can be contrasted with case of Fleischmann's potential-independent indirect oxidation where the electrochemical regeneration of the catalytically active Ni^{3+} species is not the RDS and the reaction between Ni^{3+} and the organic species does not require an applied bias to occur. Thus, PD oxidation is in fact a potential-dependent indirect oxidation if "indirect" is taken to mean that alcohol/aldehyde oxidation is mediated by a change in the valence of Ni.

2.2.5 Computational Study.

The experimental results clearly suggest that the PD oxidation must have a dehydrogenation mechanism that is different from the HAT of the α-hydrogen that is involved in Fleischmann's indirect oxidation. We expect that the ability for NiOOH to selectively oxidize alcohols and aldehydes only to their corresponding carboxylic acids instead of completely oxidizing them to CO_2 stems from its ability to selectively dehydrogenate alcohols and aldehydes through its conversion to $Ni(OH)_2$. This characteristic indicates that not only electrons but also protons need to be transferred from alcohols and aldehydes to NiOOH to form $Ni(OH)_2$. Thus, we do not expect that the PD oxidation occurs through a multisite proton-coupled electron transfer

mechanism where only electrons are transferred to the catalyst while the protons are transferred to solution species. (This is the mechanism used by metal electrocatalysts for complete oxidation of alcohols to CO_2.[25]) In contrast, hydride transfer of the α-hydrogen of the alcohol/aldehyde to a Ni^{4+} site in the catalyst does involve transfer of both electrons and a proton to the catalyst and would reduce the Ni^{4+} site to form $Ni(OH)_2$. As such, it seemed a reasonable mechanism through which the PD oxidation could be occurring. To test whether such a mechanism is truly plausible for PD oxidation, we performed computational studies modeling oxidation of ethanol, which shows the highest PD oxidation component, through a hydride transfer.

The results of our computational studies are summarized in **Table 2.1**, with the optimized structures of selected slabs shown in **Figure 2.6**. The NiOOH catalyst was first modeled as having two layers, each comprised of four NiO_2H units. To investigate the effect of Ni valence on hydride transfer energetics, the oxidation state of Ni ions in the upper layer, which is the outermost layer facing the solution, was changed from +3 to +4 and hydrogen atoms were removed from O atoms facing the solution to ensure charge neutrality during the oxidation of the slab. When all Ni ions in the slab are Ni^{3+}, the slab formula is $Ni_8O_{16}H_8$ (**Figure 2.6A**). When one and two Ni^{3+} ions in the upper layer are oxidized to Ni^{4+}, the corresponding slab formulae are $Ni_8O_{16}H_7$ (**Figure 2.6B**) and $Ni_8O_{16}H_6$ (**Figure 2.6C**), with average surface Ni valences of +3.25 and +3.5, respectively.

As alcohol oxidation on NiOOH only occurs appreciably under alkaline conditions, it is clear that base must play an important role in the mechanism.[7-9] One possibility that would account for this would be if alkoxide, rather than alcohol, is the active molecule toward hydride transfer. This is because under alkaline conditions there would be a modest equilibrium concentration of the alkoxide available to undergo oxidation. Alternatively, if the alcohol itself is the active molecule toward hydride transfer, the requirement for alkaline conditions could be explained if the

hydride transfer is accompanied by a concerted proton transfer to hydroxide in solution. Accordingly, to ascertain if hydride transfer is a plausible mechanism for the PD pathway, we examined the energetics of both a hydride transfer from EtO^- to the catalyst surface to form acetaldehyde as well as a hydride transfer from a complex comprised of EtOH hydrogen bonded to OH^- ($[EtOH—OH]^-$) to form acetaldehyde hydrogen bonded to water [$MeCHO—H_2O$].

The results in **Table 2.1** show that hydride transfer from EtO^- is highly unfavorable for a surface with a +3 average Ni valence (**row a**) and highly favorable for a surface with a +3.5 average Ni valence (**row b**). For an average valence of +3.25, hydride transfer is favorable (**row c**) but not as favorable as it is with a +3.5 average Ni valence.

For an average valence of +3.25, it is also necessary to consider if the surface exposed hydrogen of $Ni_8O_{16}H_7$ would undergo deprotonation when exposed to a strong base such as EtO^- and how that would affect hydride transfer. This examination is not needed for $Ni_8O_{16}H_6$ as it does not contain surface protons (**Figure 2.6C**), nor is it needed for $Ni_8O_{16}H_8$ where hydride transfer is already strongly unfavorable with the neutral surface. (Surface deprotonation results in a negatively charged surface, which should make hydride transfer even more unfavorable.)

We found that full deprotonation of $Ni_8O_{16}H_7$ by EtO^- to form $Ni_8O_{16}H_6^-$ (which has no protons on the surface) is not favorable (**row e**). In order to examine the possibility of partial surface deprotonation, we doubled the slab size to $Ni_{16}O_{32}H_{14}$ (eight NiO_2H units per layer with two layers). We found that deprotonation of $Ni_{16}O_{32}H_{14}$ by EtO^- to form $Ni_{16}O_{32}H_{13}^-$ (**Figure 2.6d**), which is equivalent to deprotonation of half the surface protons, is favorable (**row f**). We also found that hydride transfer from EtO^- to this $Ni_{16}O_{32}H_{13}^-$ slab is favorable (**row d**). This result indicates that with a +3.25 average Ni valence, hydride transfer can occur even to a surface that is partially deprotonated.

Table 2.1. Calculated changes in electronic energies for reactions related to the NiOOH-catalyzed oxidation of EtOH.

	Reaction	Average Valence of Ni in the Catalyst Surface[a]	ΔE / kcal mol^{-1} [b]
	Hydride transfer from EtO^- to the catalyst surface		
a	$Ni_8O_{16}H_8$ (s.) + EtO^- (aq.) → $Ni_8O_{16}H_9^-$ (s.) + MeCHO (aq.)	+3	+21.3
b	$Ni_8O_{16}H_6$ (s.) + EtO^- (aq.) → $Ni_8O_{16}H_7^-$ (s.) + MeCHO (aq.)	+3.5	−42.2
c	$Ni_8O_{16}H_7$ (s.) + EtO^- (aq.) → $Ni_8O_{16}H_8^-$ (s.) + MeCHO (aq.)	+3.25	−11.0
d	$Ni_{16}O_{32}H_{13}^-$ (s.) + EtO^- (aq.) → $Ni_{16}O_{32}H_{14}^{2-}$ (s.) + MeCHO (aq.)	+3.25	−14.7
	Deprotonation of the catalyst surface by EtO^-		
e	$Ni_8O_{16}H_7$ (s.) + EtO^- (aq.) → $Ni_8O_{16}H_6^-$ (s.) + EtOH (aq.)	+3.25	+11.1
f	$Ni_{16}O_{32}H_{14}$ (s.) + EtO^- (aq.) → $Ni_{16}O_{32}H_{13}^-$ (s.) + EtOH (aq.)	+3.25	−9.2
	Hydride transfer from EtOH to the catalyst surface coupled with deprotonation of EtOH by OH^-		
g	$Ni_8O_{16}H_6$ (s.) + $[EtOH—OH]^-$ (aq.) → $Ni_8O_{16}H_7^-$ (s.) + $[MeCHO—H_2O]$ (aq.)	+3.5	−32.9
h	$Ni_8O_{16}H_7$ (s.) + $[EtOH—OH]^-$ (aq.) → $Ni_8O_{16}H_8^-$ (s.) + $[MeCHO—H_2O]$ (aq.)	+3.25	−1.7
i	$Ni_{16}O_{32}H_{13}^-$ (s.) + $[EtOH—OH]^-$ (aq.) → $Ni_{16}O_{32}H_{14}^{2-}$ (s.) + $[MeCHO—H_2O]$ (aq.)	+3.25	−5.4

a. The average valence of Ni was inferred from the composition and charge of each slab, where O was assigned a charge of –2 and H was assigned a charge of +1.
b. Change in electronic energy for the specified reaction.

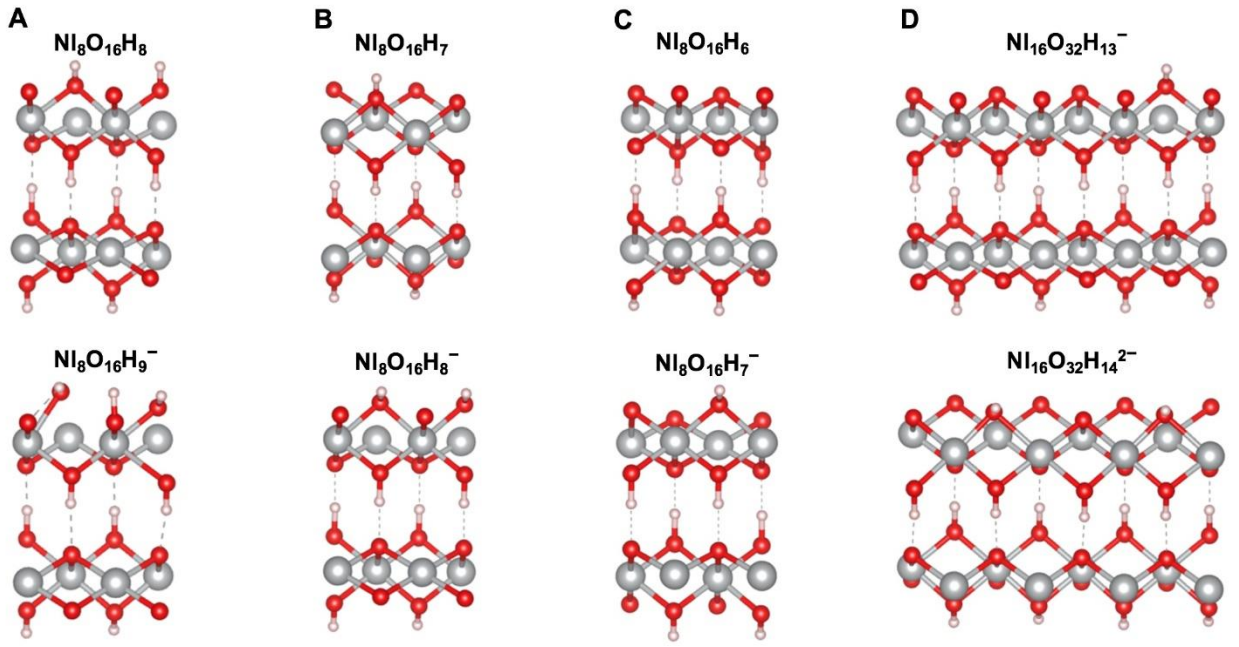

Figure 2.6. Optimized unit cell structures for selected NiOOH-derived slabs used in evaluating the energetics of hydride transfer; A) $Ni_8O_{16}H_8$, B) $Ni_8O_{16}H_7$, C) $Ni_8O_{16}H_6$, and D) $Ni_{16}O_{32}H_{13}^-$ before (top) and after (bottom) hydride transfer.

When we modeled hydride transfer to the catalyst surface from the $[EtOH—OH]^-$ complex rather than from EtO^-, our results showed that hydride transfer to the slabs with average surface Ni oxidation states of +3.25 and +3.5 is still energetically favorable (**rows g-i**), although the hydride transfer from EtO^- is more favorable by 9.3kcal/mol for all cases (**rows b-d**). In this case hydride transfer from the $[EtOH—OH]^-$ complex to the slab with an average surface Ni valence of +3 did not need to be modeled, as the transfer from EtO^- to that surface is already highly unfavorable (**row a**).

Overall, these computational results agree well with the experimental findings described above, in which we observed that Ni^{4+} was necessary for the PD oxidation to occur. Moreover, while the calculations do not provide any indication of kinetics, these results are consistent with the experimental observations that the average Ni valence is +3.2 around the onset of PD oxidation

and that the oxidation of EtOH becomes fast relative to regeneration of Ni^{4+} sites at an average valence of +3.4 (**Figure 2.5**). As such, hydride transfer, which converts a Ni^{4+} site to a Ni^{2+} site, is a plausible dehydrogenation mechanism for the PD oxidation pathway.

2.3 Conclusions

In summary, we have successfully demonstrated the mechanistic differences between Fleischmann's indirect oxidation and PD oxidation on NiOOH. Deconvoluting the rates of Fleischmann's indirect and PD oxidation for various aldehydes and alcohols revealed that, contrary to the previous belief, alcohols react primarily through the PD mechanism, not Fleischmann's indirect one. Aldehydes, on the other hand, react primarily through Fleischmann's indirect mechanism with aromaticity further enhancing this preference. By determining the average Ni valence as a function of potential during Fleischmann's indirect and PD oxidation, we uncovered that the formation of Ni^{4+} is necessary to enable PD oxidation while Fleischmann's indirect oxidation occurs with Ni^{3+}. We also discovered that the oxidation state of Ni^{4+} changes during PD oxidation, revealing that PD oxidation can also be considered a form of indirect oxidation. The reason that PD oxidation is potential-dependent is not because Ni^{4+} remains as Ni^{4+} during oxidation but rather because the electrochemical regeneration of the catalytically active species (Ni^{4+}) affects the rate and because the reaction of that Ni^{4+} sites requires applied bias to occur, unlike in the case of Fleischmann's potential-independent indirect oxidation where the electrochemical regeneration of the catalytically active species (Ni^{3+}) is not the RDS and no applied bias is required to enable the HAT. Finally, through computational studies, we showed that hydride transfer, which is enabled by the formation of Ni^{4+} and converts that Ni^{4+} to Ni^{2+}, is a plausible dehydrogenation mechanism for PD oxidation. This is distinctly different from Fleischmann's indirect oxidation, which occurs through a turnover limiting HAT to Ni^{3+} sites and thus has a potential-independent rate. This study offers a new and more comprehensive

understanding of oxidative dehydrogenation mechanisms on NiOOH and provides an essential foundation to understand electrochemical alcohol and aldehyde oxidation on oxide and hydroxide-based catalytic electrodes. This clear understanding of the mechanistic differences between Fleischmann's indirect and PD indirect oxidation as well as the substrate dependent preference for oxidation through one pathway or the other will enable a more rational design of electrocatalysts for alcohol and aldehyde oxidation, as it will allow catalyst structure and composition to be tuned to enhance either Fleischmann's indirect pathway or the PD indirect pathway based on which one is favored by a given substrate. Furthermore, the new electrochemical procedure reported in this study will allow us to conduct quantitative investigations of the effects of various solution conditions (e.g. pH, concentrations of substrates, supporting electrolytes) on the rates of Fleischmann's indirect oxidation and PD indirect oxidation as well as how those effects vary across different substrate types.

2.4 Experimental Section

2.4.1 Materials.

All chemicals used were commercially available and were used without further purification. Acetaldehyde (≥99.5%, Sigma Aldrich), ethanol (≥99.5%, Sigma Aldrich), benzyl alcohol (>99%, MP Biomedicals, LLC), benzaldehyde (≥99.5%, Sigma Aldrich), butanol (99.8%, Sigma Aldrich), Butyraldehyde (≥99.5%, Sigma Aldrich), furfural (99%, Sigma Aldrich), furfuryl alcohol (98%, Sigma Aldrich), potassium hydroxide (≥85%, Sigma Aldrich), $Ni(NO_3)_2 \cdot 6H_2O$ (99%, Acros), KNO3 (99%, Alfa Aesar). Deionized water (Barnstead E-pure water purification system, resistivity >18 MΩ cm) was used to prepare all solutions.

2.4.2 $Ni(OH)_2$ Electrode Preparation.

The thin α-$Ni(OH)_2$ films used for the rate deconvolution experiments were prepared through a well-established synthesis technique in which nitrate is electrochemically reduced, raising the local pH at the working electrode (WE) and causing $Ni(OH)_2$ to precipitate out to form a $Ni(OH)_2$ film on the WE.[26] This reaction was controlled using an SP-200 potentiostat/EIS (BioLogic Science Instrument) and was conducted with a 3-electrode setup in a single compartment cell made of glass using a fluorine doped tin oxide (FTO) working electrode (WE), Pt counter electrode, and Ag/AgCl (4 M KCl) reference electrode (RE). The FTO WE's were prepared by cutting larger FTO plates into 2.5 cm x 1 cm strips, attaching Cu tape to the top to provide electrical contact, and masking the FTO with Teflon tape with a 0.5 cm^2 hole punched in it. The Pt counter electrodes were prepared by sputter coating a 20 nm Ti adhesion layer followed by 100 nm of Pt on precleaned glass slides. The thin $Ni(OH)_2$ films used for LSVs and the rate deconvolution experiments were deposited from an aqueous plating solution of 10 mM $Ni(NO_3)_2 \cdot 6H_2O$ and 30 mM KNO_3 by galvanostatically maintaining a current of -0.25 mA/cm^2 for 45 s. The resulting $Ni(OH)_2$ films were then rinsed with >18 MΩ cm water and dried with an air stream. Thicker $Ni(OH)_2$ films used for the electrolyses were prepared though the same method, however, the exposed FTO area was larger (3.2 cm^2) and the galvanostatic current was maintained for 12 minutes.

2.4.3 Electrochemical Experiments.

Linear sweep voltammetry (LSV) was performed with a 3-electrode setup in an undivided cell made of glass. $Ni(OH)_2$ films were used as the WE, Ag/AgCl as the RE and Pt as the CE. The potential was swept from the open circuit in the positive direction at a scan rate of 10 mV/s. Electrolyses were performed in a sealed, divided cell and employed the same 3-electrode setup as

was used for the LSVs. The pH 13 KOH alcohol or aldehyde solution was added to the WE compartment while pH 13 KOH was added to the CE compartment. 0.55 V vs Ag/AgCl was maintained potentiostatically until 33.3% of the charge required for the full conversion of alcohol or aldehyde into the carboxylic acid was passed. An exception to this is that for the much more concentrated 200 mM EtOH and 200 mM butanol solutions 6.5% of the charge required for full conversion was passed. We chose to pass only a portion of the charge required for full conversion when conducting these electrolyses to ensure that the results provided a more accurate reflection of the selectivities and Faradic efficiencies that would have been present during the rate deconvolution experiments, as those were conducted at a substrate concentration equal to the concentrations at the beginning of the electrolyses. Additionally, doing so minimized the risk that any of the aldehydes would undergo degradation during the course of a longer electrolysis in the highly alkaline reaction solution. For the 200 mM EtOH and 200 mM butanol solutions, the smaller 6.5% of charge was used to keep the electrolysis times comparable across the different solutions.

2.4.4 Product Analysis.

Quantification of electrolysis products and evaluation of the geminal diol component of the aldehydes was achieved via ^{1}H NMR spectroscopy using a Bruker Avance III 400 MHz NMR spectrometer. NMR samples were prepared by adding 0.450 mL of the electrolysis solution and 0.050 mL of D_2O with 12.5 mM of a dimethyl sulfone internal standard to an NMR tube and shaking vigorously. NMR analyses were conducted with a relaxation delay of 30 s and using a WATERGATE method with excitation sculpting to remove the background signal due to the water solvent. Product quantification was performed by comparing the product integrations in the post electrolysis solutions to those in a standard of known concentration.

2.4.5 ICP-MS.

$Ni(OH)_2$ films were deposited and subjected to a 2 cycle CV in pH 13 KOH according to the methods laid out above to ensure that the samples used for ICP were in the same state as those used for the rate deconvolution experiments. These films were then dissolved in 10 mL of 1 wt% nitric acid (Fisher Chemical, TraceMetal Grade) in a polypropylene centrifuge tube. Three samples were prepared for ICP analysis, one with 2 films dissolved, one with 3 films dissolved, and one with 4 films dissolved. Standard solutions containing 0, 50, 100, 200, 350, 500, and 750 ppb Ni in 1 w% nitric acid were prepared to construct a calibration curve. The standards and samples were analyzed using inductively coupled plasma optical emission spectrometry (ICP–MS) (Shimadzu ICP Mass Spectrometer-2030) and the Ni concentration in the samples used to determine the average Ni per film. The linearity of a plot of the mol Ni in the samples as a function of number of films dissolved was assessed to confirm the deposition described above resulted in only a minor variance of Ni from film to film. All containers and pipet tips used to prepare the ICP samples were washed with 10wt% nitric acid prior to use to remove any trace metal ions on them.

2.4.6 Computational Methods.

All calculations were performed using DFT in the computational chemistry package Quantum-ESPRESSO.[28,29] The core electrons were described with norm-conserving pseudopotentials,[30,31] and a kinetic energy cutoff of 80 Ry was used for the planewaves. The solvent was modeled using the self-consistent continuum (SCCS) method implemented in the Environ module[29,32] of Quantum Espresso. In this method, the solute cavity is determined from the electronic density of the atomistic system, and the solvation contribution to the energy is computed by solving the Poisson equation self-consistently with the Kohn-Sham equations. A dielectric

constant of 78.3 was used to simulate water as the solvent. For charged systems, a neutralizing background charge was included to ensure a neutral supercell.

The $Ni_xO_yH_z$ catalyst was represented with two-layer slabs derived from the (0001) facet of β-NiOOH. All geometry optimizations of these slabs were performed with Γ-point calculations using the PBE functional[33] with a Hubbard *U* correction[34,35] of 6.6 eV[36] applied to Ni. For the $Ni_xO_yH_z$ slabs, the top layer of Ni, O, and H atoms, together with any molecular adsorbates, were optimized with no constraints, while the atoms of the second layer were fixed at the positions found in bulk Ni(O)(OH). Single point calculations were performed on these geometry-optimized slabs using the hybrid PBE0 functional,[37,38] the Brillouin zone being sampled by a 4-by-4 (for slabs containing 4 Ni atoms in each layer) or 2-by-2 (for slabs with 8 Ni atoms in each layer) k-point Monkhorst-Pack grid for the in-slab dimensions. The cell dimension was set to 40 Å in the surface-normal direction to minimize unphysical interactions between slabs. For molecular species such as acetaldehyde, geometry optimizations were performed with Γ-point calculations using the PBE0 functional.[37,38] A cube of 20 Å was used as the unit cell, and optimizations were performed without constraints.

2.4.7 Rate Deconvolution Procedure.

Before being used for the 3-step rate deconvolution experiment each thin $Ni(OH)_2$ film was used as the WE for 2 CVs in a pH 13 KOH solution to ensure that the deposition had occurred correctly and that the $Ni(OH)_2$/NiOOH peak had the normal shape and position. After this, the $Ni(OH)_2$ film was transferred to a single-cell sealed container made of glass with a 3-electrode setup. The $Ni(OH)_2$ film was used as the WE, Ag/AgCl as the RE, and platinum mesh as the CE. The cell was filled with 30 mL of a pH 13 alcohol or aldehyde solution. For most alcohols/aldehydes tested the concentration was 10 mM, however, for butanol and EtOH 200 mM

was used because at 10 mM the indirect rate was too slow to be accurately measured. Additionally, pH 13 was chosen rather than pH 14 for these experiments to limit the risk of aldehyde degradation under highly alkaline conditions affecting our results and to minimize potential interference from water oxidation, which is more competitive with alcohol/aldehyde oxidation at pH 14. This solution was stirred rapidly throughout the rate deconvolution experiment to mimic the conditions during an electrolysis, minimize mass transport induced limitations on the current, and to allow us to model the alcohol/aldehyde concentration at the surface of the electrode as constant for the purpose of the kinetics equations. The same stir speed was used for every substrate and was selected to be sufficiently fast such that for all the substrates tested, further increasing the stir speed no longer resulted in a noticeable increase to current.

For step one of the rate deconvolution procedure, 0.55 V vs Ag/AgCl was applied for long enough for the current to stabilize to a steady state value (typical 20 s). At this point the NiOOH film has achieved a steady state composition and the observed current is all caused by turnover due to alcohol/aldehyde oxidation rather than being due in part to oxidation of the original $Ni(OH)_2$ film. We chose 0.55 V vs Ag/AgCl for this measurement because this was one of the most positive potentials we could apply before the onset of significant water oxidation. This allowed us to achieve the highest rates of alcohol/aldehyde oxidation we could without water oxidation significantly lowering the Faradic efficiency (FE) toward their oxidation.

During the second step, the potential was no longer applied and the film was allowed to sit in the stirred solution under open circuit conditions. During this time the NiOOH film acts as a chemical oxidizing agent reacting with alcohol/aldehyde in solution through the indirect process and thus loses positive charge stored in it during the first step. The length of this step was varied from trial to trial to collect a dataset showing the disappearance of charge from the NiOOH film

over time. For each solution data points were collected at 0.1, 0.3, 0.7, 1, 1.5, 2, 3.5, 5, and 7 seconds under open circuit conditions. For each time under open circuit conditions, 3 measurements were made using 3 different $Ni(OH)_2$ films (for a total of 27 measurements per organic substrate tested) so the results could be averaged. These relatively short times stirring under open circuit conditions were chosen because our goal was to determine the instantaneous rate of disappearance of positive charge at 0 s (when the film is in the same state as it is during an electrolysis) and these short times stirring under open circuit conditions are when the film is in a state most similar to the one in which it would be under applied bias.

The third, reductive step was conducted in two parts. In the first part, the potential was rapidly swept at a scan rate of 1 V/s from open circuit to 0 V vs Ag/AgCl. Then, in the second part, the potential was held at 0 V for 20 s. This two-part process of a rapid reductive sweep followed by holding the potential was employed rather than just stepping the potential to 0 V and holding it because we found that simply stepping the potential resulted in a slight undermeasurement of the charge stored in the film. This was determined by comparing the charge passed in this reductive step in a pH 13 KOH solution with the charge that corresponds to the area under the cathodic peak of the $NiOOH/Ni(OH)_2$ couple in a CV obtained in pH 13 KOH. We believe this is due to a slight lag between when the potential was stepped and when the potentiostat begins recording the current, resulting in a small amount of the charge passed going uncounted. By splitting the reductive step into the 2-part sweep-and-hold this issue was avoided and the total charge passed across these two parts matched closely with the area under the cathodic peak of the $NiOOH/Ni(OH)_2$ couple in a CV in pH 13 KOH. The magnitude of the total charge passed during this two-part reductive step in the presence of an alcohol/aldehyde after a given time stirring at open circuit is the measured value of the charge still stored in the NiOOH film after the length of time chosen in step 2 for the

film to sit at open circuit. However, before averaging this value with the others measured after the same time at open circuit, it was first adjusted according to a calibration procedure described below in section 2.4.8 and it is the averages of these adjusted data points that were used to construct the 1/charge vs time plots shown in **Figure 2.3**. To enable this calibration, immediately after each of the 27 3-step rate deconvolution measurements used to produce a data point (9 different open circuit times with each time measured in triplicate) a separate instance of the 3-step procedure was performed with 0.1 s chosen as the time at open circuit. This means for each organic species tested a total of 54 3-step measurements were performed (27 to produce data points, 27 to calibrate those data points). The calculations used to convert this data set into a rate for the direct and indirect processes will be described below in section 2.4.8.

In addition to the above, there were some other techniques and features of the experiment that we employed to ensure more accurate results that bear further explanation. Regarding the choice of times at open circuit in step 2, we did not collect data at 0 s at open circuit even though this was the time we were most interested in because of a measurement artifact we observed at t = 0 s which resulted in an abnormally high loss of charge from the film when going from 0 s to 0.1 s at open circuit. This same unusually large loss of charge was also observed when the film was tested in a pH 13 KOH solution without alcohol or aldehyde present and thus where the indirect mechanism is not in effect. This is why we concluded that this significant difference in charge passed between 0 s and 0.1 s at open circuit was not due to the indirect process but rather was likely a measurement artifact introduced by suddenly stepping the potential. Therefore, to avoid this measurement artifact biasing our results we did not collect data at 0 s at open circuit and instead used 0.1 s as the lowest time and extrapolated the charge at $t = 0$ from the $1/(Q_{film})$ vs t plot where Q_{film} refers to the charge stored in the NiOOH film.

Regarding film reuse, we observed that repeated cycling of the $Ni(OH)_2$ films between the reduced and oxidized form resulted in a gradual loss of their ability to store charge. This in turn risked biasing the rate deconvolution results as the charge passed in the reductive step was affected not only by the rate of the indirect process but also by the number of previous measurements the film had been used for. To avoid this issue two steps were taken. First, each film was used to measure no more than 3 data points. This limited the extent to which the films could lose the ability to store charge and thus bias our data. The three-measurement limit was chosen based on the empirical observation that at this level of reuse we could still obtain highly linear plots and reproducible results for the rate of the indirect process when collecting multiple datasets for the oxidation of the same substrate. It is possible a greater number of data points can be collected without introducing a significant error into the results, but this would need to be experimentally verified. The second step was the calibration method mentioned above and described below in section 2.4.8.

Regarding reuse of the alcohol/aldehyde solutions, we observed that, at least for alcohols at longer times at open circuit (minutes rather than seconds) a greater amount of charge would be lost from the film during the same time stirring under open circuit conditions in a solution in which more than one film had been tested than in a solution in which the same number of tests had been performed with only a single film. This effect was further exaggerated when films with higher surface areas were used, suggesting that it is tied to a reaction that a newly prepared film undergoes in the solution. It was unclear to what extent this solution effect was present for aldehydes and for the much shorter times stirring at open circuit presented in this paper, but to avoid the possibility of this influencing the results the alcohol/aldehyde solutions were replaced every time a new $Ni(OH)_2$ film was used.

2.4.8 Mathematical adjustment of measured charge values

As described in section 2.4.7, the number of active Ni sites in the $Ni(OH)_2$ films employed in this study can vary slightly from film to film and measurement to measurement (generally decreasing slightly with successive measurements). Therefore, the linearity and accuracy of the 1/charge vs time plots reported could be improved by mathematically adjusting the measured charge stored in the $Ni(OH)_2$ films to account for these differences such that the differences in charge stored in films after different times at open circuit are due only to the changes to reaction time for the indirect process (i.e. time at open circuit) and not due to differences in the initial number of Ni active sites. To enable this adjustment, immediately after performing each measurement for a data point in the rate deconvolution trials, a separate instance of the measurement was performed with 0.1 s as the time at open circuit. This enabled us to adjust the observed charge required to reduce the film in step 3 to the value it would have been had the $Ni(OH)_2$ film started with the average number of active Ni sites. The was done using equation 5 where $Q_{obs}(t)$ is the magnitude of the observed charge required to reduce the film in the rate deconvolution trial after t seconds at open circuit, $Q_{cal}(t=0.1)$ is the magnitude of the charge required to reduce the film during the trial conduced immediately afterward with 0.1 s at open circuit in step 2, $Q_{ave}(t=0.1)$ is obtained by averaging the magnitude of the charge required to reduce all of the films tested in their first trial conducted at 0.1 s at open circuit and $Q_{adj}(t)$ is the adjusted value for the charge required to reduce the film in the third step of the rate deconvolution process after t seconds at open circuit in step 2. It is these $Q_{adj,}(t)$ values that were used to produce all the 1/charge vs time plots shown in **Figure 2.3**.

$$\frac{1}{Q_{\mathrm{adj}}(t)} = \frac{1}{Q_{\mathrm{ave}}(t=0.1)} - \frac{1}{Q_{\mathrm{cal}}(t=0.1)} + \frac{1}{Q_{\mathrm{obs}}(t)} \qquad (5)$$

The derivation for equation 5 can be obtained by noting that for all the organic species tested here, over the timespan of interest the indirect process behaves as if it follows pseudo second order kinetics with respect to charge stored in the $Ni(OH)_2$ films. This gives equation 6, which is the pseudo second order equation expressed in terms of coulombs where $Q_{obs}(t)$ is the magnitude of the charge required to reduce the NiOOH film back to $Ni(OH)_2$ in step 3 of the rate deconvolution procedure after t time stirring at open circuit while Q_o is the charge required to reduce the NiOOH film when it is in its steady state condition under the bias applied in step 1 (i.e. 0s at open circuit).

$$\frac{1}{Q_{obs}(t)} = \frac{1}{Q_o} + k_{obs}t \tag{6}$$

Based on this, we can note that the difference between the actual charge required to reduce the film after t seconds at open circuit ($Q_{obs}(t)$) and the charge that would have been required had the film started with the average amount of active Ni in the steady state condition in step 1 ($Q_{adj}(t)$) is given by equation 7. This equation can then be rearranged to yield equation 4 above.

$$\frac{1}{Q_{adj}(t)} - \frac{1}{Q_{obs}(t)} = \frac{1}{Q_{ave}(t=0.1)} - \frac{1}{Q_{obs}(t=0.1)} \tag{7}$$

We note here though that while this adjustment does result in more linear and, we believe, more precise plots, removing this adjustment would not substantially affect either the slopes or y-intercepts of any of the linear fits for the $1/(Q_{film})$ vs time plots shown in **Figure 2.3**. As such, the absence of this adjustment would not substantially change the results of any of our calculations for the rate for the indirect process nor would it alter any of the conclusions presented in this work.

2.4.9 Measurement of Average Ni valence.

The rate deconvolution procedure outlined above was, with minor modifications, used alongside inductively coupled plasma mass spectrometry (ICP–MS) data to determine the average

Ni valence as a function of potential in various solutions. This was achieved by conducting the same 3 steps outlined above; however, the time at open circuit was held constant at 0.1 s and the potential applied in step 1 was instead varied across the trials. Additionally, the time this potential was held in step 1 was increased to 2 minutes to ensure that even at low applied potentials enough time passed for the catalyst to achieve a steady state composition. The magnitude of the charge passed in the reductive step was observed and compared to the amount of Ni in a film as determined by ICP. This allowed the average valence to be calculated based on the assumption that the reduced film is entirely $Ni(OH)_2$ and that the charged stored in the film after 0.1 s at open circuit is not significantly different than the steady state charge stored in the film while potential is applied. This average valence was calculated with equation 4 (listed in section 2.2.4 and reproduced here for clarity) where Q_E is the magnitude of the adjusted charge passed in the reductive step, n_{Ni} is the average mols of Ni in a film as determined by ICP-MS, and F is Faraday's constant.

$$\langle \text{Ni valence} \rangle = 2 + \frac{Q_E}{n_{Ni}F} \tag{4}$$

The adjustment was carried out through the same procedure as outlined above for the rate deconvolution procedure. After every measurement of the steady state charge stored in a film at a given potential another measurement was immediately conducted with the same film with 0.55 V vs Ag/AgCl applied in step 1. The charge passed in the reductive step of the first of these trials conducted at 0.55 V vs Ag/AgCl for each film was averaged to obtain the average steady state charge stored in a NiOOH film at 0.55 V vs Ag/AgCl, $Q_{ave,0.55V}$. This was used to adjust the observed charge passed at each potential according to eq. 8 where $Q_{adj,E}$ is the adjusted steady state charge stored in the NiOOH film when applying potential E, $Q_{obs,E}$ is the magnitude of the observed charge passed in the reductive step after applying potential E in step 1, and $Q_{obs,0.55V}$ is the observed

magnitude of the charge passed in the reductive step of the trial conducted applying 0.55 V in step 1 after the measurement applying potential *E* in step 1.

$$\frac{1}{Q_{\mathrm{adj},E}} = \frac{1}{Q_{\mathrm{ave,0.55V}}} - \frac{1}{Q_{\mathrm{obs,0.55V}}} + \frac{1}{Q_{\mathrm{obs},E}} \tag{8}$$

2.5 References

1. Bender, M. T.; Yuan, X.; Choi, K.-S. Alcohol oxidation as alternative anode reactions paired with (photo)electrochemical fuel production reactions. Nat. Commun. 2020, 11, 4594.
2. Cha, H. G.; Choi, K.-S. Combined biomass valorization and hydrogen production in a photoelectrochemical cell. Nat. Chem. 2015, 7, 328-333.
3. Lhermitte, C. R.; Sivula, K. Alternative oxidation reactions for solar-driven fuel production. ACS Catal. 2019, 9, 2007–2017.
4. Bajada, M. A.; Roy, S.; Warnan, J.; Abdiaziz, K.; Wagner, A; Roessler, M. M.; Reisner, E. A precious-metal-free hybrid electrolyzer for alcohol oxidation coupled to CO2-to-syngas conversion. Angew.Chem. Int. Ed. 2020, 59,15633–15641.
5. You, B.; Liu, X.; Liu, X.; Sun Y. Efficient H2 evolution coupled with oxidative refining of alcohols via a hierarchically porous nickel bifunctional electrocatalyst. ACS Catal. 2017, 7, 4564–4570.
6. Taitt, B. J.; Nam, D.-H.; Choi, K.-S. A comparative study of nickel, cobalt, and iron oxyhydroxide anodes for the electrochemical oxidation of 5-hydroxymethylfurfural to 2,5-furandicarboxylic acid. ACS Catal. 2019, 9, 660–670.
7. Miao. Y.; Ouyang, L.; Zhou, S.; Xu, L.; Yang, Z.; Xiao, M.; Ouyang, R. Electrocatalysis and electroanalysis of nickel, its oxides, hydroxides and oxyhydroxides toward small molecules. Biosens. Bioelectron. 2014, 53, 428–439.
8. Schäfer, H.-J. Oxidation of organic compounds at the nickel hydroxide electrode. Top. Curr. Chem. 1987, 142, 101–129.
9. Lyalin, B. V.; Petrosyan, V. A. Oxidation of organic compounds on NiOOH electrode. Russ. J. Electrochem. 2010, 46, 1199–1214.
10. Fleischmann, M.; Korinek, K.; Pletcher, D. The oxidation of organic compounds at a nickel anode in alkaline solution. J. Electroanal. Chem. Interfacial Electrochem. 1971, 31, 39-49.
11. Fleischmann, M.; Korinek, K.; Pletcher, D. The kinetics and mechanism of the oxidation of amines and alcohols at oxide-covered nickel, silver, copper, and cobalt electrodes J. Chem. Soc., Perkin Trans. 2 1972, 10, 1396–1403.
12. Kowal, A.; Port, S. N.; Nichols R. J. Nickel hydroxide electrocatalysts for alcohol oxidation reactions: An evaluation by infrared spectroscopy and electrochemical methods. Catal. Today 1997, 38, 483–492.

13. Rahim, M. A. A.; Hameed, R. M. A.; Khalil, M. W. The role of a bimetallic catalyst in enhancing the electro-catalytic activity towards methanol oxidation. J. Power Sources 2004, 135, 42–51.
14. Martín-Yerga, D.; Henriksson, G.; Cornell, A. Effects of incorporated iron or cobalt on the ethanol oxidation activity of nickel (oxy)hydroxides in alkaline media. Electrocatalysis 2019, 10, 489–498.
15. Deng, X.; Kang, X.; Li, M. Xiang, K.; Cheng, W.; Guo, Z.; Zhang, J.; Fu, X.-Z.; Luo, J.-L. Coupling efficient biomass upgrading with H2 production via bifunctional CuxS@NiCo-LDH core– shell nanoarray electrocatalysts. J. Mater. Chem. A 2020, 8, 1138–1146.
16. Sivasakthi, P.; Sangaranarayanan, M. V. Pulse electrodeposited nickel with structure directing agents as an electrocatalyst for oxidation of glycerol. New J. Chem. 2019, 43, 8352–8362.
17. Zhang, W.; Xiong, Z.; Gao, Y.; Gao, H.; Zhang, Y. Roles of the base in the electrocatalytic reactions: A case study of glycine electrooxidation. J. of Electroanal. Chem. 2017, 785, 216–219.
18. Toghill, K. E.; Xiao, L.; Stradiotto, N. R.; Compton, R. G. The determination of methanol using an electrolytically fabricated nickel microparticle modified boron doped diamond electrode. Electroanalysis 2010, 22, 491–500.
19. Francke, R.; Quell, T.; Wiebe, A.; Waldvogel, S. R. Organic Electochemistry: Revised and Expanded Ch. 26 “Oxygen-Containing Compounds” (CRC Press 2016).
20. Vértes, G.; Horányi, G. Some problems of the kinetics of organic compounds at oxide-covered nickel electrodes. J. Electroanal. Chem. Interfacial Electrochem. 1974, 52, 47–53.
21. Robertson, P. M. On the oxidation of alcohols and amines at nickel oxide electrodes: mechanistic aspects. J. Electroanal. Chem. Interfacial Electrochem. 1980, 111, 97–104.
22. Houache, M. S. E.; Hughes, K.; Ahmed, A.; Safari, R.; Liu, H.; Botton, G. A., Baranova, E. A. Electrochemical valorization of glycerol on Ni-rich bimetallic NiPd nanoparticles: insight into product selectivity using in situ polarization modulation infrared-reflection absorption spectroscopy. ACS Sustainable Chem. Eng. 2019, 7, 14425−14434.
23. Kapałka, A.; Cally, A.; Neodo, S.; Comninellis, C.; Wächter, M.; Udert K. M. Electrochemical behavior of ammonia at Ni/Ni(OH)2 electrode. Electrochem. Commun. 2010, 12, 18–21.
24. Görlin, M.; Chernev, P.; Araújo, J. F.; Reier, T.; Dresp, S.; Paul, B.; Krähnert, R. Dau, H. Strasser, P. Oxygen evolution reaction dynamics, faradaic charge efficiency, and the active

metal redox states of Ni–Fe oxide water splitting electrocatalysts. J. Am. Chem. Soc. 2016, 138, 5603–5614.

25. Yu, E. H.; Krewer, U.; Scott K. Principles and Materials Aspects of Direct Alkaline Alcohol Fuel Cells. Energies 3, 2010, 1499–1528.
26. Kang, D.; Kim, T. W.; Kubota, S. R.; Cardiel, A.C.; Cha, H. G.; Choi. K.-S. Electrochemical synthesis of photoelectrodes and catalysts for use in solar water splitting. Chem. Rev. 2015, 115, 12839–12887.
27. Klaus, S.; Cai, Y.; Louie, M. W.; Trotochaud, L.; Bell, A. T. Effects of Fe electrolyte impurities on Ni(OH)2/NiOOH structure and oxygen evolution activity. J. Phys. Chem. C, 2015, 119, 7243–7254.
28. Giannozzi, P.; Baroni S., Bonini; Calandra, M; Car, R.; Cavazzoni, C.; Ceresoli, D.; Chiarotti, G. L.; Cococcioni, M.; Dabo, I.; Corso1, A. D.; Gironcoli, S.; Fabris, S.; Fratesi, G.; Gebauer, R.; Gerstmann, U.; Gougoussis, C.; Kokalj, A.; Lazzeri, M.; Martin-Samos, L.; Marzari, N.; Mauri, F.; Mazzarello, R.; Paolini, S.; Pasquarello, A.; Paulatto, L.; Sbraccia, C.; Scandolo, S.; Sclauzero, G.; Seitsonen, A. P.; Smogunov, A.; Umari1, P.; Wentzcovitch, R. M. QUANTUM ESPRESSO: A modular and open-source software project for quantum simulations of materials. J. Phys.: Condens. Matter 2009, 21, 395502.
29. Giannozzi, P.; Andreussi, O.; Brumme, T.; Bunau, O.; Nardelli, M. B.; Calandra, M.; Car, R.; Cavazzoni, C.; Ceresoli, D.; Cococcioni, M; Colonna, N.; Carnimeo, I.; Corso, A. D.; Gironcoli, S.; Delugas, P.; DiStasio, R. A.; Ferretti, A.; Floris, A.; Fratesi, G.; Fugallo, G.; Gebauer, R.; Gerstmann, U.; Giustino, F.; Gorni, T.; Jia, J.; Kawamura, M; Ko, H.-Y.; Kokalj, A.; Küçükbenli, E.; Lazzeri, M.;Marsili, M.; Marzari, N.; Mauri, F.; Nguyen, N. L.; Nguyen, H.-V.;Otero-de-la-Roza, A.; Paulatto, L.; Poncé, S.; Rocca, D.; Sabatini, R.; Santra, B.; Schlipf, M.; Seitsonen, A. P.; Smogunov, A.; Timrov, I.; Thonhauser, T.; Umari, P.; Vast, N.; Wu, X.; S Baroni Advanced capabilities for materials modelling with quantum ESPRESSO. J. Phys.: Condens. Matter 2017, 29, 465901.
30. Hamann, D. R.; Schlüter, M.; Chiang, C. Norm-conserving pseudopotentials. Phys. Rev. Lett. 1979, 43, 1494-1497.
31. Schlipf, M.; Gygi, F. Optimization algorithm for the generation of ONCV pseudopotentials. Comput. Phys. Commun. 2015, 196, 36–44.

32. Andreussi, O.; Dabo, I.; Marzari, N. Revised self-consistent continuum solvation in electronic-structure calculations. J. Chem. Phys. 2012, 136, 064102.
33. Perdew, J. P., Burke, K. & Ernzerhof, M. Generalized gradient approximation made simple. Phys. Rev. Lett. 1996, 77, 3865–3868.
34. Anisimov, V. I.; Zaanen, J.; Andersen, O. K. Band theory and mott insulators: Hubbard U instead of Stoner I. Phys. Rev. B 1991, 44, 943–954.
35. Anisimov, V. I.; Aryasetiawan, F.; Lichtenstein, A. I. First-principles calculations of the electronic structure and spectra of strongly correlated systems: The LDA + U method. J. Phys.: Condens. Matter 1997, 9, 767–808.
36. Goldsmith, Z. K.; Harshan, A. K.; Gerken, J. B.; Vörös, M.; Galli, G. Stahl, S. S.; Hammes-Schiffer, S. Characterization of NiFe oxyhydroxide electrocatalysts by integrated electronic structure calculations and spectroelectrochemistry. Proc. Natl. Acad. Sci. 2017, 114, 3050–3055.
37. Perdew, J. P.; Ernzerhof, M.; Burke, K. Rationale for mixing exact exchange with density functional approximations. J. Chem. Phys. 1996, 105, 9982–9985.
38. Adamo, C. & Barone, V. Toward reliable density functional methods without adjustable parameters: The PBE0 model. J. Chem. Phys. 1999, 110, 6158–6170.

Chapter 3: Understanding Hydrogen Atom and Hydride Transfer Processes During Electrochemical Alcohol and Aldehyde Oxidation

Portions of this chapter have been adapted from:

Bender, M. T.; Warburton, R. E.; Hammes-Schiffer, S.; Choi, K.-S. Understanding hydrogen atom and hydride transfer processes during electrochemical alcohol and aldehyde oxidation. *ACS Catal.* **2021**, *11*, 15110–15124. DOI 10.1021/acscatal.1c04163

3.1 Introduction

Electrochemical oxidation of alcohols and aldehydes is an important topic with applications not only within the realm of organic synthesis but also as anodic reactions that can be paired with electrochemical and photoelectrochemical water reduction to simultaneously lower energy costs of hydrogen generation while also producing a value-added product at the anode.[1-5] NiOOH is among the most promising electrocatalysts for selectively oxidizing alcohols and aldehydes to carboxylic acids, combining high performance and selectivity, good stability, and low cost.[5-10] As such, understanding the mechanism of alcohol and aldehyde oxidation to carboxylic acid on NiOOH is of great interest.[1,11]

For decades, the electrochemical oxidation of alcohols on NiOOH was understood to proceed through an indirect mechanism proposed by Fleischmann *et al.* (**Scheme 3.1**).[10,12] In this mechanism, NiOOH is first electrochemically generated by oxidizing $Ni(OH)_2$, which is the relevant bulk stoichiometry at open circuit (**Scheme 3.1, step 1**). That NiOOH then acts as a chemical oxidizing agent, oxidizing the alcohol through a rate limiting hydrogen atom transfer of the α-hydrogen to Ni^{3+} sites in NiOOH (**Scheme 3.1, step 3**).[10,12] This reduces the NiOOH back to $Ni(OH)_2$; however, under the applied bias this $Ni(OH)_2$ is then rapidly reoxidized into the active NiOOH state (**Scheme 3.1, step 1**). Fleischmann *et al.* report that after the rate limiting step 3, further oxidation of the organic species to produce carboxylic acid (**Scheme 3.1, step 4**) is fast.[12]

For this mechanism, the applied potential only drives the NiOOH regeneration and does not directly drive alcohol oxidation. Accordingly, the effective overpotential for alcohol oxidation is set by the potential of the $Ni(OH)_2$/NiOOH couple regardless of the actual applied potential because NiOOH serves as a chemical oxidizing agent. Thus, once the potential is sufficient to rapidly oxidize $Ni(OH)_2$ to NiOOH, the rate for alcohol oxidation though this pathway becomes potential independent.[10,12] Although the original studies by Fleishmann *et al.* did not examine

aldehyde oxidation, subsequent works have claimed aldehyde oxidation also proceeds through this mechanism.[9,11,13-14] This is possible because aldehydes in solution will be in equilibrium with their hydrate, a 1,1-geminal diol, which is an alcohol and thus can undergo an identical reaction pathway to the one shown in **Scheme 3.1**.[11,15]

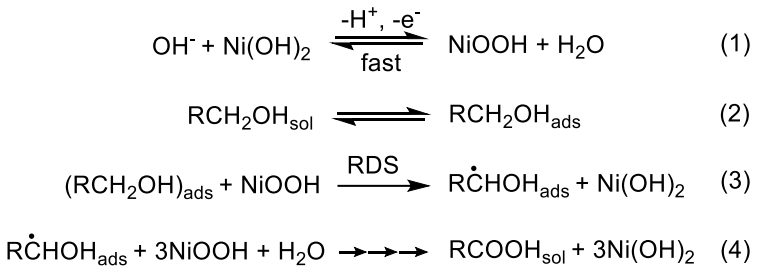

Scheme 3.1. Mechanism proposed by Fleischmann *et al*. for the indirect oxidation of alcohols at NiOOH electrodes in alkaline aqueous media.

When a linear sweep voltammogram (LSV) is recorded, alcohol oxidation through this indirect mechanism results in a characteristic enhancement in the peak associated with oxidation of $Ni(OH)_2$ to NiOOH (**Figure 3.1**). This is because alcohol oxidation consumes NiOOH and generates $Ni(OH)_2$ during the LSV, thereby requiring more current to fully oxidize $Ni(OH)_2$ to NiOOH. The degree of enhancement of this peak is directly related to the rate at which a given alcohol is oxidized by NiOOH during the LSV. However, our recent study using thin NiOOH films, where current profiles were collected with a better resolution, revealed a second, potential dependent, oxidation wave in the more positive potential region in addition to the enhancement of the $Ni(OH)_2$/NiOOH peak (**Figure 3.1**).[11] This second feature cannot be explained by the $Ni(OH)_2$/NiOOH-mediated oxidation depicted in **Scheme 3.1** and therefore indicates there is a second oxidation pathway that competes with the well-known one proposed by Fleischmann *et al*.

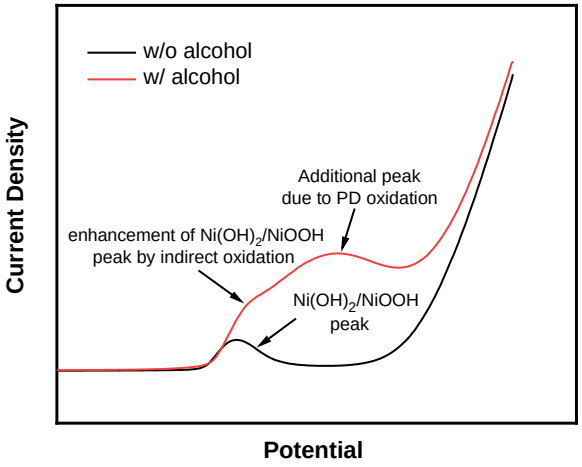

Figure 3.1. Schematic LSVs comparing representative current profiles for a $Ni(OH)_2$ working electrode with (red) and without (black) the presence of an alcohol.

Using an electrochemical rate deconvolution technique we developed, we demonstrated that this second oxidation pathway involves Ni^{4+} as the active site and that its rate is potential dependent.[11] Thus, we refer to the second pathway as potential-dependent (PD) oxidation to distinguish it from the indirect oxidation mechanism proposed by Fleischmann *et al*, which will be referred to as indirect oxidation in this chapter. Using our electrochemical rate deconvolution technique, we also showed that for alcohol oxidation, the PD pathway is dominant while for aldehyde oxidation the indirect pathway is preferred, with aromaticity further enhancing the preference for the indirect pathway.[11] We then proposed hydride transfer from the organic substrate to Ni^{4+} sites in the electrocatalyst as a plausible mechanism for PD oxidation (**Scheme 3.2**).[11] In **Scheme 3.2**, the hydride transfer step is shown in step 4. The electrochemical (re)generation of the Ni^{4+} sites, which is a required step for hydride transfer, is shown in steps 1 and 5. For PD oxidation, the electrochemical (re)generation of the Ni^{4+} sites affects the rate, accounting for the potential dependence.

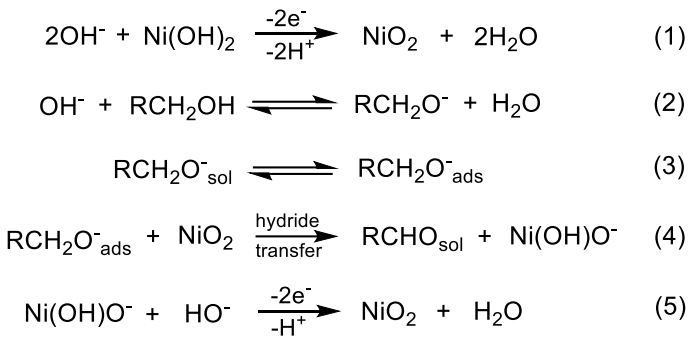

Scheme 3.2. Hydride transfer mechanism we proposed for oxidation of alcohols to aldehydes through the PD oxidation pathway. The oxidation of aldehydes to carboxylic acids proceeds through the same steps because aldehydes in solution are in equilibrium with their hydrate, a 1,1-geminal diol, which is an alcohol.

While the existence of two oxidation pathways has been revealed, our mechanistic understanding for them is currently very limited. As such, identifying key factors that affect the oxidation rates through these two pathways and improving our mechanistic insight into them is vital for properly understanding the process of alcohol and aldehyde oxidation on NiOOH catalysts. The goal of this study is to examine the effect of pH and substrate concentration on these oxidation pathways. Solution pH is an important factor that can influence alcohol oxidation in multiple ways, including affecting the regeneration of Ni^{3+} and Ni^{4+} centers, the deprotonation of alcohols and aldehydes, the equilibrium between aldehydes and their active geminal diol state, and the competition with water oxidation. Thus, developing a clear understanding of the effect pH has on both pathways is of paramount importance in achieving atomic level understanding of the mechanisms. Elucidating the effect of substrate concentration is also critical because different pathways can have different concentration dependences, and, therefore, the major pathway can change in different concentration regions. Furthermore, by examining the effect concentration has on the oxidation rate and the average Ni valence in NiOOH, we can elucidate which mechanistic steps among adsorption, oxidation of the organic species, and catalyst regeneration limit the rate

of the two pathways. We used four different substrates: benzyl alcohol, benzaldehyde, butanol, and butanal, which represent an aromatic alcohol, an aromatic aldehyde, an aliphatic alcohol, and an aliphatic aldehyde, respectively. Using the results obtained from this study, we provide a comprehensive and thorough mechanistic understanding of the two alcohol/aldehyde oxidation pathways available on NiOOH.

2.2 Results and Discussion

2.2.1 pH dependence study.

LSVs obtained with and without 10 mM butanol, butanal, benzyl alcohol, and benzaldehyde in pH 12, 13, and 14 are provided in **Figure 3.2**. To quantitatively examine the impact of pH on the PD and indirect oxidation pathway, rate deconvolution experiments were performed for each organic species at each pH condition at a potential of 1.52 V versus the reversible hydrogen electrode (RHE). To determine the potential vs RHE, the potentials measured verses the Ag/AgCl reference electrodes used in our study were adjusted according to equation 1.

$$E_{RHE} = E_{Ag/AgCl} + 0.197V + 0.0591V*pH \quad (1)$$

A constant potential on the RHE scale was employed so we could compare the oxidation of the compounds at the same overpotential regardless of the pH condition. Specifically, 1.52 V vs RHE was chosen because it provided relatively fast kinetics for alcohol and aldehyde oxidation while still being before the onset of significant oxygen evolution reaction (OER) current (**Figure 3.2**). To confirm that this potential is before the onset of significant OER current we performed potentiostatic electrolyses at pH 14 (the solution condition where OER is most facile) and confirmed that for all four alcohols/aldehydes the Faradic efficiency for alcohol/aldehyde oxidation is ≥95%. We did not examine pH values below 12 because alcohol and aldehyde

oxidation on NiOOH only occurs under alkaline conditions, and at pH values below 12 the rate becomes quite slow.[7-9]

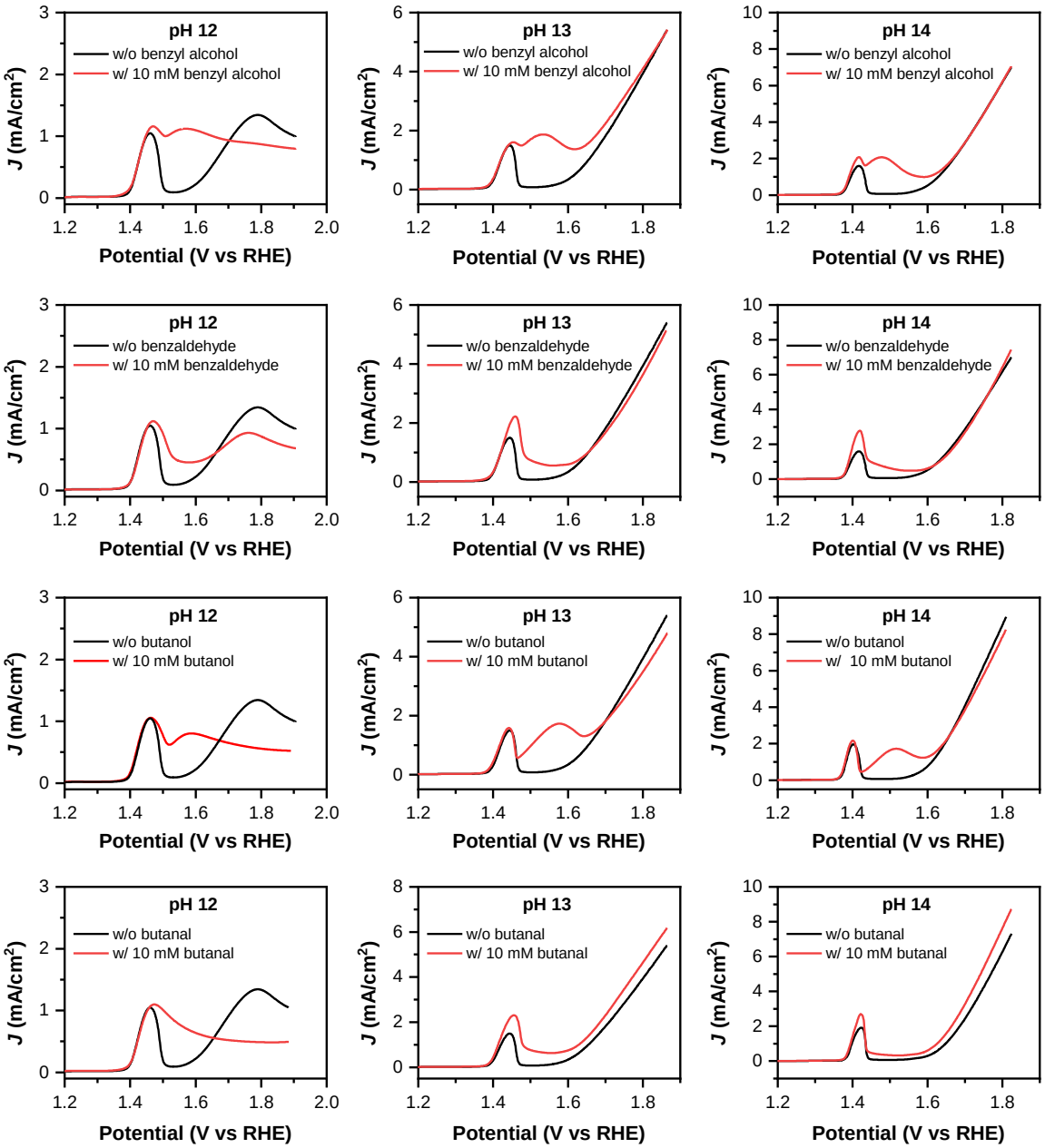

Figure 3.2. LSVs collected at a scan rate of 10 mV/s using a $Ni(OH)_2$ working electrode with (red) and without (black) 10 mM of alcohol/aldehyde in pH 12, 13 and 14 KOH solutions. For the pH 12 solutions, 90mM $KClO_4$ was added as a supporting electrolyte to ensure adequate solution conductivity.

The principles and experimental details of our rate deconvolution method were described in Chapter 2 so we will provide only a brief overview here. In short, our method allows us to measure the change in charge in the NiOOH due to indirect oxidation of any given organic species under open circuit condition, which is directly related to the rate of oxidation of the organic species through the indirect pathway and can be converted to the oxidation current through the indirect pathway at a given applied potential ($I_{indirect}$). Once $I_{indirect}$ is obtained, by subtracting it from the total oxidation current (I_{tot}) the current for PD oxidation (I_{PD}) at the given potential can be obtained (equation 2).

$$I_{\text{tot}} = I_{\text{indirect}} + I_{\text{PD}} \tag{2}$$

For all substrates and conditions tested in this study, the plots of 1/(charge in the film) vs time were linear (**Figure 3.3**). This indicates that within the timeframe of interest, the indirect pathway is behaving as if it is second order with respect to charge in the NiOOH film and allows us to calculate the indirect rate according to the pseudo second order rate law equation shown in equation 3, where k_{obs} is the slope and $Q_{film}(t=0)$ is the reciprocal of the y-intercept of the plots shown in **Figure 3.3**. $Q_{film}(t=0)$ represents the positive charge stored in the NiOOH film and available to oxidize the organic species after 0 seconds at open circuit during the second step of our rate deconvolution experiments (see Chapter 2.4.7 and the experimental section for more details).

$$I_{indirect} = k_{\text{obs}} C_{\text{film}}{}^{2}(t = 0) \tag{3}$$

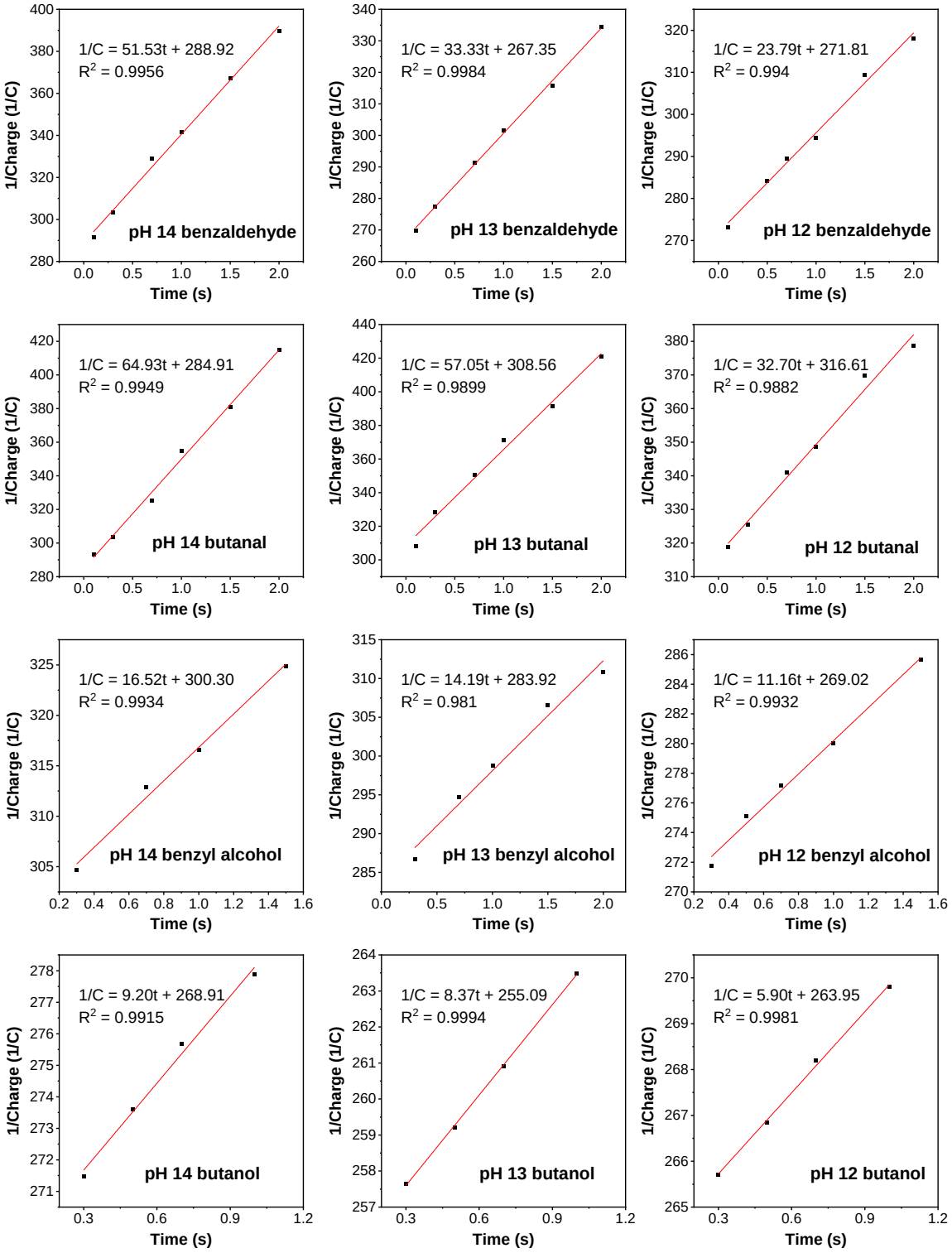

Figure 3.3. 1/Charge vs time plots for rate convolution experiments using 10mM substrate solutions at 1.52V vs RHE in different pH solutions. Charge represents the magnitude of charge required to reduce the films back to $Ni(OH)_2$ in the third step of the rate deconvolution procedure.

We use k_{obs} in equation 3 instead of k to represent the effective rate constant because our solution is rapidly stirred, meaning the organic species is effectively "flooded" and its concentration is included in k_{obs}, i.e., $k_{obs}=k[\text{organic species}]^a$, where *a* is the reaction order with respect to the organic species. Furthermore, we note that while we use a pseudo-second order rate equation to model the kinetics of the indirect pathway, the true rate equation may be more complicated. For our purposes, though, it is not necessary that the reaction truly be second order with respect to charge stored in the NiOOH film, but rather only that this accurately model the behavior in the timespan of interest. The linearity of all the 1/charge vs time plots shown in **Figure 3.3** indicates this is true for all of the substrates and conditions tested here. The results of our rate deconvolution experiments in the different pH conditions are shown in **Figure 3.4**. Using these results, we discuss the effect of pH on PD and indirect oxidation individually.

3.2.2 The effect of pH on PD oxidation.

For alcohol oxidation, the PD pathway shows a strong pH dependence, with more basic conditions significantly enhancing the current for both butanol and benzyl alcohol oxidation (**Figure 3.4**). This is consistent with the mechanism proposed in Chapter 2 for PD oxidation consisting of hydride transfer of an α-hydrogen from the alcohol to Ni^{4+} sites in the NiOOH catalyst. In that mechanism, to enable hydride transfer either the alcohol must have already been deprotonated to form the alkoxide or the hydride transfer must occur in concert with deprotonation of the alcohol group by a hydroxide ion in solution. Either way, the rate of the hydride transfer step would be expected to be faster under more alkaline conditions. Moreover, regeneration of the active Ni^{4+} sites from the $Ni(OH)_2$ formed following hydride transfer requires deprotonation of the $Ni(OH)_2$ by a base in solution and should also occur faster at higher pH. Accordingly, since both

the hydride transfer step and the regeneration of the catalyst are expected to occur faster under more alkaline conditions, the hydride transfer mechanism we proposed for PD oxidation predicts a faster oxidation rate under more basic conditions and is in line with the observed results for the alcohols.

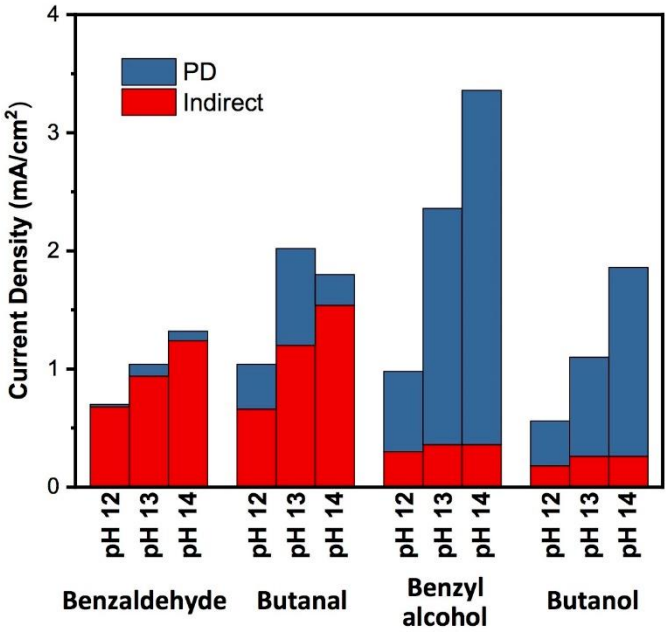

Figure 3.4. The component of the current due to indirect (red) and PD (blue) oxidation of alcohols and aldehydes at 1.52V vs RHE in different pH solutions.

For the oxidation of the aldehydes, the trend observed for PD oxidation is more complicated. For both aldehydes, the predicted enhancement in PD oxidation is observed as the pH is increased from 12 to 13. The trend, however, is broken when the pH is further increased to 14, with both aldehydes showing a decrease in the PD current. To probe this unexpected behavior and determine if it might be tied to the potential we selected for our rate deconvolution experiments, we collected an LSV of 10 mM benzaldehyde in a rapidly stirred pH 14 solution (**Figure 3.5**). That LSV shows the current for benzaldehyde oxidation actually declines as the potential is increased above 1.47V vs RHE. Since this LSV was collected in a rapidly stirred solution this decline in current cannot be attributed to mass transport limitation. Instead, it suggests that

increasing the potential enables a process that inhibits benzaldehyde oxidation. The most likely cause of this inhibition is the increased potential enabling the oxidation of OH^- to form OER intermediates on the Ni^{4+} sites needed for PD oxidation. Because the rate for OER is extremely slow at these potentials, once formed these adsorbed intermediates are long lived and block the Ni^{4+} sites from catalyzing aldehyde oxidation, leading to a decline in the observed current until a sufficiently positive potential is reached to allow for rapid OER. This process would be most severe at pH 14, as the increased OH^- concentration relative to that of the aldehyde would lead to greater difficulty for the aldehyde to outcompete the OH^- for adsorption on active sites.

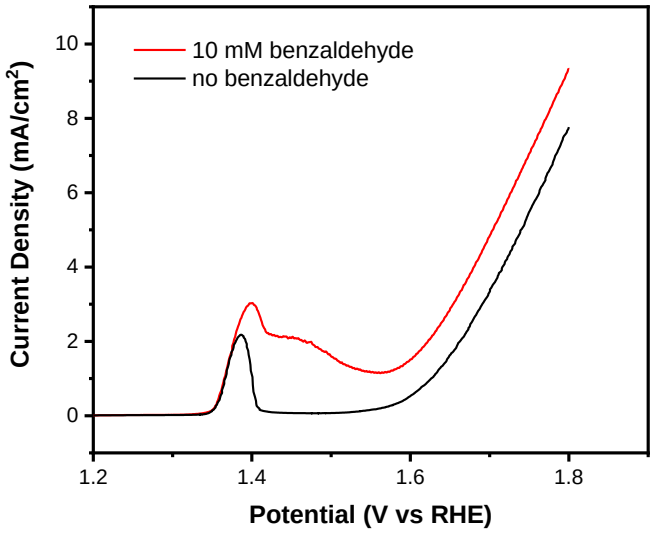

Figure 3.5. Linear sweep voltammograms (LSVs) collected at a scan rate of 10 mV/second in a rapidly stirred pH 14 solution with (red) and without (black) 10mM benzaldehyde.

To further test if the above hypothesis could explain the low PD current for aldehyde oxidation at pH 14, we performed our rate deconvolution experiment for benzaldehyde at a potential of 1.48V vs RHE instead of 1.52 V vs RHE (**Figure 3.6**). As suggested by the LSV, the decrease in applied potential led to a higher oxidation current. Moreover, the rate deconvolution results reveal that the increase in overall current is entirely due to an enhancement of the PD pathway and show that the partial current for PD oxidation at 1.48V vs RHE in pH 14 far exceeds

that at 1.52V vs RHE in pH 13. This suggests that, were it not for competition from OER intermediates for adsorption at Ni^{4+} sites, aldehyde oxidation through the PD pathway at pH 14 would be enhanced relative to its rate at less basic pH values. Furthermore, the fact that increasing the potential in pH 14 to 1.52V vs RHE suppresses only the PD pathway provides further support for our previously reported claim that the indirect and PD pathways occur at two different active sites.[11] The PD pathway requires Ni^{4+} sites to occur and thus is suppressed when OER intermediates form on those sites and prevent adsorption of the organic substrate. Conversely, the indirect pathway occurs without issue on Ni^{3+} sites, which are inactive for OER and do not suffer from OER intermediates undergoing competitive adsorption; thus, no loss of indirect current is observed as the potential is increased.

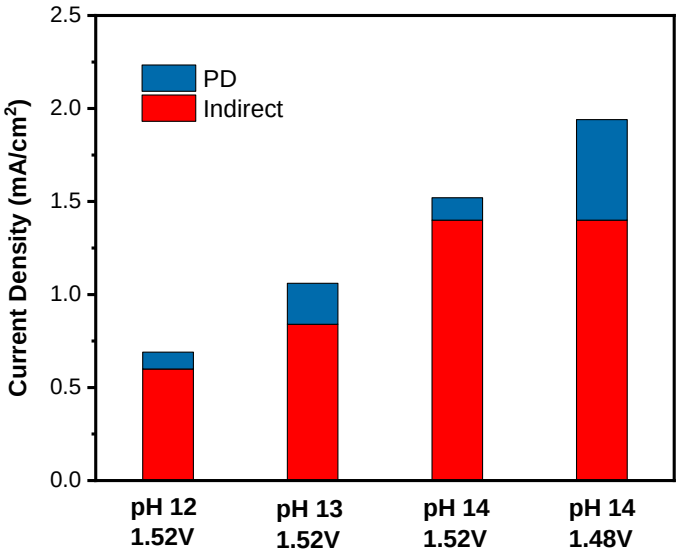

Figure 3.6. The component of the current due to the indirect (red) and PD (blue) pathways for oxidation of 10 mM benzaldehyde solutions at different pHs and potentials.

2.2.3 The effect of pH on indirect oxidation.

Figure 3.4 also provides insight into the pH dependence of indirect oxidation. For the alcohols, there is a small increase in indirect current when the pH is increased from 12 to 13, and

no change when the pH is further increased to 14. The observed minor or no impact of pH on the rate of indirect oxidation of alcohols is consistent with the well-known mechanism proposed by Fleishmann *et al.* because there is no deprotonation involved in the rate limiting HAT step in that mechanism (**Scheme 3.1, Step 3**). Unexpectedly, however, for the aldehydes the rate of indirect oxidation increases considerably as pH increases, suggesting aldehydes and alcohols may not have the same rate determining steps for indirect oxidation.

It is possible that the pH dependence of indirect aldehyde oxidation may stem from the fact that the active form of the aldehyde toward oxidation is not the aldehyde itself but rather the 1,1-geminal diol formed following hydration.[11,15] NMR results show that for benzaldehyde the proportion of molecules existing in the hydrated 1,1-geminial diol state increases significantly as pH increases (**Table 3.1**). Such an increase in the equilibrium concentration of the active species would be expected to increase the rate of indirect oxidation and could explain the observed trend for benzaldehyde. This explanation, however, does not explain the similar trend observed for butanal, as even at pH 12 butanal is entirely hydrated (**Table 3.1**).

	Benzaldehyde % diol	**Butanal % diol**
pH 12	20%	100%
pH 13	65%	100%
pH 14	100%	100%

Table 3.1. The equilibrium percent of benzaldehyde and butanal molecules existing as the 1,1-geminal diol following hydration in pH 12, 13 and 14 solutions. The percentage was determined by comparing the observed ratio of the integration of the aldehyde H peak in the NMR and all the other H peaks with that of the expected ratio (1:5 for benzaldehyde, 1:7 for butanal).

Another possible explanation for the pH dependence is faster regeneration of the active NiOOH species following HAT (**Scheme 3.1, Step 1**). As shown in **Figure 3.7**, the $Ni(OH)_2$/NiOOH couple does not follow ideal Nernstian behavior as pH changes as, if it did, the $Ni(OH)_2$ oxidation peak should appear at the same potential on the RHE scale. This is because, as indicated by equation 1 above, the RHE scale shares the Nernstian shift of -59 mV per pH unit. Instead, **Figure 3.7** shows that under more basic conditions the $Ni(OH)_2$/NiOOH peak shifts cathodically on the RHE scale, meaning that when a fixed potential is applied vs RHE, at higher pH values this provides a greater overpotential relative to the $Ni(OH)_2$/NiOOH couple, which would allow for faster regeneration of NiOOH. As will be discussed more below, this faster regeneration enabled by more basic pH likely plays a role in enhancing the rate of indirect oxidation for butanal and benzaldehyde. It cannot, however, fully explain the observed results because much of the enhancement of the indirect rate as pH increases is attributable to an increase in the pseudo-second order rate constant, k_{obs} (**Figure 3.3**). This substantial increase in k_{obs} as pH increases suggests that the pH-independent HAT may not be the only rate affecting step for aldehyde oxidation through the indirect pathway. Instead, there appears to be a pH-dependent reaction that influences the rate. Such a reaction could, for example, be a deprotonation involving the NiOOH catalyst, which influences the equilibrium abundance of active sites. Alternatively, it could be a reaction involving the organic species in solution, such as conversion of the aldehyde into the 1,1-geminal diol or even deprotonation of that geminal diol to form a more active alkoxide. As none of these possibilities are accounted for by the indirect mechanism proposed by Fleishmann *et al.*[10,12] nor can that mechanism explain the observed pH dependence of the indirect pathway, our results suggest that the understanding provided by this mechanism is incomplete, particularly as applied to aldehydes.

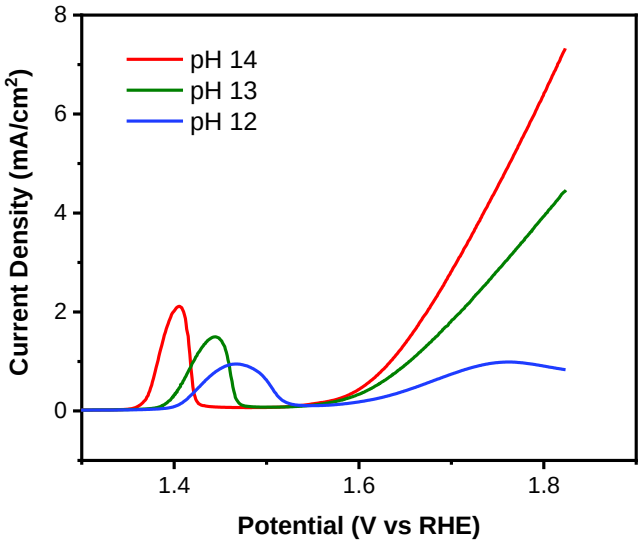

Figure 3.7. LSVs conducted at a 10 mV/s scan rate using a $Ni(OH)_2$ working electrode in a pH 14 KOH (red) pH 13 KOH (green) and pH 12 KOH, 90 mM $KClO_4$ (blue) solution.

2.2.4 Concentration dependence study.

We also explored the impact concentration had on the indirect and PD oxidation pathways. This was achieved by performing rate deconvolution experiments in pH 13 KOH solutions at 1.52V vs RHE for 5, 10, 20, 35, and 50 mM solutions of butanol, benzyl alcohol, butanal, and benzaldehyde. The results of these trials are shown in **Figure 3.8**.

For the alcohols, the rate of indirect oxidation is slow and effectively zeroth order in concentration. In contrast, the PD oxidation rate is relatively fast even at lower concentrations and increases significantly along with concentration for all substrates, except for 50 mM benzyl alcohol where the rate plateaued. As a result, for alcohols the PD pathway is dominant at all concentrations, and the increase in current as concentration increases is almost entirely due to faster PD oxidation.

For the aldehydes, the rate of indirect oxidation is higher than that of PD oxidation at lower concentrations. The rate of indirect oxidation increases only slightly with concentration, and at higher concentrations it either approaches a plateau (butanal) or even decreases (benzaldehyde). In contrast, the rate of PD oxidation increases more significantly with concentration. As a result,

while the indirect pathway dominates at low concentrations, the PD pathway becomes the dominant pathway at higher concentrations.

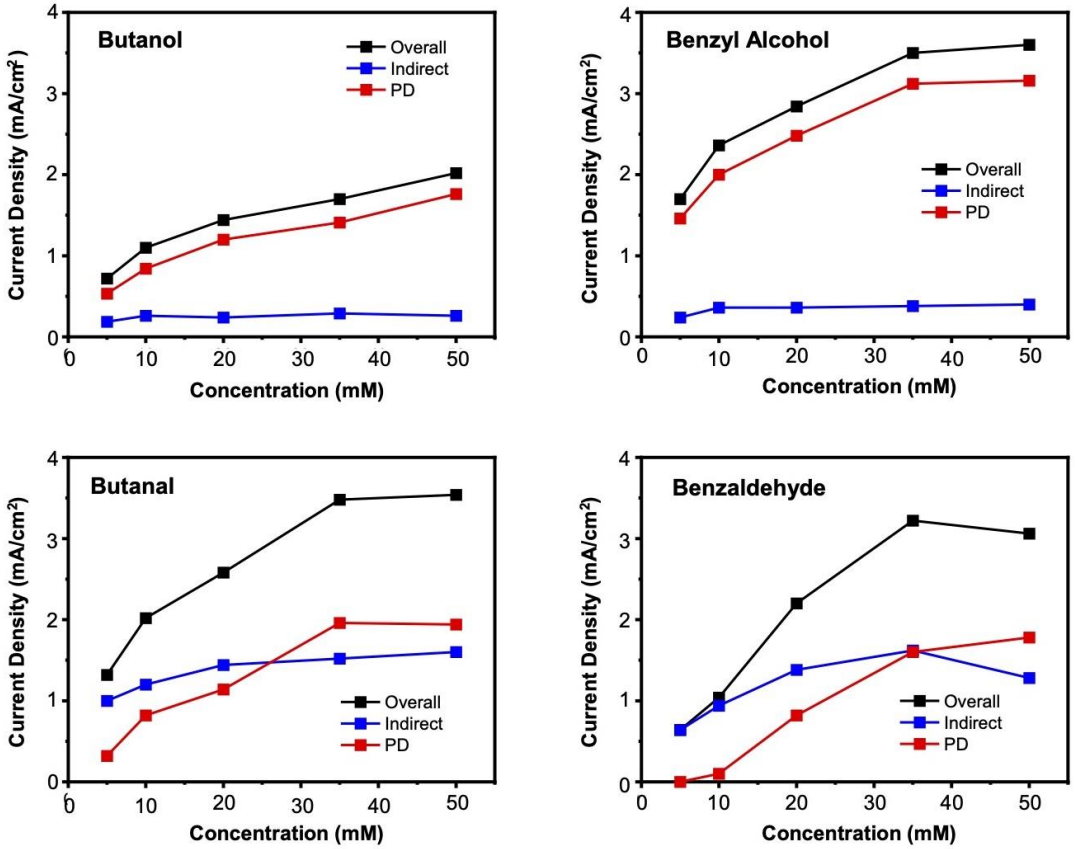

Figure 3.8. Plots depicting the trend in overall current at 1.52 V vs RHE (black) and the partial currents for indirect (blue), and PD (red) oxidation of various organic substrates as substrate concentration is varied in a rapidly stirred pH 13 solution.

In addition to revealing how concentration affects the rate and relative prominence of the two oxidation pathways, a careful analysis of our concentration dependent rate deconvolution results also provides insight into which steps impact the rate of the two pathways. In order to perform this analysis, it is useful to split each mechanism into three general steps that could be limiting the rate: (i) adsorption of the organic species, (ii) the reaction between the adsorbed organic species and the oxidized Ni sites (this includes HAT for the indirect pathway or hydride transfer for the PD pathway), and (iii) regeneration of the oxidized Ni sites. **Scheme 3.3a-c** shows

how current, k_{obs}, and the average steady state Ni valence under applied bias would change as concentration increases for three extreme cases where one of these steps is slow and entirely limits the rate while the other two steps are fast and very thermodynamically favorable.

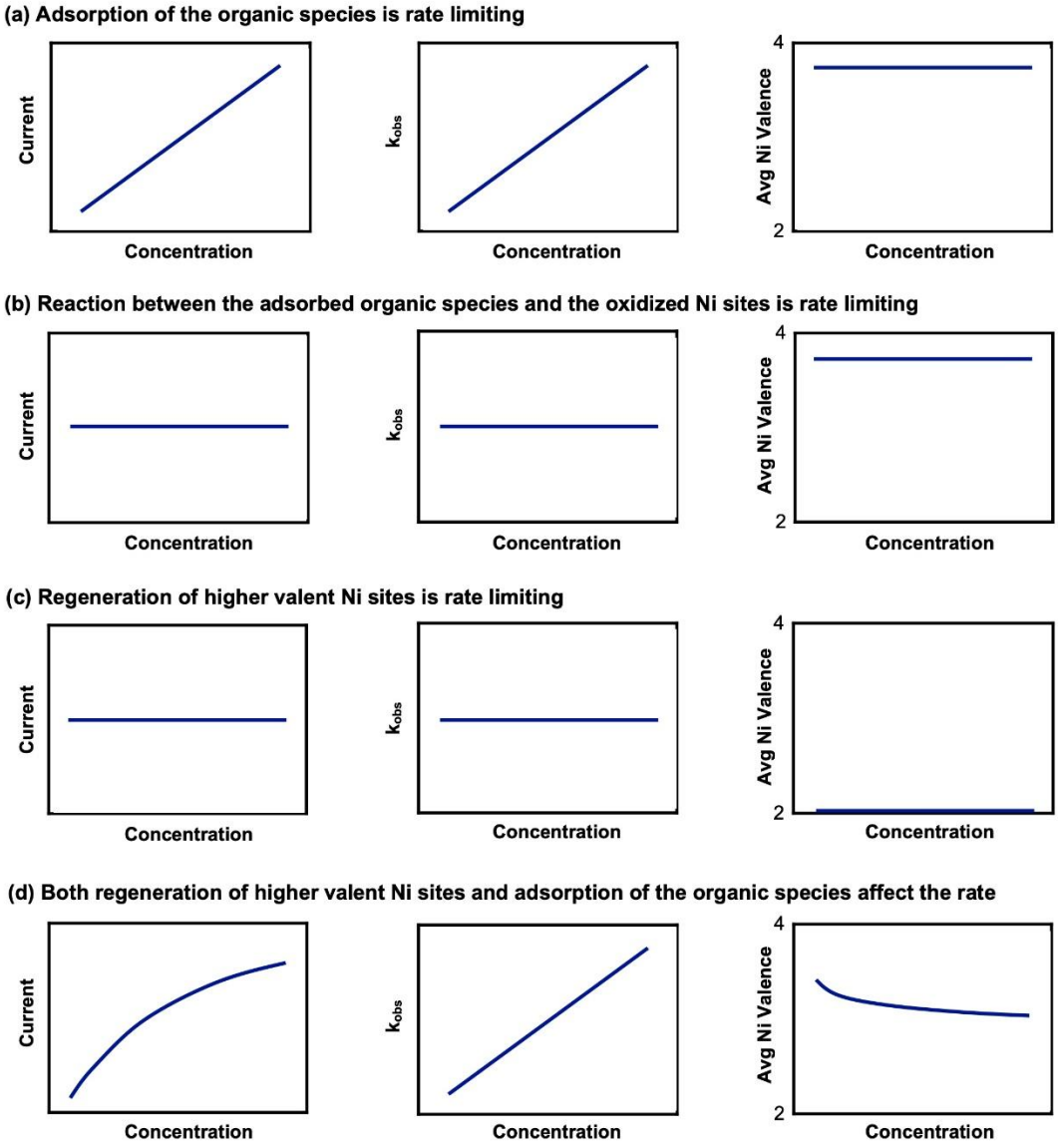

Scheme 3.3. Schemes depicting the relationship between concentration and current, k_{obs}, and the average Ni valence for a pathway (a) when the adsorption step is slow, (b) when the oxidation of the organic species is slow, and (c) when the regeneration step is slow. In all three limiting cases, we have assumed that the other steps are both fast and very thermodynamically favorable. (d) depicts the more moderate case where regeneration is neither exceedingly fast nor exceedingly slow and both it and the adsorption step influence the rate.

Scheme 3.3a depicts a case where the adsorption of the organic species is slow while the other two steps are fast and very thermodynamically favorable. In such a case, we would expect the proportion of catalyst active sites covered with an adsorbed organic species to be low. The rate of the adsorption step would depend on the concentration of the organic species in solution. Accordingly, as the concentration increases, the rate of this rate limiting adsorption step would also increase, resulting in an enhancement in the partial oxidation current through the pathway in question. Since our rapidly stirred solution means the organic species is effectively "flooded" and included in the k_{obs} term, k_{obs} should also increase with concentration. Meanwhile, if adsorption is the slow step, regeneration of the oxidized Ni sites should be fast relative to their consumption, so we would expect the average Ni valence to be as high as when no organic substrate is present (~+3.7 at 1.52V vs RHE in pH 13) and independent of concentration.

Scheme 3.3b depicts a case where the reaction between the adsorbed organic species and the oxidized Ni sites is slow while the other two steps are fast and very thermodynamically favorable. In such a case, the active sites should be saturated with the adsorbed organic substrate. As such, increasing the concentration cannot lead to more adsorbed species and therefore would not increase the reaction rate. Accordingly, we would expect both the partial current through the mechanism in question and k_{obs} to be concentration independent. Furthermore, as was the case for a rate limiting adsorption step, because regeneration of the oxidized Ni sites would be fast relative to their consumption, we would expect a high and concentration independent average Ni valence in this case too.

Finally, **Scheme 3.3c** depicts the case where the regeneration of the oxidized Ni sites is slow while the other two steps are fast and very thermodynamically favorable. In this extreme case, we would not expect to see any meaningful accumulation of charge in the catalyst, as any higher

valent Ni sites would be consumed immediately after formation. Thus, the average Ni valence would remain the Ni^{2+} of $Ni(OH)_2$, and neither the oxidation rate nor k_{obs} would have a concentration dependence because the rate of $Ni(OH)_2$ oxidation should not be affected by the concentration of the organic species. We note that this extreme case cannot be applicable to the 1.52V vs RHE potential condition used in this study (though it may apply in less positive potential regions) because it is clear that at 1.52V vs RHE the film does accumulate positive charge and thus is not entirely $Ni(OH)_2$. Accordingly, should regeneration be limiting the rate, it is not the sole limiting step. Rather, it would determine the rate in balance with one or both of the other steps (**Scheme 3.3d**). In such a case, because regeneration is neither extremely fast nor extremely slow, we would expect the average Ni valence to be significantly higher than the extreme case where regeneration is the sole rate determining step (**Scheme 3.3c**) while still being lower than when no organic substrate is present. Moreover, if either the kinetics or the thermodynamics of the adsorption step are not sufficient to ensure the active sites remain saturated with adsorbed organic species, the average Ni valence will decrease as concentration increases. This is because an increase in concentration would increase the percentage of active sites covered by adsorbed organic species, increasing k_{obs} and thus the rate at which oxidized Ni sites are consumed. The overall rate will also increase, although by a smaller factor than k_{obs} because the loss of some of the active sites as the average Ni valence decreases will partially offset the higher k_{obs} provided by the higher degree of active site coverage.

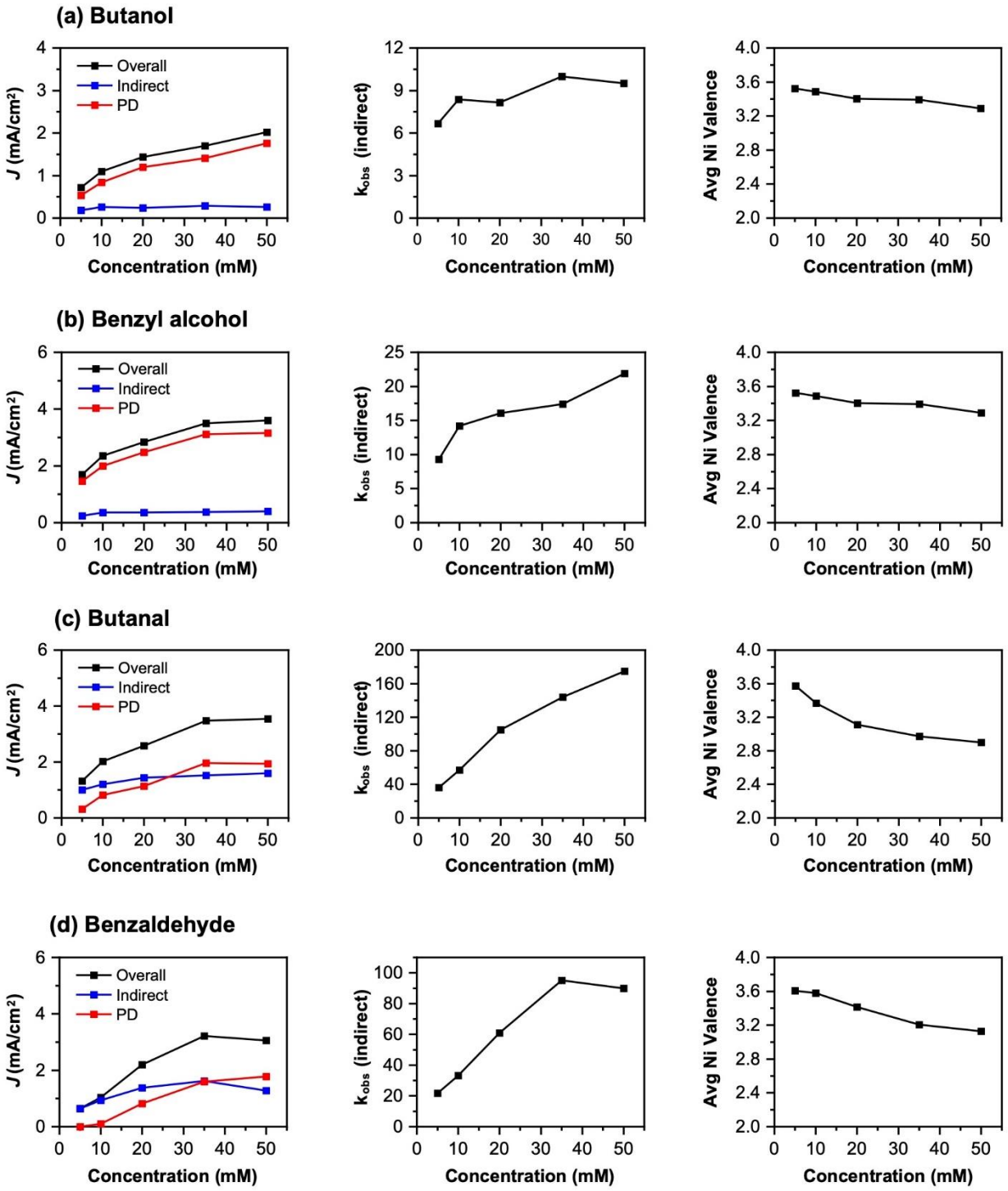

Figure 3.9. Plots depicting the partial current for oxidation through the indirect and PD pathways, k_{obs} for the indirect pathway, and the average steady state Ni valence at 1.52V vs RHE in a rapidly stirred pH 13 solution of differing concentrations of (a) butanol, (b) benzyl alcohol, (c) butanal, and (d) benzaldehyde. For reference, the average Ni valence at 1.52V vs RHE without the presence of an organic substrate is +3.68.[11]

Now that the general behavior expected for a mechanism limited by each of these steps has been outlined, we can look at our experimental data for indirect and PD oxidation of the alcohols and aldehydes to see which cases match best (**Figure 3.9**). For the indirect oxidation of alcohols, our experimental data best matches a case where the reaction between the adsorbed alcohol and the Ni^{3+} sites is the main factor limiting our current (**Scheme 3.3b**). This suggests the coverage of the active Ni^{3+} sites with adsorbed alcohol is high, although the small increases in k_{obs} as concentration increases means this coverage is not complete and is modestly enhanced at higher concentrations, a sign that the adsorption step is playing a minor role in governing the rate. The average Ni valence does decline modestly as concentration increases, which could indicate a rate partially limited by a regeneration step. The average Ni valence, however, is determined not only by the behavior of the indirect pathway but also by that of the concurrently occurring PD pathway. Moreover, because the PD pathway is dominant for alcohols and becomes even faster as alcohol concentration increases, any decline in the average Ni valence as alcohol concentration increases is likely due to the behavior of the PD pathway rather than the indirect one. As will be discussed more below, the observed modest decrease in average Ni valence as concentration increases is better attributed to a regeneration step limiting the rate of the PD pathway rather than the indirect one.

For indirect oxidation of the aldehydes, k_{obs} increases roughly proportionally with concentration. This indicates that the effective rate constant, k_{obs} (which contains concentration terms as noted previously) has a linear (i.e., first order) dependence on the benzaldehyde and butanal concentration. The partial current for indirect oxidation also increases as concentration increases, though by less than the first order dependence on aldehyde concentration suggested by the k_{obs}. This is because, while k_{obs} does increase with aldehyde concentration, the average Ni

valence falls quite a bit, decreasing from initial values of approximately +3.6 at 5mM to values of +2.9 (butanal) and +3.1 (benzaldehyde) at 50 mM. Overall, this is consistent with the mechanistic picture shown in **Scheme 3.3d**, where both the regeneration step and the inability of the adsorption step to ensure the available active sites are fully saturated with adsorbed aldehydes play a role in limiting the rate. The relative weight of each step's influence on the overall rate is determined by the concentration. At low concentrations the proportion of Ni^{3+} sites covered by an adsorbed aldehyde is likely low and regeneration fairly fast relative to the cumulative aldehyde adsorption and oxidation steps. As concentration of the aldehyde increases, k_{obs} increases and gradually levels off at higher concentrations. This plateauing of k_{obs} at higher concentrations is likely due to the active sites becoming saturated with adsorbed organic species such that any further increases in concentration cannot further increase the surface coverage. At these high concentrations, regeneration of the Ni^{3+} sites plays a greater role in limiting the rate, as shown by the decline in the average Ni valence (and thus the number of available active sites).

Evaluating which step limits the PD pathway using our rate deconvolution data is more difficult, since our rate deconvolution method provides a k_{obs} value only for the indirect pathway. Still, some insights can be obtained by looking at the trends in current and average Ni valence. For both the alcohols and the aldehydes, the PD current increases significantly as concentration increases, with the relative impact of concentration on the rate being larger for the aldehydes than for the alcohols. This indicates that for all the species and conditions examined here, the kinetics and/or thermodynamics of the adsorption step are insufficient to fully saturate the active Ni^{4+} sites with adsorbed organic species. This limits the rate of the PD pathway, with the relative size of the impact being larger for the aldehydes than for the alcohols, suggesting the proportion of Ni^{4+} sites covered with an adsorbed organic species is lower for the aldehydes than for the alcohols. This is

consistent with the hypothesis laid out above in the pH dependence section that in order to undergo the PD pathway, the substrates must outcompete hydroxide ions in solution for adsorption on Ni^{4+} sites, and that aldehydes struggle more than alcohols to win this competition.

In addition to the importance of the adsorption step, the decline in the average Ni valence as concentration increases for both alcohols and aldehydes indicates that the rate of regeneration of the Ni^{4+} sites is not extremely fast. As noted previously, interpreting the average Ni valence data can be ambiguous, since it is affected by the rate of both the indirect and PD pathways. In the case of the alcohols, however, because the PD pathway is so dominant and the indirect current does not increase with concentration, we can be confident that the decline in the average Ni valence as concentration increases is primarily due to the PD pathway consuming Ni^{4+} sites more quickly and that the regeneration of those sites is not exceedingly fast. For the aldehydes, because as concentration increases both the indirect and PD pathway are enhanced and contribute significantly to the overall current, we cannot say with certainty that enhancement of the PD pathway is contributing to the decline in the average Ni valence. Given, however, the large size of the decline in the average Ni valence and the fact that at higher concentrations the PD currents for butanal and benzaldehyde are roughly comparable to that of butanol, it seems likely that at higher concentrations regeneration of Ni^{4+} sites is also not exceedingly fast for the aldehydes and that this step also plays a role in limiting the current.

Overall, our concentration dependence rate deconvolution results obtained at 1.52V vs RHE indicate that for indirect alcohol oxidation the rate is primarily limited by the reaction between the adsorbed alcohols and Ni^{3+} sites. This is in agreement with the well-known mechanism proposed by Fleischmann *et al.* shown in **Scheme 3.1**.[10,12] In contrast, for indirect oxidation of aldehydes, a balance between the adsorption step and the regeneration step is

important in governing the rate, with higher concentrations increasing the percentage of the active sites covered with an adsorbed aldehyde and thus enhancing the importance of the regeneration step. Notably, neither of these steps involves the HAT considered to be rate limiting in Fleischmann *et al.*'s proposed mechanism for the indirect pathway, which helps explain the unexpected increase in the indirect oxidation rate as pH was increased that we described above for the aldehydes. For the PD oxidation of both alcohols and aldehydes, both the regeneration of Ni^{4+} sites and the inability of the adsorption step to maintain a high degree of coverage of the available Ni^{4+} sites with adsorbed organic species play a role in determining the rate. Whether or not the reaction between the adsorbed organic species and the oxidized Ni sites also plays a role in determining the rate of PD oxidation could not be determined from these experiments because the rate deconvolution experiments do not provide a k_{obs} for PD oxidation. However, the kinetic isotope effect (KIE) experiments discussed below reveal that for benzyl alcohol this step also affects the rate of PD oxidation while for benzaldehyde it does not.

2.2.5 KIE experiments.

In order to verify and supplement the conclusions from the concentration dependence study, we also performed kinetic isotope effect (KIE) experiments comparing the oxidation of benzyl alcohol with benzyl-α,α-d_2 alcohol and benzaldehyde with benzaldehyde-α-d_1. LSVs taken in pH 13 KOH with 10 mM of the deuterated and undeuterated compounds show that the LSVs for benzaldehyde are identical regardless of whether the aldehyde position is occupied by protium or deuterium (**Figure 3.10a**). Conversely, there is a clear suppression of the current for benzyl-α,α-d_2 alcohol relative to that for benzyl alcohol (**Figure 3.10b**).

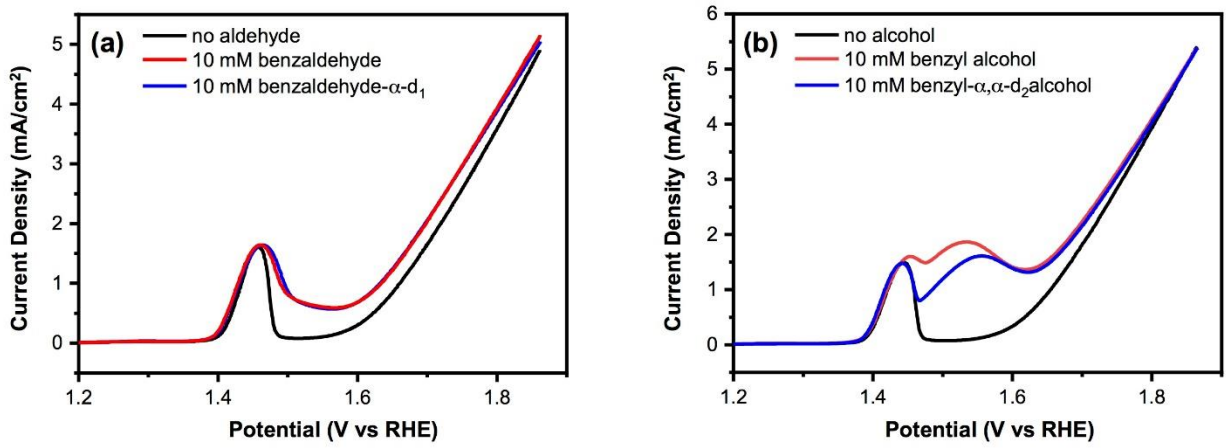

Figure 3.10. LSVs comparing the current in pH 13 solutions without (black) and with 10mM of normal (red) and deuterated (blue) (a) benzaldehyde and (b) benzyl alcohol. Scan rate 10 mV/cm^2.

We also performed rate deconvolution experiments at 1.52V vs RHE for pH 13, 10 mM solutions of benzyl-α,α-d_2 alcohol and benzaldehyde-α-d_1. The resulting 1/charge vs time plots are shown in (**Figure 3.11**) while the partial currents for indirect and PD oxidation are shown in (**Figure 3.12**). For benzaldehyde, substituting protium for deuterium at the aldehyde position produces no KIE and has no significant impact either pathway's rate. Moreover, there is no significant change in k_{obs} or the average Ni valence (33.3 and +3.58 for benzaldehyde versus 31.3 and +3.59 for benzaldehyde-α-d_1). These results agree with the identical LSVs seen in **Figure 3.10**.

These results augment the conclusions drawn through the concentration dependence study. Because we do not observe a KIE for indirect aldehyde oxidation, we can conclude that it is rate limited by a combination of the adsorption step and the regeneration of higher valent Ni sites, neither of which would be expected to result in a KIE. We similarly did not observe suppressed PD current for oxidation of benzaldehyde-α-d_1; instead, our KIE experiments suggest that hydride transfer from the adsorbed benzaldehyde to the Ni^{4+} sites is fast relative to the other steps and thus does not limit the rate of PD oxidation. Thus, we can conclude that the PD oxidation pathway for aldehydes is also rate limited by a combination of the adsorption and regeneration steps.

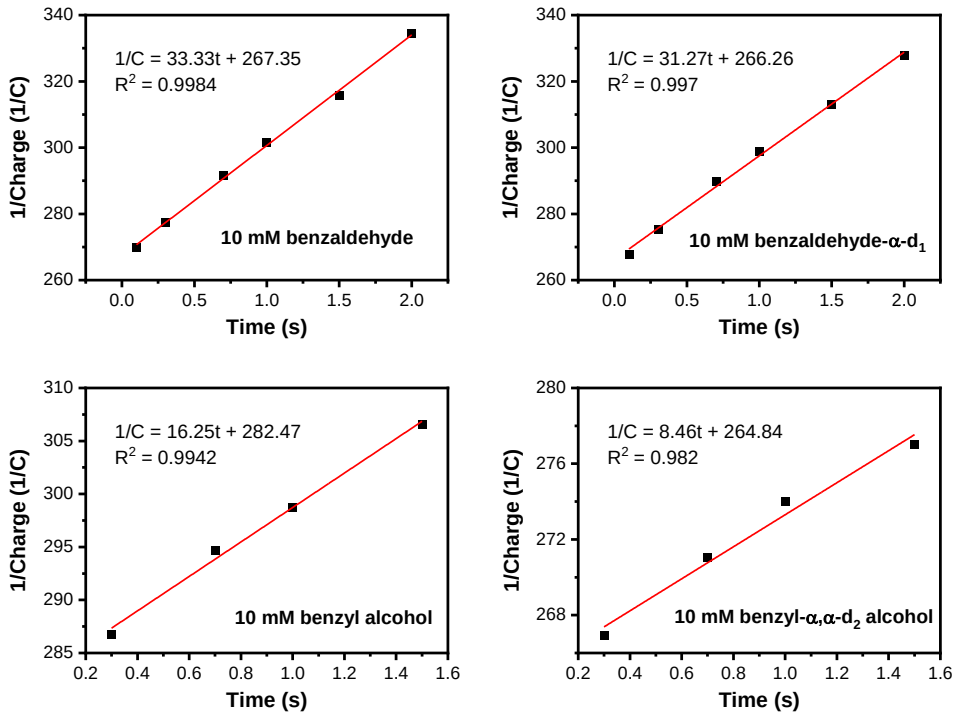

Figure 3.11. 1/Charge vs time plots for rate convolution experiments with normal and deuterated benzyl alcohol and benzaldehyde in a pH 13 solution. In all cases the potential applied in step 1 of the rate deconvolution procedure was 1.52V vs RHE.

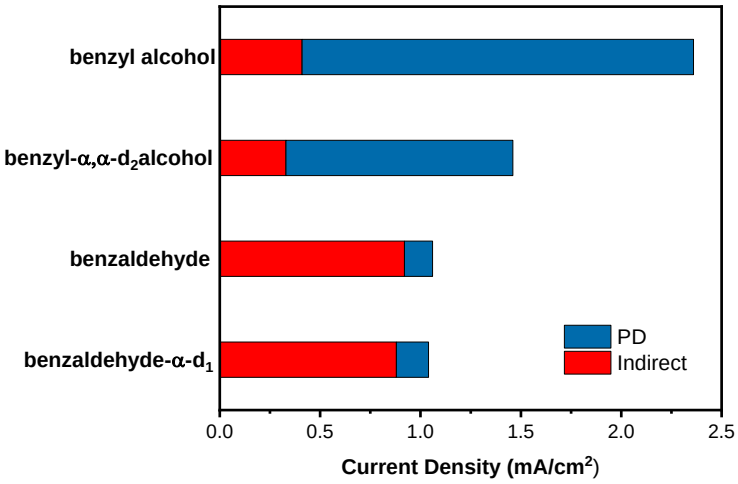

Figure 3.12. The component of the current due to the indirect (red) and PD (blue) pathways when oxidizing rapidly stirred pH 13 solutions of 10mM normal and deuterated benzyl alcohol and benzaldehyde at 1.52V vs RHE.

For benzyl alcohol, the results in **Figure 3.12** show a significantly slower rate of PD oxidation following D substitution, with I_H/I_D = 1.7. The KIE observed for the PD pathway confirms that, unlike for benzaldehyde, the reaction between the adsorbed benzyl alcohol and the Ni^{4+} sites does limit the current. Moreover, it indicates that the rate limiting step in this oxidation reaction involves breaking the C-H/D bond at the alpha position, which is consistent with our proposed hydride transfer mechanism. Furthermore, it is worth noting that the decrease in the PD oxidation current following deuterium substitution occurs despite the average steady state Ni valence in the presence of benzyl-α,α-d_2 alcohol (+3.59) being higher than the average Ni valence in the presence of normal benzyl alcohol (+3.49). This means that benzyl-α,α-d_2 alcohol has a lower current despite having more Ni^{4+} sites available for the PD oxidation reaction. This in turn means that the ratio of the turnover rate of the active Ni^{4+} sites in the presence of benzyl alcohol vs benzyl-α,α-d_2 alcohol is greater than the observed ratio of 1.7 for I_H/I_D. Overall, our combined concentration dependence and KIE experiments indicate that all three steps (adsorption, the reaction between the adsorbed species and Ni^{4+} sites, and regeneration of Ni^{4+} sites) play a role in controlling the current for benzyl alcohol oxidation through the PD pathway. More discussions that can help clarify how that can be the case will be provided in section 3.2.6 below.

For indirect oxidation of benzyl alcohol, we observe only a minimal KIE of I_H/I_D = 1.2. This result at first appears to contradict our conclusion from the concentration dependence study that the reaction between the adsorbed alcohol and the oxidized Ni sites is rate determining and also with Fleishmann et al.'s proposed mechanism that HAT of the hydrogen at the α position is the rate limiting step.[10,12] Our result can be understood, however, by looking not just at how the deuterium substitution affects the current but also how it affects k_{obs} for the indirect pathway and the average Ni valence. With normal benzyl alcohol, k_{obs} is 16.3 and the average Ni valence is

+3.49. These are notably different than the values observed for benzyl-α,α-d_2 alcohol, which has a k_{obs} of only 8.5 (giving a k_H/k_D of 1.9) but a higher average Ni valence of +3.59. This means that, as expected, substitution of H for D at the alpha position does significantly lower the rate constant for the oxidation reaction between the adsorbed benzyl alcohol and the NiOOH catalyst. However, the more considerable decrease in k_{obs} does not result in a correspondingly large decrease in the actual indirect rate because, as noted above, the D substitution also significantly lowers the rate of PD oxidation, which is in competition with indirect oxidation, resulting in a higher steady state average Ni valence and thus more available active sites for indirect oxidation. In other words, were the indirect pathway to be considered in isolation, its rate would indeed be substantially inhibited by the deuterium substitution. In reality, however, the KIE on indirect oxidation, a minor oxidation pathway for benzyl alcohol, is affected considerably by the KIE on the dominant PD oxidation pathway.

2.2.6 Factors determining the rate of PD oxidation

Our combined concentration dependence and KIE experiments indicate that all three steps (adsorption, the reaction between the adsorbed species and Ni^{4+} sites, and regeneration of Ni^{4+} sites) play a role in controlling the current for benzyl alcohol oxidation through the PD pathway. The following discussion can help clarify how that can be the case. PD oxidation occurs at Ni^{4+} sites and first requires the benzyl alcohol to adsorb at those sites before oxidation can occur. Moreover, this adsorption step occurs in competition with hydroxide adsorption at those same Ni^{4+} sites. Knowing this, we can express the rate of PD oxidation with equation 4, where I_{PD} is the partial current for PD oxidation, N_{Ni4+} is the total number of Ni^{4+} sites, θ is the fraction of Ni^{4+} sites with an adsorbed alcohol, and TF is the average turnover frequency of the Ni^{4+} sites with an adsorbed alcohol.

$$I_{PD} = (TF)(N_{Ni4+})\theta \quad (4)$$

Improving the adsorption step will increase θ, leading to a greater coverage of the Ni^{4+} sites available in the catalyst and thereby increasing I_{PD} (assuming the other two terms remain the same). Improving the rate of the reaction between the adsorbed organic species and oxidized Ni sites will increase TF, which also increases I_{PD}. Finally, increasing the rate of the regeneration step will cause more Ni^{4+} sites to exist under steady state conditions, increasing N_{Ni4+} and thereby increasing I_{PD}. In considering the effects of these steps, however, it also is necessary to consider what effect increasing the rate of one of the steps will have on the other terms in equation 4. If the adsorption step is improved, leading to an increase in θ, this will cause Ni^{4+} sites to be reduced at a faster rate, while the driving force for regenerating those Ni^{4+} sites remains the same. As a result, there will be fewer Ni^{4+} sites available in the steady state (a lower N_{Ni4+}), meaning I_{PD} will not increase by as much as would be predicted by the change in θ alone. Moreover, should the change in θ be due to a difference in the adsorption energy, this could also affect the energetics of the subsequent reaction steps and lead to a change in TF. Similarly, in the case where there is a faster reaction between the adsorbed alcohol and the Ni^{4+} sites, the increase in TF will be accompanied by both a decrease in N_{Ni4+} (for the same reasons discussed for improved adsorption) and a decrease in θ. The decrease in θ is because the faster reaction between the Ni^{4+} sites and the adsorbed alcohol causes a decrease in the average lifetime of the Ni^{4+} sites with an adsorbed alcohol, while the average lifetime of Ni^{4+} sites with an adsorbed hydroxide remains unchanged. As a result, under steady state conditions a greater proportion of the Ni^{4+} sites will have an adsorbed hydroxide rather than an adsorbed alcohol. Because of this accompanying decrease in N_{Ni4+} and θ, an increase in TF will also not increase I_{PD} by as much as might first be thought.

2.2.7 Competition between PD oxidation and OER on Ni^{4+}.

As noted earlier, our rate deconvolution results from the aldehydes in pH 14 suggest that the rate of PD oxidation can be inhibited by OER intermediates blocking the Ni^{4+} sites. Moreover, the fact that this inhibition was observed only for the aldehydes and not for the alcohols suggests that the aldehydes may adsorb more weakly on Ni^{4+} sites and thus might be more easily outcompeted by OH^- for adsorption on those sites than the alcohols. This would be consistent with the results from the concentration dependence study outlined above suggesting that, in general, alcohols have a higher degree of surface coverage and the rate of their oxidation is less controlled by an adsorption step. The fact that PD oxidation is dominant for alcohols at all concentrations but is favored for aldehydes only at high concentrations led us to hypothesize that the ability of an organic substrate to outcompete OER intermediates for adsorption on Ni^{4+} sites may be a key predictor for that substrate's tendency to undergo PD oxidation. Alcohols, which appear to adsorb more strongly, may be capable of winning this competition at all concentrations and thus always have a large PD component. Aldehydes, on the other hand, appear to adsorb more weakly and may not be able to outcompete OH^- for access to the Ni^{4+} sites until higher concentrations.

In order to test this hypothesis, we performed computational experiments to compare the adsorption strength of benzyl alcohol and benzaldehyde on a NiOOH surface with an average valence of +3.25.

2.2.8 Density Functional Theory Calculations.

To gain further mechanistic insight into these experimental findings, we performed periodic density functional theory (DFT) calculations to evaluate the adsorption energetics of alcohol and aldehyde substrates, as well as subsequent hydride transfer steps. Undercoordinated Ni sites are hypothesized to play a role in the PD oxidation mechanisms. We therefore performed

these calculations on a NiOOH($01\bar{1}5$) slab model, which contains undercoordinated Ni sites in the surface layer.[16-17] Concomitant with the oxidizing conditions required for PD oxidation, we also removed some surface H atoms to introduce Ni^{4+} sites into the slab model. Although the NiOOH electrodes used in the experimental measurements are polycrystalline, this model is used to establish trends in the reactivity of alcohol and aldehyde substrates on these materials. As described further in the Methods section, total energies were obtained from single-point calculations with the hybrid PBE0 functional using geometries optimized using the PBE+*U* functional.

The molecular substrates for the benzyl alcohol and phenylmethanediol (geminal diol form of benzaldehyde) oxidation reactions were optimized on a NiOOH($01\bar{1}5$) slab using periodic DFT. Since these reactions occur in alkaline media (pH 12–14), the relevant reference states for the adsorption energy calculations are the deprotonated forms of benzyl alcohol (benzyl alkoxide, denoted BO^-) and phenylmethanediol (phenylmethane-ol-alkoxide, denoted $PMOOH^-$). Benzyl alcohol is slightly less acidic (pK_a = 15.4) than water (pK_a = 14),[18] but the pK_a value of phenylmethanediol has not been measured experimentally. We calculated the relative pK_a values of phenylmethanediol and benzyl alcohol at the PBE0 level of theory and estimate that phenylmethanediol is ~5.4 pK_a units more acidic (i.e., the estimated pK_a value is ~10). The adsorption energies $\Delta E_{ads,X*}$ were calculated using equation 5:

$$\Delta E_{ads,X*} = E_{[X*]^0} - E_{[*]^+} - E_{X^-} \quad (5)$$

where $E_{[X*]^0}$, $E_{[X*]^+}$, and E_{X^-} are the energies of the anion X^- adsorbed on the NiOOH slab, the bare NiOOH slab with a single added positive charge, and the X^- molecule in dielectric continuum solvent, respectively. The $E_{[X*]^0}$ and $E_{[X*]^+}$ values were determined from the calculated periodic

DFT energies. The E_{X^-} values were determined relative to E_{OH^-} using the charge-neutral protonated molecules along with the experimentally measured and DFT computed pK_a values. This procedure accounts for the over-stabilization of BO^- in solution, as indicated by the under-estimation of the benzyl alcohol pK_a at the PBE0 level of theory; however, we note that the relative reactivity between BO^- and $PMOOH^-$ is the same if DFT energies are used directly for E_{X^-}.

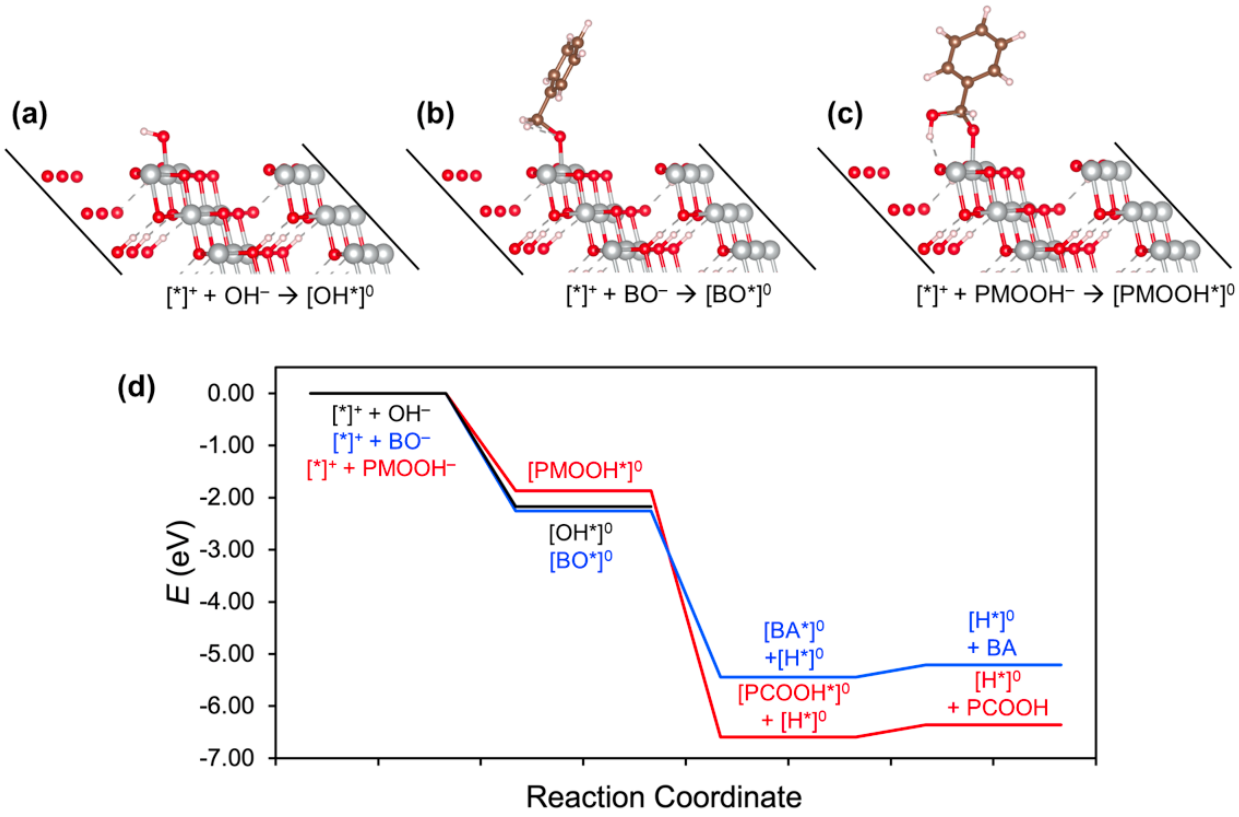

Figure 3.13. (a–c) Converged geometries for adsorbed (a) hydroxyl (OH*), (b) benzyl alkoxide (BO*), and (c) phenylmethane-ol-alkoxide (PMOOH*) on NiOOH($01\bar{1}5$) slab. (d) Energies associated with adsorption, hydride transfer, and desorption for these systems.

Figure 3.13a-c shows the optimized configurations of OH^-, BO^-, and $PMOOH^-$ adsorbed on oxidized NiOOH($01\bar{1}5$), as well as the energetics of adsorption and substrate oxidation. The BO^- and $PMOOH^-$ adsorption energies are –2.26 eV and –1.61 eV, respectively. This difference most likely arises because the second OH group in $PMOOH^-$ can act as an electron

withdrawing group, stabilizing the negative charge on $PMOOH^-$ through inductive withdrawal. As a result, $PMOOH^-$ is more stable in solution than BO^-, as suggested by the lower pK_a of phenylmethanediol. The finding that adsorbed BO^- (BO*) is 0.65 eV more stable than adsorbed $PMOOH^-$ (PMOOH*) suggests that it is much more facile for the anionic substrates to adsorb to NiOOH during alcohol oxidation than during aldehyde oxidation. We identified similar trends when performing these calculations starting with a neutral NiOOH($01\bar{1}5$) slab model (**Figure 3.14**). Moreover, the results in **Figure 3.13d** show that the adsorption energy of BO^- (–2.26 eV) is similar to that of OH^- (–2.17 eV). These similar adsorption energies suggest that BO^- could displace OH* intermediates involved in OER, whereas $PMOOH^-$ is unlikely to do so.

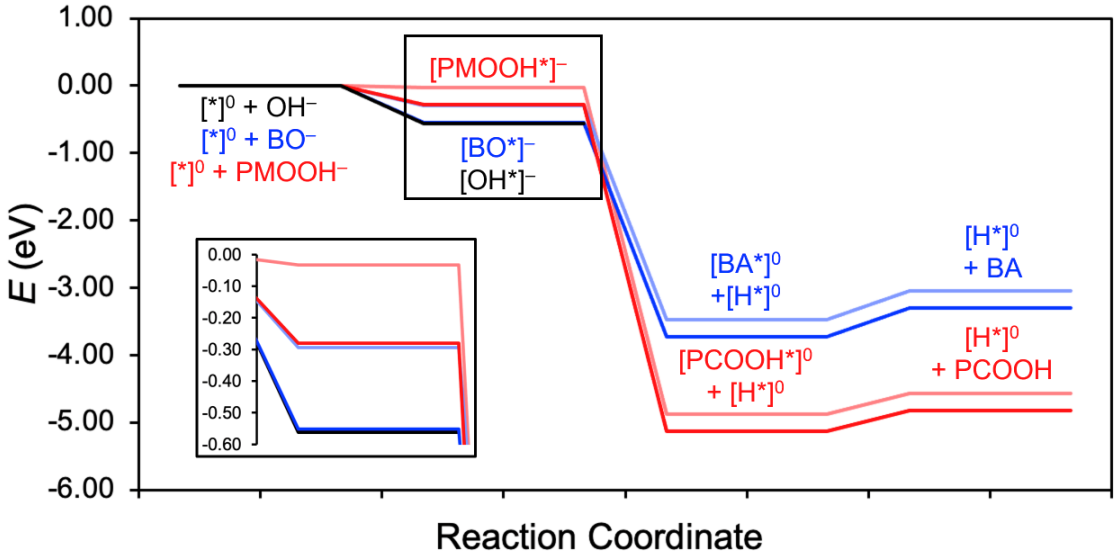

Figure 3.14. DFT calculated energy diagram for adsorption and oxidation of BO^- and $PMOOH^-$ starting on a neutral NiOOH($01\bar{1}5$) slab. The adsorption energies calculated using DFT energies for the solvated anions are shown in light red and blue, whereas the diagram utilizing pK_a-corrected energies are shown in bolder shades of red and blue. The inset shows a closer view of the adsorption energy step (boxed in the energy diagram) to show the splitting between the different data series.

Following adsorption, hydride transfer to surface oxygen sites is downhill in both the alcohol and aldehyde oxidation pathways (**Figure 3.13d**). This hydride transfer converts BO* into benzaldehyde (denoted BA*) and PMOOH* into benzoic acid (denoted PCOOH*). Desorption of these oxidized products is modestly uphill, by 0.21 eV for BA* and 0.23 eV for PCOOH*. We note that these numbers reflect the differences in DFT energies and that the free energy of solution-phase molecules should be decreased further because of higher entropy compared to their surface-bound analogues.[19] Moreover, PCOOH* is likely to be deprotonated under the alkaline conditions of the experiments given the relative acidity of carboxylic acids compared to alcohols. We find that desorption of benzoate is similarly uphill in energy by 0.08 eV, suggesting that either the protonated or deprotonated form may desorb after it is formed. Overall, these computational results suggest that hydride transfer should be thermodynamically favorable from either adsorbed species.

An important finding is that deprotonated geminal diols such as $PMOOH^-$ adsorb more weakly than alkoxides such as BO^- and may not effectively compete with OER intermediates such as OH^- at the Ni^{4+} sites required for PD oxidation. During PD aldehyde oxidation, the coverage of PMOOH* is likely to be low, limiting the rate of hydride transfer. Following desorption of the product, the catalytic cycle is closed when hydrogen transferred from the organic species to NiOOH is removed as a proton by OH^- in solution (**Scheme 3.2, step 5**) and Ni^{4+} sites are regenerated. This dependence on Ni^{4+} site regeneration, in combination with the substrate surface coverage effects between alcohol and aldehyde oxidation, support the experimental mechanistic assumptions outlined above and lend further insights into the difference in reactivity of alcohols and aldehydes in PD oxidation mechanisms on NiOOH materials.

3.3 Conclusion

In summary, our study offers a comprehensive understanding of the effects of pH and concentration on electrochemical alcohol and aldehyde oxidation on NiOOH. An increase in pH strongly promotes the PD oxidation of alcohols. It can also promote PD oxidation of aldehydes, but only in the potential region where OER intermediates do not form. In the potential region where such intermediates do form, aldehydes, unlike alcohols, cannot effectively compete with the OER intermediates for adsorption at the Ni^{4+} sites critical for PD oxidation, leading to a suppression of the PD pathway. This conclusion was supported by computational results indicating that deprotonated geminal diols adsorb more weakly than alkoxides. Since an increase in pH promotes OER, it leads to a suppression of PD oxidation for aldehydes when applying potentials that allow for the formation of OER intermediates. The indirect oxidation of alcohols appears to show no pH dependence, agreeing with the mechanism proposed by Fleishmann *et al* where the rate limiting HAT step involves no deprotonation. However, the indirect oxidation of aldehydes shows a strong pH dependence, suggesting that the pH-independent HAT may not be the only rate affecting step for indirect aldehyde oxidation. Instead, there appears to be a pH-dependent reaction that influences the rate of indirect oxidation. Such a reaction may involve conversion of aldehydes to a more reactive form or may be a deprotonation step affecting the steady state abundance of active sites in the NiOOH catalyst.

The results obtained from concentration-dependence studies along with the KIE experiments also enabled us to elucidate the rate determining steps for alcohol and aldehyde oxidation for both the indirect and PD pathways. For the indirect oxidation of alcohols, our experimental results suggest the reaction between the adsorbed alcohol and Ni^{3+} sites is the main step limiting the current. On the other hand, for indirect oxidation of aldehydes, a balance between an adsorption step and a catalyst regeneration step mainly limits the current. For the PD oxidation

of alcohols, the rate is controlled by the interplay between all three steps (adsorption step, hydride transfer, and regeneration of Ni^{4+} sites), whereas for the PD oxidation of aldehydes, the rate is controlled only by the balance between the adsorption and regeneration step. Overall, this work adds significantly to our understanding of the mechanism of alcohol and aldehyde oxidation on NiOOH surfaces, a highly important class of reactions.

3.4 Experimental Section

3.4.1 Materials.

All chemicals used were commercially available and were used without further purification. Benzyl alcohol (>99%, MP Biomedicals, LLC), benzaldehyde (≥99.5%, Sigma Aldrich), butanol (99.8%, Sigma Aldrich), Butyraldehyde (≥99.5%, Sigma Aldrich), potassium hydroxide (≥85%, Sigma Aldrich), $Ni(NO_3)_2 \cdot 6H_2O$ (99%, Acros), KNO_3 (99%, Alfa Aesar), $KClO_4$ (≥99%, Sigma Aldrich). Deionized water (Barnstead E-pure water purification system, resistivity >18 MΩ cm) was used to prepare all solutions.

3.4.2 $Ni(OH)_2$ Electrode Preparation.

Amorphous α-$Ni(OH)_2$ films were prepared through an established technique in which nitrate is electrochemically reduced, raising the local pH at the working electrode (WE) and causing $Ni(OH)_2$ to precipitate out to form a $Ni(OH)_2$ film.[20] This reaction was controlled using an SP-200 potentiostat/EIS (BioLogic Science Instrument) and was conducted with a 3-electrode setup in a single compartment glass cell using a fluorine doped tin oxide (FTO) working electrode (WE), Pt counter electrode (CE), and Ag/AgCl (4 M KCl) reference electrode (RE). The FTO WE's were prepared by cutting larger FTO plates into 2.5 cm x 1 cm strips, attaching Cu tape to

the top to provide electrical contact, and masking the FTO with electroplating tape (3M Company) with a 0.5 cm^2 hole punched in it. The Pt counter electrodes were prepared by sputter coating a 20 nm Ti adhesion layer followed by 100 nm of Pt on precleaned glass slides. The $Ni(OH)_2$ films were deposited from an aqueous plating solution of 10 mM $Ni(NO_3)_2 \cdot 6H_2O$ and 30 mM KNO_3 by galvanostatically maintaining a current of -0.25 mA/cm^2 for 45 s. The resulting $Ni(OH)_2$ films were rinsed with >18 MΩ cm water and dried with an air stream.

3.4.3 Electrochemical Experiments.

Linear sweep voltammetry and electrolyses were performed with a 3-electrode setup in an undivided glass sealed cell. $Ni(OH)_2$ films were used as the WE, Ag/AgCl as the RE and Pt mesh as the CE. For the LSVs, the potential was swept from the open circuit in the positive direction at a scan rate of 10 mV/s. The electrolyses were performed by applying 1.52V vs RHE potentiostatically to a rapidly stirred alcohol or aldehyde solution until the stochiometric charge required for 25% (benzyl alcohol, butanol, benzaldehyde) or 12.5% (butanal) conversion of the starting substrate to carboxylic acid had been passed. The lower charge passed used for butanal was to allow the electrolysis to be completed more quickly due to concerns about the long-term stability of the butanal in the pH 14 solution. We chose to pass only a portion of the charge required for full conversion when conducting these electrolyses to ensure that the results would accurately reflect the selectivities and Faradic efficiencies present during the rate deconvolution experiments, which were conducted at substrate concentration equal to the concentrations at the beginning of the electrolyses and to decrease the chance of aldehyde degradation during longer reaction times at pH 14. The pH of all solutions used for our electrochemical experiments was adjusted using KOH, and for pH 12 solutions 90mM $KClO_4$ was added as a supporting electrolyte.

2.4.4 Product Analysis.

Quantification of electrolysis products and evaluation of the geminal diol component of the aldehydes was achieved via ^{1}H NMR spectroscopy using a Bruker Avance III 400 MHz NMR spectrometer. NMR samples were prepared by adding 0.450 mL of the electrolysis solution and 0.050 mL of D_2O with 12.5 mM of a dimethyl sulfone internal standard to an NMR tube and shaking vigorously. NMR analyses were conducted with a relaxation delay of 30 s and used a WATERGATE method with excitation sculpting to remove the background signal of the water solvent. Product quantification was performed by comparing the product integrations of the post electrolysis solutions to those of standards of known concentration.

2.4.5 Rate Deconvolution Procedure.

A detailed explanation of our three-step rate deconvolution procedure is provided in Chapter 2.4.7; however, a brief description and overview of the process will be provided here along with specification of a few experimental details that were different in this study. The procedure was performed with 30 mL of rapidly stirred alcohol or aldehyde solution in a single-cell sealed cell with a 3-electrode setup. The WE was a thin $Ni(OH)_2$ film deposited through the procedure detailed above, the RE was Ag/AgCl, and the CE was platinum mesh. Prior to use for the rate deconvolution experiments, each $Ni(OH)_2$ film was tested using cyclic voltammetry (CV) (2 cycles starting at OCP and with switching potentials of 1 V vs Ag/AgCl and 0 V vs Ag/AgCl (pH 12), 0.9V vs Ag/AgCl and 0 vs Ag/AgCl (pH 13), or 0.8V vs Ag/AgCl and 0V vs Ag/AgCl (pH 14) to confirm the $Ni(OH)_2$/NiOOH peak and water oxidation behavior of each film were consistent.

In the first step of the three-step procedure, 1.52V vs RHE was applied potentiostatically to the WE in a rapidly stirred solution for long enough for the current to stabilize to a steady state value (typical 30 s). This converts the film into the steady state condition it would be in during a potentiostatic electrolysis at 1.52V vs RHE and during this step both the indirect and PD oxidation pathways are active. During the second step, the potential is no longer applied and the film is allowed to sit in the stirred solution under open circuit conditions. During this time neither the PD pathway nor reoxidation of $Ni(OH)_2$ can occur as both require potential, however, the indirect pathway, which proceeds through a chemical (rather than electrochemical) HAT step still occurs, reducing higher valent Ni sites back to $Ni(OH)_2$. During the third step, the remaining higher valent sites still left after step 2 are rapidly reduced back to $Ni(OH)_2$ by sweeping the potential from open circuit to 0 V vs Ag/AgCl at a scan rate of 1V/s and then holding the potential at 0V for 20 s. The magnitude of the charge passed during this third, reductive step corresponds to the amount of charge that was still stored in the film after some of it was used to oxidize the organic substrate through the indirect pathway in step 2. By repeating this whole 3-step process with different times stirring at open circuit in step two, we were able to construct plots showing the disappearance of charge from the film as a function of time. This can be used to generate kinetics equations and determine the rate of charge loss from the NiOOH film at 0s at open circuit, which corresponds to the rate of the indirect pathway under electrolysis conditions at the potential of 1.52V vs RHE applied in step 1.

When conducting the rate deconvolution trials for a given substrate and condition, the three step process was repeated four separate times using four different $Ni(OH)_2$ films for each length of time tested at open circuit in step two, with the results being averaged to get the data points shown in the 1/charge vs time plots. When conducting these trials, the $Ni(OH)_2$ films were replaced

after being used to collect no more than 4 data points. Additionally, the alcohol/aldehyde solution was replaced with a fresh 30 mL solution each time the $Ni(OH)_2$ working electrode was replaced. To account for small variations in the active Ni content from film to film and trial to trial, after the measurement of each data point an additional instance of the 3-step procedure was immediately performed with 0.1 s as the time at open circuit in step 2. This was used to adjust the measured charge stored in the NiOOH film observed in the previous measurement according to the method described in Chapter 2.4.8.

2.4.7 Calculation of Average Ni valence

The average Ni valence for the plots in **Figure 3.9** was calculated using equation 6 where Q_0 is the charge in coulombs required to reduce the Ni film to $Ni(OH)_2$ from its steady state condition at 1.52V vs RHE in the presence of the organic substrate and is obtained from the y-intercept of the 1/charge vs time plots obtained in the rate deconvolution analysis, and n_{Ni} is the moles of Ni in one of the films, which we previously determined to be 23.6 ± 0.4 nmol for our films.[11]

$$\langle \text{Ni valence} \rangle = 2 + \frac{Q_0}{n_{Ni}F} \tag{5}$$

2.4.8 Computational methods.

Periodic DFT calculations were performed using the Quantum ESPRESSO code.[21-22] We used the optimized norm-conserving Vanderbilt psuedopotentials[23-24] with a plane-wave kinetic energy cutoff of 80 Ry. We employed Fermi–Dirac smearing of the electronic states with smearing widths of 0.001 Ry (0.0136 eV) and 0.005 Ry (0.068 eV) for condensed-phase and molecular systems, respectively. Total energies were converged to a tolerance of 10^{-3} Ry with a force convergence criterion of 10^{-3} Ry/Bohr for geometry optimizations. Geometry optimizations of the

NiOOH systems were performed using the PBE functional[25] with a Hubbard *U* correction[26-28] of 6.6 eV[29-30] applied to the nickel d states. A single-point calculation with the hybrid PBE0 functional[31] was used for the final energies, utilizing the optimized PBE+*U* geometries. PBE0 calculations utilized the adaptively compressed exchange (ACE) operator[32] for Hartree–Fock exchange with a kinetic energy cutoff of 160 Ry.

We modeled the aqueous solvent as dielectric continuum water using the self-consistent continuum solvation (SCCS) method within the Environ module[33] of Quantum ESPRESSO. A dielectric constant of 78.3 was used for liquid water. We used the parabolic point-counter-charge periodic boundary condition correction to the total DFT energies. Calculations involving species with a net charge are compensated by a homogeneous background charge to maintain charge neutrality in the unit cell.

NiOOH($01\bar{1}5$) was modeled as a five-layer periodic slab with stoichiometry $Ni_{30}O_{60}H_{26}$, containing six Ni atoms in each layer. The bottom two layers were constrained to their computed bulk positions to represent the bulk NiOOH, and the top three layers were allowed to relax during geometry relaxations. Two-thirds of the hydrogen atoms were removed from the surface layer to introduce Ni^{4+} ions into the system, representing a partially oxidized surface. Due to the size of the slab and the expense of the hybrid PBE0 calculations, all calculations were performed using a single *k*-point (Γ).

Molecular geometries for the ions in solution (OH^-, BO^-, and $PMOOH^-$) and their conjugate acids (H_2O, benzyl alcohol, and phenylmethanediol) were optimized using the PBE0 functional. In the main text, the energies of the ions were adjusted to account for deviations between calculated and experimental pK_a values due to the difficulties associated with treating charged species using periodic DFT. This adjustment was done by referencing all anion energies

to the DFT energy of OH^- in dielectric continuum water. Since the experimental pK_a of phenylmethanediol was not available, we computed the ΔpK_a between the molecularly similar phenylmethanediol and benzyl alcohol to be 5.4, thereby estimating the phenylmethanediol pK_a value to be 10. The experimental pK_a values for H_2O and benzyl alcohol (14 and 15.4, respectively), as well as the pK_a value of 10 obtained from the ΔpK_a calculation for phenylmethanediol, were used to correct the energy of the anions in solution. According to this correction scheme, the energy of the anion was calculated relative to OH^- using equation 7.

$$E_{X^-} = E_{OH^-} + (E_{XH} - E_{H_2O}) + (0.059\,\text{eV}) \times \left[pK_a(XH) - pK_a(H_2O) \right] \quad (7)$$

3.5 References

1. Bender, M. T.; Yuan, X.; Choi, K.-S. Alcohol oxidation as alternative anode reactions paired with (photo)electrochemical fuel production reactions. *Nat. Commun.* **2020**, *11*, 4594.
2. Cha, H. G.; Choi, K.-S. Combined biomass valorization and hydrogen production in a photoelectrochemical cell. *Nat. Chem.* **2015**, *7*, 328-333.
3. Lhermitte, C. R.; Sivula, K. Alternative oxidation reactions for solar-driven fuel production. *ACS Catal.* **202,** *9*, 2007–2017.
4. Bajada, M. A.; Roy, S.; Warnan, J.; Abdiaziz, K.; Wagner, A; Roessler, M. M.; Reisner, E. A precious-metal-free hybrid electrolyzer for alcohol oxidation coupled to CO_2-to-syngas conversion. *Angew.Chem. Int. Ed.* **2020**, *59*,15633–15641.
5. You, B.; Liu, X.; Liu, X.; Sun Y. Efficient H_2 evolution coupled with oxidative refining of alcohols via a hierarchically porous nickel bifunctional electrocatalyst. *ACS Catal.* **2017**, *7*, 4564–4570.
6. Taitt, B. J.; Nam, D.-H.; Choi, K.-S. A comparative study of nickel, cobalt, and iron oxyhydroxide anodes for the electrochemical oxidation of 5-hydroxymethylfurfural to 2,5-furandicarboxylic acid. *ACS Catal.* **2019**, *9*, 660–670.
7. Miao. Y.; Ouyang, L.; Zhou, S.; Xu, L.; Yang, Z.; Xiao, M.; Ouyang, R. Electrocatalysis and electroanalysis of nickel, its oxides, hydroxides and oxyhydroxides toward small molecules. *Biosens. Bioelectron.* **2014**, *53*, 428–439.

8. Schäfer, H.-J. Oxidation of organic compounds at the nickel hydroxide electrode. *Top. Curr. Chem.* **1987**, *142*, 101–129.
9. Lyalin, B. V.; Petrosyan, V. A. Oxidation of organic compounds on NiOOH electrode. *Russ. J. Electrochem.* **2010**, *46*, 1199–1214.
10. Fleischmann, M.; Korinek, K.; Pletcher, D. The oxidation of organic compounds at a nickel anode in alkaline solution. *J. Electroanal. Chem. Interfacial Electrochem.* **1971**, *31*, 39-49.
11. Bender, M. T.; Lam, Y. C.; Hammes-Schiffer, S.; Choi, K.-S. Unraveling two pathways for electrochemical alcohol and aldehyde oxidation on NiOOH. *J. Am. Chem. Soc.* **2020**, *142*, 21538–21547.
12. Fleischmann, M.; Korinek, K.; Pletcher, D. The kinetics and mechanism of the oxidation of amines and alcohols at oxide-covered nickel, silver, copper, and cobalt electrodes *J. Chem. Soc., Perkin Trans. 2* **1972**, *10*, 1396–1403.
13. Francke, R.; Quell, T.; Wiebe, A.; Waldvogel, S. R. *Organic Electochemistry: Revised and Expanded* Ch. 26 "Oxygen-Containing Compounds" (CRC Press 2016).
14. Deng, X.; Kang, X. Li, M.; Xiang, K.; Wang, C.; Guo, Z.; Zhang, J. Fu, X.-Z.; Luo, J.-L. Coupling efficient biomass upgrading with H_2 production via bifunctional Cu_xS@NiCo-LDH core– shell nanoarray electrocatalysts. *J. Mater. Chem. A* **2020**, *8*, 1138–1146.
15. Kaulen, J.; Schäfer, H.-J. Oxidation of alcohols by electrochemically regenerated nickel oxide hydroxide. Selective oxidation of hydroxysteroids. *Tetrahedron*. **1982**, *38*, 3299-3308.
16. Li, Y.-F.; Selloni, A. Mechanism and activity of water oxidation on selected surfaces of pure and Fe-doped NiO_x. *ACS Catal.* **2014**, *4*, 1148–1153.
17. Fidelsky, V.; Toroker, M. C. Enhanced water oxidation catalysis of nickel oxyhydroxide through the addition of vacancies. *J. Phys. Chem. C* **2016**, *120*, 25405–25410.
18. Serjeant, E.P., Dempsey B. Ionisation constants of organic acids in aqueous solution. International Union of Pure and Applied Chemistry; Pergamon: Oxford, 1979.
19. Campbell, C.T.; Sellers, J.R.V. The entropies of adsorbed molecules. *J. Am. Chem. Soc.* **2012**, *134*, 18109–18115.
20. Kang, D.; Kim, T. W.; Kubota, S. R.; Cardiel, A.C.; Cha, H. G.; Choi. K.-S. Electrochemical synthesis of photoelectrodes and catalysts for use in solar water splitting. *Chem. Rev.* **2015**, *115*, 12839–12887.

21. Giannozzi, P.; Baroni S., Bonini; Calandra, M; Car, R.; Cavazzoni, C.; Ceresoli, D.; Chiarotti, G. L.; Cococcioni, M.; Dabo, I.; Corso1, A. D.; Gironcoli, S.; Fabris, S.; Fratesi, G.; Gebauer, R.; Gerstmann, U.; Gougoussis, C.; Kokalj, A.; Lazzeri, M.; Martin-Samos, L.; Marzari, N.; Mauri, F.; Mazzarello, R.; Paolini, S.; Pasquarello, A.; Paulatto, L.; Sbraccia, C.; Scandolo, S.; Sclauzero, G.; Seitsonen, A. P.; Smogunov, A.; Umari1, P.; Wentzcovitch, R. M. QUANTUM ESPRESSO: A modular and open-source software project for quantum simulations of materials. J. *Phys.: Condens. Matter* **2009**, *21*, 395502.
22. Giannozzi, P.; Andreussi, O.; Brumme, T.; Bunau, O.; Nardelli, M. B.; Calandra, M.; Car, R.; Cavazzoni, C.; Ceresoli, D.; Cococcioni, M; Colonna, N.; Carnimeo, I.; Corso, A. D.; Gironcoli, S.; Delugas, P.; DiStasio, R. A.; Ferretti, A.; Floris, A.; Fratesi, G.; Fugallo, G.; Gebauer, R.; Gerstmann, U.; Giustino, F.; Gorni, T.; Jia, J.; Kawamura, M; Ko, H.-Y.; Kokalj, A.; Küçükbenli, E.; Lazzeri, M.;Marsili, M.; Marzari, N.; Mauri, F.; Nguyen, N. L.; Nguyen, H.-V.;Otero-de-la-Roza, A.; Paulatto, L.; Poncé, S.; Rocca, D.; Sabatini, R.; Santra, B.; Schlipf, M.; Seitsonen, A. P.; Smogunov, A.; Timrov, I.; Thonhauser, T.; Umari, P.; Vast, N.; Wu, X.; S Baroni Advanced capabilities for materials modelling with quantum ESPRESSO. *J. Phys.: Condens. Matter* **2017**, *29*, 465901.
23. Hamann, D. R. Optimized norm-conserving Vanderbilt pseudopotentials. *Phys. Rev. B* **2013**, *88*, 085117.
24. Schlipf, M.; Gygi, F. Optimization algorithm for the generation of ONCV pseudopotentials. *Comput. Phys. Commun.* **2015**, *196*, 36–44.
25. Perdew, J. P., Burke, K.; Ernzerhof, M. Generalized gradient approximation made simple. *Phys. Rev. Lett.* **1996**, *77*, 3865–3868.
26. Anisimov, V. I.; Zaanen, J.; Andersen, O. K. Band theory and mott insulators: Hubbard U instead of Stoner I. *Phys. Rev. B* **1991**, *44*, 943–954.
27. Anisimov, V. I.; Solovyev, I. V.; Korotin, M. A. Density-functional theory and NiO photoemission spectra. *Phys. Rev. B **1993**, 48*, 16929-16934.
28. Liechtenstein, A. I.; Anisimov, V. I.; Zaanen, J. Density-functional theory and strong interactions: Orbital ordering in Mott-Hubbard insulators. *Phys. Rev. B* **1995**, *52*, R5467-R5470.
29. Cococcioni, M.; de Gironcoli, S. Linear response approach to the calculation of the effective interaction parameters in the LDA+U method. *Phys. Rev. B* **2005**, *71*, 035105.

30. Goldsmith, Z. K.; Harshan, A. K.; Gerken, J. B.; Vörös, M.; Galli, G. Stahl, S. S.; Hammes-Schiffer, S. Characterization of NiFe oxyhydroxide electrocatalysts by integrated electronic structure calculations and spectroelectrochemistry. *Proc. Natl. Acad. Sci.* **2017**, *114*, 3050–3055.
31. Adamo, C.; Barone, V. Toward reliable density functional methods without adjustable parameters: The PBE0 model. *J. Chem. Phys.* **1999**, *110*, 6158–6170.
32. Lin, L. Adaptively compressed exchange operator. *J. Chem. Theory Comput.* **2016**, *12*, 2242–2249.
33. Andreussi, O.; Dabo, I.; Marzari, N. Revised self-consistent continuum solvation in electronic-structure calculations. *J. Chem. Phys.* **2012**, *136*, 064102.

Chapter 4: Electrochemical Dehydrogenation Pathways of Amines to Nitriles on NiOOH

Portions of this chapter have been adapted from:

Bender, M. T.; Choi, K.-S. Electrochemical dehydrogenation pathways of amines to nitriles on NiOOH. *JACS Au* **2022**, *2*, 1169–1180. DOI 10.1021/jacsau.2c00150

4.1 Introduction

Nitriles are highly important synthetic intermediates with applications in a wide variety of organic reactions including production of pharmaceuticals, fine chemicals, and agricultural chemicals.[1-3] Traditional methods of preparing nitriles (e.g. ammoxidation, Sandmeyer reaction, displacement of halides with cyanide ions), however, suffer from several unattractive features including the use and production of toxic chemicals, harsh reaction conditions, and the generation of significant amounts of chemical waste.[3-5] As such, there is great interest in developing greener synthetic routes to produce nitriles. One promising alternative is the oxidation of primary amines to nitriles using molecular oxygen and transition metal-based catalysts, notably ones based on Ru or Cu.[3,5-8] While these methods are greener than the traditional nitrile synthesis methods and offer several important advantages, there are still challenges that must be overcome with most methods facing some combination of drawbacks including low turnover numbers, requiring the use of elevated temperatures and O_2 pressures, or requiring the use of complex ligands and catalysts that can be challenging or expensive to produce.[3,5,9] Furthermore, side reactivity can be an issue, often stemming from the electrophilic imine intermediate undergoing nucleophilic attack before it can undergo dehydrogenation to form the nitrile.[2,5,9]

Another promising method that has been explored is the electrochemical oxidation of primary amines to nitriles.[10-14] This method shares the benefits of using the transition metal-based catalysts and molecular oxygen in that it eliminates the need for harsh chemicals and stoichiometric oxidizing agents, but it offers additional benefits. First, electrochemical amine oxidation can be performed efficiently at ambient temperatures and pressures without needing O_2 or a sacrificial oxidant. Second, the electrons gained by the oxidation of amines at the anode are transferred to the cathode and can be used for reduction reactions that produce valuable products such as fuels (e.g., H_2 by water reduction) or chemicals (e.g., reductive valorization of other

organic species), increasing the economic viability. Third, electrochemical oxidation can be driven by electricity generated from renewable energy sources and will only become more appealing as an increase in renewable energy sources lowers electricity prices. As such, electrochemical oxidization of primary amines has the potential to be among the greenest methods of producing nitriles.

NiOOH is one of the most promising and practical electrode materials for catalyzing these electrochemical conversions. Previous reports have shown that it can efficiently and selectively convert a variety of primary amines into nitriles under alkaline conditions.[13-17] As shown in **Scheme 4.1**, the oxidation of amines to nitriles bears many similarities to the oxidation of alcohols to carboxylic acids, another class of electrochemical reaction NiOOH is well known to effectively catalyze.[13-19] Both processes (alcohol oxidation to carboxylic acid and amine oxidation to nitrile) are $4e^-$ dehydrogenations occurring in two successive $2e^-$ steps, with the first producing an aldehyde/imine and the second then converting that aldehyde/imine into a carboxylic acid/nitrile. One key difference is that before aldehyde oxidation, the aldehyde must first undergo nucleophilic attack by an OH^- from solution to form the 1,1-geminal diol.[20] However, for imine oxidation, nucleophilic attack by an OH^- from solution must be suppressed as it results in the formation of aldehyde, which can be further oxidized to carboxylic acid.[13,16]

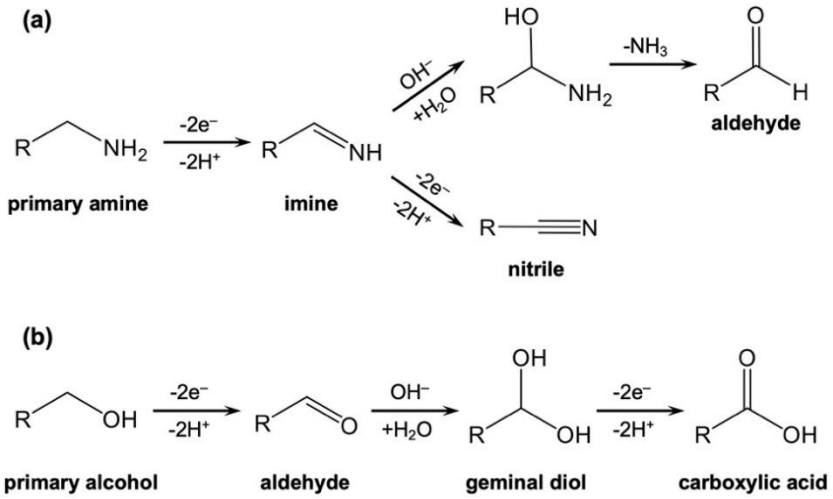

Scheme 4.1. Scheme depicting (a) oxidation of a primary amine to either a nitrile or an aldehyde and (b) oxidation of a primary alcohol to a carboxylic acid.

The electrochemical dehydrogenation of both amines and alcohols on NiOOH has long been understood to proceed through the same general mechanism proposed by Fleischmann *et al.* (**Scheme 4.2**).[16,17] In this mechanism, NiOOH serves as a chemical oxidizing agent, undergoing a chemical reaction with the amine/alcohol that features a rate limiting hydrogen atom transfer (HAT) in which a hydrogen radical from the α-C of the alcohol/amine is transferred to the NiOOH (**Scheme 2, step 3**).[16,17] Accordingly, the oxidation of alcohol/amine through this mechanism is accompanied by reduction of NiOOH to $Ni(OH)_2$. The role of electrochemistry is simply to allow the $Ni(OH)_2$ formed following alcohol/amine oxidation to be reconverted to NiOOH (**Scheme 4.2, step 1**). As such, the actual oxidation reaction with amine is the same as when NiOOH is used as a stoichiometric chemical oxidizing agent, with the potential serving to enable regeneration of NiOOH and thus its use in a catalytic rather than stochiometric amount.[13,16,17] This regeneration of NiOOH from $Ni(OH)_2$ is reported to become fast at relatively low overpotentials relative to the $Ni(OH)_2$/NiOOH couple.[16,17] Thus, the overall rate of alcohol/amine oxidation is reported to be dictated by the rate of the chemical HAT step and thus unaffected by the applied potential (so long

as the bias is sufficient to ensure fast regeneration for NiOOH).[16,17] As such, we will refer to this pathway as indirect oxidation.

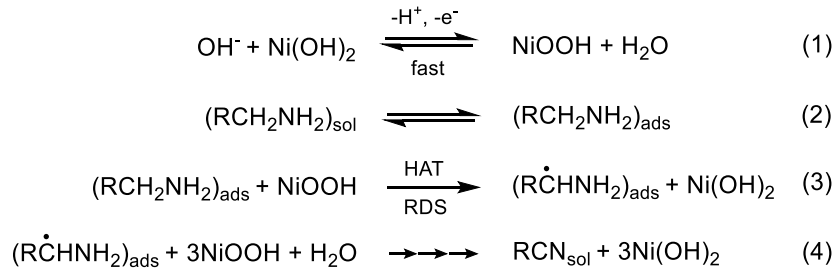

Scheme 4.2. Literature mechanism propsed by Fleischmann *et al.* for the indirect oxidation of amines at NiOOH electrodes in alkaline aqueous media. An identical mechasim was also proposed for oxidation of primary alcohols to carboxylic acids.

Recently, we revealed that for oxidation of alcohols and aldehydes to carboxylic acids on NiOOH there is a second, potential dependent (PD) pathway that occurs in addition to the indirect one and that this PD pathway is dominant for alcohol oxidation.[20,21] Unlike indirect oxidation which uses Ni^{3+} as the catalytic center and achieves dehydrogenation through HAT, PD oxidation uses Ni^{4+} as the catalytic center and achieves dehydrogenation through hydride transfer.[20,21] This recent finding made us wonder if the oxidation of amines to nitriles on NiOOH truly occurs through indirect oxidation as it has been believed or if it also occurs partly or dominantly through PD oxidation.

The goal of this study is to interrogate and establish the oxidation mechanisms of amines to nitriles on NiOOH using various electrochemical techniques that can qualitatively and quantitatively analyze the indirect and PD oxidation pathways. We used aliphatic propylamine and aromatic benzylamine as model systems and examined how the structure and concentration of amines, pH, and oxidation potential influence the indirect and PD oxidation processes. By comparing the results obtained from amine oxidation with those of alcohol oxidation, this study

will establish a general foundation for understanding electrochemical dehydrogenation, one of the major oxidation reactions in organic chemistry, on metal oxyhydroxide electrocatalysts.

4.2 Results and Discussion

4.2.1 CV Analysis

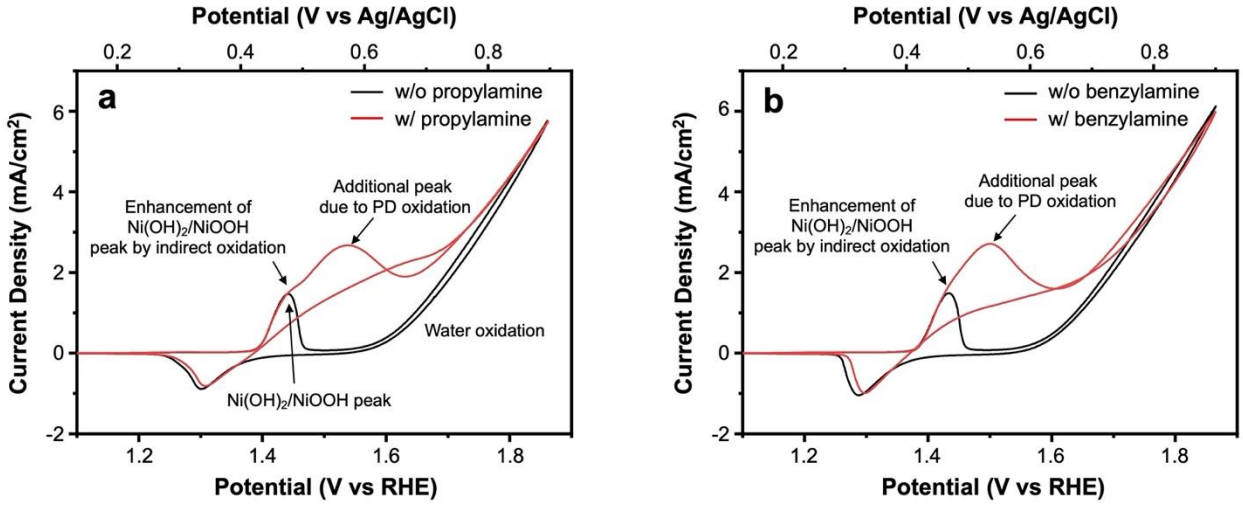

Figure 4.1. CVs collected using a $Ni(OH)_2$ working electrode in pH 13 solutions with (red) and without (black) 10mM solutions of (a) propylamine and (b) benzylamine (scan rate, 10 mV/s).

We first examined cyclic voltammograms (CVs) of NiOOH in a pH 13 solution with and without propylamine or benzylamine (**Figure 4.1**). If amine oxidation on NiOOH occurs only through indirect oxidation, we would expect the addition of amines to only enhance the anodic peak associated with the oxidation of $Ni(OH)_2$ to NiOOH. This is because in the indirect mechanism the amine is not directly oxidized by the applied bias.[16,17] Instead, it chemically reacts with NiOOH to reform $Ni(OH)_2$ which would then be re-oxidized to NiOOH during the CV scan, enhancing the $Ni(OH)_2$/NiOOH peak. Our results, however, show that there is only a minor enhancement of the $Ni(OH)_2$/NiOOH peak when the amines are present and instead the $Ni(OH)_2$/NiOOH peak is followed by a separate oxidation peak in the more positive potential

region (**Figure 4.1**). This cannot be explained by indirect oxidation. Additionally, we note that the second oxidation peak is significantly larger than the enhancement of the $Ni(OH)_2$/NiOOH peak, indicating it, rather than the indirect process, accounts for the majority of amine oxidation. Furthermore, we note that, according to the indirect mechanism, the current for a solution rapidly stirred to minimize mass transport limitation should settle into a potential independent plateau shortly after reaching potentials anodic enough to oxidize $Ni(OH)_2$. In reality, however, CVs we collected in rapidly stirred amine solutions show the current is highly potential dependent and keeps increasing as the potential is swept to the positive direction without ever settling into a plateau (**Figure 4.2**).

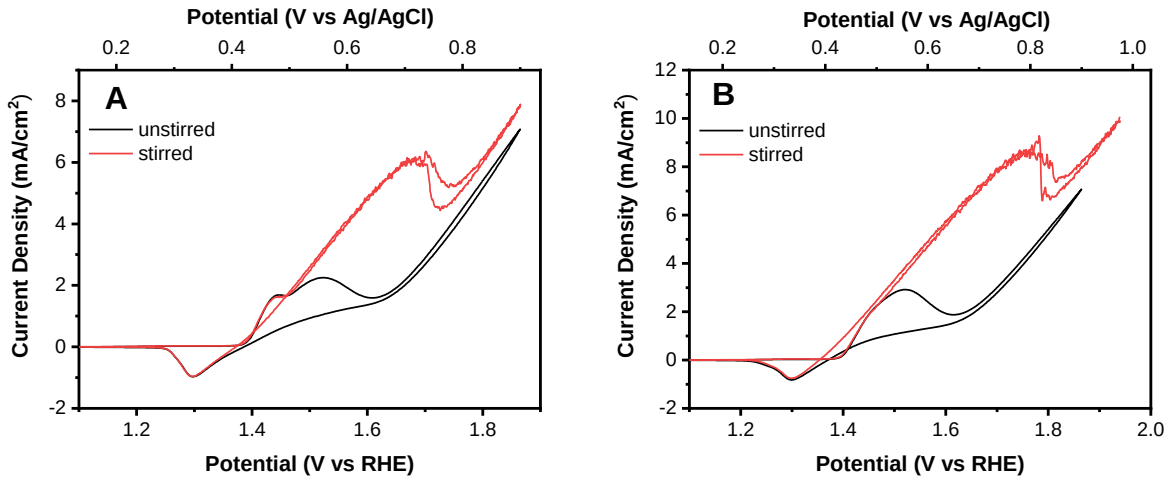

Figure 4.2. CVs collected using a $Ni(OH)_2$ working electrode in stirred (red) and unstirred (black) pH 13 solutions with 10 mM of A) propylamine and B) benzylamine (scan rate, 10 mV/s).

While the CV's depicted in **Figure 4.1** deviate significantly from the those expected for indirect oxidation mechanisms, their shape is nearly identical to those we have previously observed for alcohol oxidation where PD oxidation dominates.[20,21] This suggests amine oxidation also occurs predominantly through PD oxidation. The PD oxidation mechanism we proposed for alcohol oxidation is shown in **Scheme 4.3**.[20,21] In this mechanism, Ni^{4+} is the active center (**Step 1, Scheme 4.3**), which is why PD oxidation is enabled in a more positive potential region than

indirect oxidation (which uses Ni^{3+}). The alcohol is oxidized through a hydride transfer from the alpha position of the organic substrate to a Ni^{4+} site in the catalyst (**Step 4, Scheme 4.3**), thereby reducing that site back to Ni^{2+}. In order to activate the alcohol to hydride transfer its OH group must also be deprotonated. We believe for alcohols this most often occurs as a separate step in solution prior to adsorption (**Step 2, Scheme 4.3**); however, it is also possible it occurs either after the alcohol adsorbs or in concert with the hydride transfer. After the hydride transfer, the now reduced Ni site will be electrochemically re-oxidized to regenerate Ni^{4+}, closing the catalytic cycle (**Step 5, Scheme 4.3**).

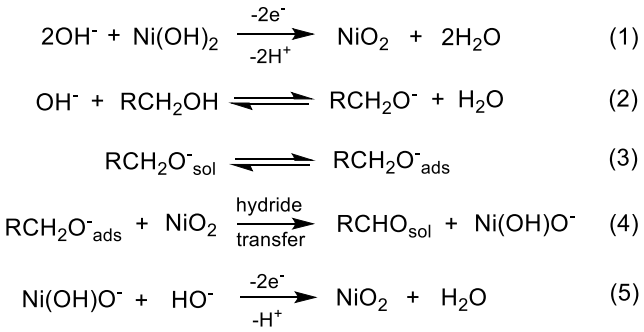

Scheme. 4.3. Hydride transfer mechanism we have previously proposed for oxidation of alcohols to aldehydes through the PD oxidation pathway. The oxidation of aldehydes to carboxylic acids proceeds through the same steps because aldehydes in solution are in equilibrium with their hydrate, a 1,1-geminal diol, which is an alcohol.

Our proposed PD oxidation mechanism for amines is shown in **Scheme 4.4**. It is very similar to that for alcohol oxidation, still featuring a hydride transfer from the alpha position of the adsorbed organic substrate to a Ni^{4+} site in the catalyst. The biggest difference with the mechanism for alcohol oxidation is that because amines are much less acidic than alcohols, the deprotonation that enables the organic species to undergo hydride transfer is unlikely to occur in solution. Instead, the deprotonation is expected to occur after adsorption. This is written in the scheme as a separate step (**Step 3, Scheme 4.4**) to hydride transfer (**Step 4, Scheme 4.4**); however, it is also possible

the two occur in a concerted manner. Another notable difference in the mechanism comes after the imine is formed. Unlike with aldehyde oxidation, the imine does not undergo nucleophilic attack by OH^- before undergoing further oxidation to the imine. Because the imine is highly reactive and its further oxidation very fast, we did not detect any imine intermediates and could not directly probe its mechanism as we could for aldehyde oxidation. Accordingly, while we expect imine oxidation proceeds though a similar combination of indirect and PD mechanisms as does aldehyde oxidation, we could not experimentally confirm this. Accordingly, in **Scheme 4.4** we do not propose specific steps for imine oxidation, instead showing it as an undefined set of fast steps resulting in a nitrile (**Step 5, Scheme 4.4**).

$$2OH^- + Ni(OH)_2 \xrightarrow[-2H^+]{-2e^-} NiO_2 + 2H_2O \quad (1)$$

$$(RCH_2NH_2)_{sol} \rightleftharpoons (RCH_2NH_2)_{ads} \quad (2)$$

$$OH^- + (RCH_2NH_2)_{ads} \rightleftharpoons (RCH_2NH^-)_{ads} + H_2O \quad (3)$$

$$(RCH_2NH^-)_{ads} + NiO_2 \xrightarrow{\text{hydride transfer}} (RCHNH)_{ads} + Ni(OH)O^- \quad (4)$$

$$(RCHNH)_{ads} \xrightarrow[-2H^+]{-2e^-} RCN_{sol} \quad (5)$$

$$Ni(OH)O^- + HO^- \xrightarrow[-H^+]{-2e^-} NiO_2 + H_2O \quad (6)$$

Scheme 4. Proposed hydride transfer mechanism for the PD oxidation of primary amines to nitriles on a NiOOH elecrocatalyst.

To summarize, there are several key differences between the indirect pathway laid out in **Scheme 4.2** and the PD one shown in **Scheme 4.4**. The two mechanisms feature different key mechanistic steps with PD oxidation involving a hydride transfer (1 H^+/2e^-) and a deprotonation instead of two hydrogen atom transfers (1H^+/1e^-). Additionally, they differ in the primary active site they occur at, with PD oxidation occurring only on Ni^{4+} while indirect can occur on Ni^{3+} (and also possibly Ni^{4+}). Finally, as will be expanded upon below, they differ in the role potential plays

in the mechanism. For indirect oxidation the potential is important only for generating the oxidized Ni site while for PD oxidation the applied bias is critical not only for generating the Ni^{4+} sites but also for enabling their reaction with the amine.

4.2.2 Deconvolution of indirect and PD oxidation currents

In order to quantitatively determine the contributions the indirect and PD pathways have toward amine oxidation, we performed a rate deconvolution analysis using the procedure that we developed to study alcohol and aldehyde oxidation on NiOOH.[20] Only a brief overview of the principles behind our rate deconvolution process will be provided here as a detailed description is included in Chapter 2 and the specific details used for this chapter are contained in the experimental section. Our method for measuring the rate of a potential independent, indirect oxidation pathway is described in depth in Chapter 2 and in the methods section. We first pre-oxidize $Ni(OH)_2$ to NiOOH by applying a fixed potential at the working electrode in a rapidly stirred amine solution long enough for the current to settle into a steady state. We then stop applying a bias, allowing the NiOOH to sit at open circuit in the rapidly stirred amine solution. As the system is under open circuit condition, during this time NiOOH cannot be regenerated nor will any potential dependent process occur; however, NiOOH can act as a stoichiometric chemical oxidizing agent, oxidizing the amine while being reduced back to $Ni(OH)_2$. After a specified amount of time at open circuit, a reducing potential is applied, rapidly converting the remaining NiOOH back to $Ni(OH)_2$. The charge passed during this reduction shows how much NiOOH "reactant" remained after undergoing the potential independent chemical oxidation process for the amount of time the system was at open circuit. By repeating this process for several different open circuit times, a data series can be constructed showing the disappearance of the NiOOH reactant due to acting as a chemical oxidant as a function of reaction time (i.e. the length of time sitting at open circuit). Kinetics

equations can then be derived from this describing the rate of the indirect process. For all the reactions examined here, at relatively short times at open circuit a plot of 1/charge vs time is linear. This means during the time frame of interest the indirect process behaves as if it is second order with respect to charge in the NiOOH film and therefore its rate can be described according to equation 1 where Q_{Ni} is the positive charge stored in the film beyond its $Ni(OH)_2$ resting state (i.e., the positive charge available for organic oxidation), which will be referred to as charge stored in the NiOOH film. We note that this does not necessarily mean the reaction is truly "second order" with respect to charge stored in the NiOOH film. Indeed, we suspect the true rate law is probably more complicated. For our purposes, however, it is not necessary that equation 1 be the true rate law but rather just that it accurately model the disappearance of charge from the NiOOH across the timeframe of interest. The linearity of the 1/charge vs time plots shows that this is true for all the conditions tested in this this work.

$$\text{Rate}_{ind} = k_{obs,ind} Q_{Ni}^2 \quad (1)$$

We use $k_{obs,ind}$ rather than k_{ind} in equation 1 because the solution is rapidly stirred during our rate deconvolution trials, meaning the concentration of the organic species at our electrode surface is constant over the duration of the experiments and thus is effectively "flooded". This means the influence the concentration of the organic species has on the reaction rate will be incorporated into $k_{obs,ind}$ according to equation 2 where *a* is the reaction order with respect to the organic species.

$$k_{obs,ind} = k_{ind} [\text{organic species}]^a \quad (2)$$

By solving equation 1 for when the positive charge stored in the Ni film (Q_{Ni}) is equivalent to its steady state value when a constant potential is applied (obtained from the y-intercept of the 1/charge vs time plots), the current due to the indirect pathway can be obtained. We can then use

this to obtain the current for the PD pathway by noting that, as long as we have chosen a potential before the onset of water oxidation when generating our pre-oxidized NiOOH film, the total current will be equal to the sum of the indirect and PD partial currents (equation 3).

$$I_{tot} = I_{ind} + I_{PD} \quad (3)$$

We note that our rate deconvolution method works only because PD oxidation cannot occur under the open circuit condition; when the applied potential is removed, PD oxidation stops and only indirect oxidation continues until all existing Ni^{3+} (and likely Ni^{4+}) is reduced by HATs from the organic species, which is experimentally observed.[20-21] This means that unlike for indirect oxidation where the potential is needed only to (re)generate the oxidized Ni sites, for PD oxidation the potential is critical not only to (re)generate the Ni^{4+} catalytic centers but also to enable the actual hydride transfer to the Ni^{4+} centers.

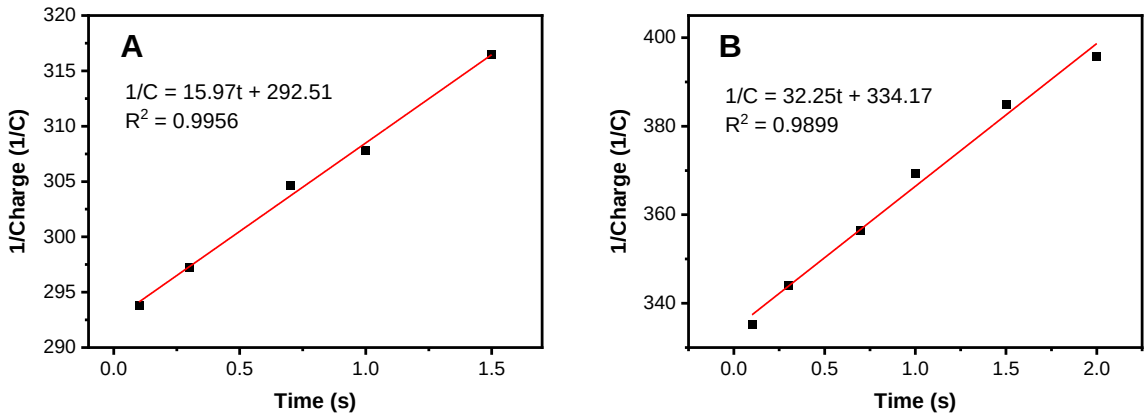

Figure 4.3. 1/Charge vs time plots measuring the disappearance of positive charge from NiOOH films due to indirect oxidation of A) 10 mM propylamine or B) 10 mM benzylamine as a function of time at open circuit in a rapidly stirred pH 13 solution. The NiOOH used for these measurements was pre-oxidized at 1.52 V vs RHE in the given solutions.

The 1/charge plots obtained from the rate deconvolution experiments performed with 10 mM benzylamine and propylamine solutions at pH 13 and 1.52 V vs RHE are shown in **Figure 4.3** while the deconvoluted partial current densities for indirect and PD oxidation are given in **Figure 4.4.** The results confirm that, as was suggested qualitatively by the CVs, for both the aliphatic propylamine and the aromatic benzylamine the indirect mechanism only accounts for a small fraction of the oxidation current (13% for propylamine and 19% for benzylamine), with the clear majority being due to a PD process. Additionally, we note that the aromatic benzylamine is more reactive for both PD and indirect oxidation than aliphatic propylamine.

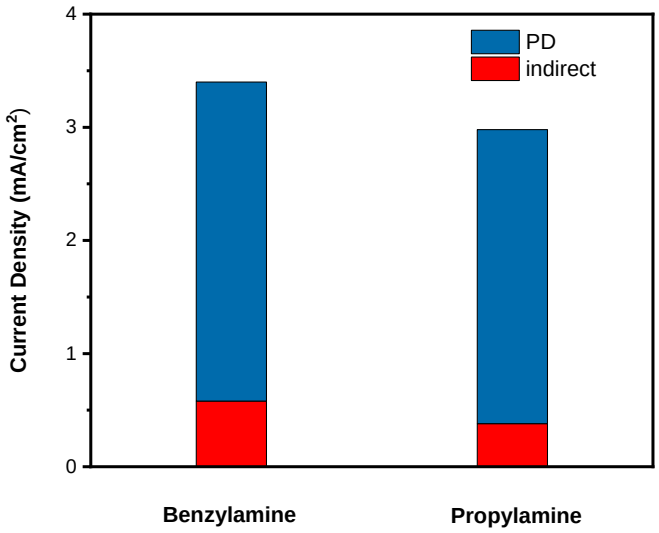

Figure 4.4. The component of the current due to indirect (red) and PD (blue) oxidation of pH 13 solutions of 10 mM benzylamine and 10 mM propylamine at 1.52 V vs RHE.

4.2.3 pH dependence

We next considered how pH affects the rate of indirect and PD oxidation by comparing the rate deconvolution analyses obtained at 1.52 V vs the reversible hydrogen electrode (RHE) in pH 12, 13, and 14 solutions. Before the rate deconvolution analysis, we confirmed that the Faradaic efficiency for amine oxidation to nitrile in all these solutions is high with no detectable side products, which is an important prerequisite for the rate deconvolution analysis. The fact that no

aldehydes and carboxylic acids are detected suggests that once the imine intermediate is formed, further oxidation to the nitrile is rapid. The pH dependent rate-deconvolution results, $k_{obs,ind}$, and average Ni valence are shown in **Figure 4.5**. The steady state average Ni valence at the various conditions in the presence of the amines was calculated by comparing the value of the y-intercept of the 1/charge vs time plots to the total amount of Ni in the NiOOH film (see experimental section for more details).

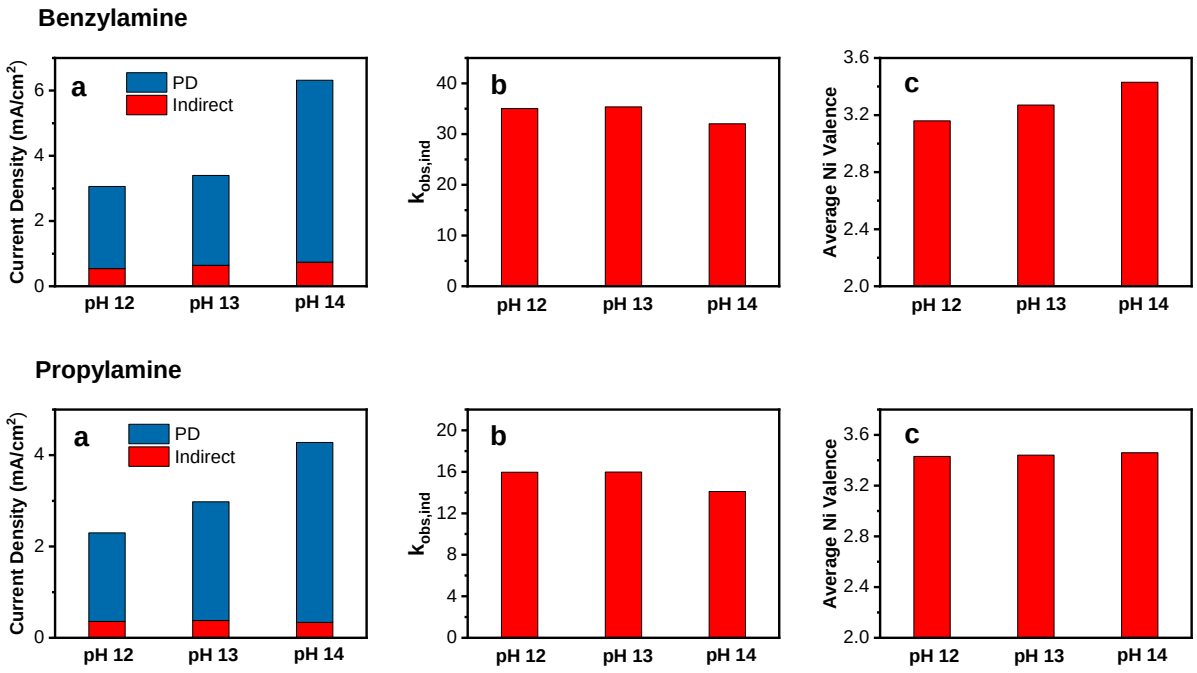

Figure 4.5. Plots displaying (a) the deconvoluted indirect and PD current, (b) $k_{obs,ind}$, and (c) the average Ni valence at 1.52V vs RHE in pH 12, 13, and 14 solutions of 10 mM benzylamine (top) and 10 mM propylamine (bottom).

Figure 4.5 shows that for both propylamine and benzylamine the PD current increases considerably as pH increases. This pH dependence can be attributed to two factors. The first is that the $Ni(OH)_2$/NiOOH couple follows a non-Nernstian shift as pH changes (**Figure 4.6**). As a consequence, even when the same potential is applied vs RHE, under more basic conditions this same potential vs RHE will represent a greater overpotential with respect to the $Ni(OH)_2$/NiOOH

peak, leading to faster regeneration of higher valent Ni. This improves the kinetics for the PD process as the rate of this pathway is limited in part by the regeneration of Ni^{4+} sites as can be seen by noting that the average Ni valence is significantly lower in the presence of amine than in its absence. For example, at 1.52 V vs RHE in a pH 13 solution the average Ni valence without amine was determined to be +3.68 in our previous study[20] while in the presence of 10 mM propylamine it is +3.44 and in the presence of the more reactive benzylamine it is only +3.27. The faster regeneration of Ni^{4+} sites as pH increases can lead to an increase in the average Ni valence and thus the number of active sites available to do PD oxidation, accounting for an increase in the observed current.

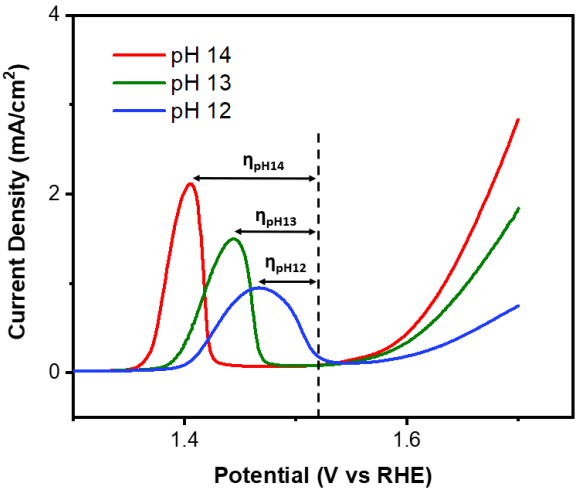

Figure 4.6. LSVs collected with a scan rate of 10 mV/s using a $Ni(OH)_2$ working electrode in pH 14 KOH (red), pH 13 KOH (green), and pH 12 KOH (blue) solutions. For the pH 12 solution, 90 mM $KClO_4$ was added as a supporting electrolyte to ensure adequate solution conductivity. The dashed line indicates the potential 1.52 V vs RHE applied in the rate deconvolution measurements.

This first factor (faster Ni^{4+} regeneration) alone, however, cannot explain the effect of pH on the increase in the PD oxidation current for the less reactive propylamine, where the Ni valence is relatively high even in pH 12 and does not meaningfully increase as pH does. The results of propylamine oxidation suggests that the effective rate constant for the PD oxidation, $k_{obs,PD}$, must

include an [OH^-] term as shown in equation 4 where *b* is the order with respect to [OH^-]. In fact, equation 4 can also explain why propylamine does not show an enhancement in the average Ni valence as pH increases. While a higher pH does enhance the rate of Ni^{4+} regeneration, it also enhances the rate of consumption of Ni^{4+} through the PD process. In the case of propylamine these two effects seem to net out to zero, leading to no change in the average Ni valence while for benzylamine the effect on the regeneration step is greater, leading to a higher average Ni valence as pH increases.

$$k_{obs,PD} = k_{PD}[\text{organic species}]^a [OH^-]^b \quad (4)$$

The most likely reason $k_{obs,PD}$ has a [OH^-] dependence is because, in addition to the hydride transfer, conversion of a primary amine into a nitrile through the PD process involves removing two protons from the $–NH_2$ group. The pH dependence suggests that, for the PD pathway, at least one of these deprotonation steps affects the rate. Moreover, due to the high reactivity of the imine and the lack of any observed aldehyde product (indicating the lifetime of any imine formed is quite short), we can conclude that the first deprotonation step (**Step 3, Scheme 4.4**) is the one much more likely to be rate-affecting. As was mentioned when discussing **Scheme 4.4**, this deprotonation is very unlikely to occur in solution and instead is expected to occur after the amine adsorbs, either shortly before hydride transfer or in concert with hydride transfer. In either case, it appears that this deprotonation of the adsorbed amine is critical to activate it toward hydride transfer. This is analogous to the case of PD oxidation involving alcohols, where previous computational results have indicated hydride transfer to Ni^{4+} sites is favorable so long as the alcohol either has already undergone deprotonation to form the alkoxide or does so in concert with the hydride transfer.[20]

While the PD pathway was dominant at all pHs, there was also always a modest indirect component to the current. For propylamine, both the current from indirect oxidation and $k_{obs,ind}$ remain more or less the same. This is as expected since HAT, which is reportedly the rate determining step for indirect oxidation, is pH independent. For benzyl amine, however, there is a modest enhancement in the indirect oxidation under more basic conditions, with the current increasing from 0.54 mA/cm^2 to 0.74 mA/cm^2. This occurs despite $k_{obs,ind}$ remaining constant, meaning the reactivity of the higher valent Ni sites toward HAT has not changed (which is as expected). The reason for the increased current is because, for a highly reactive amine like benzylamine, the rate of HAT is quite fast and, at 1.52V vs RHE, HAT is not actually the sole rate determining step. Instead, the overall rate for the indirect pathway is also partially limited by the regeneration of the catalytic center which, as discussed above, is faster under more basic conditions due to the non-Nernstian shift of the $Ni(OH)_2$/NiOOH couple as pH changes.

4.2.4 Concentration dependence study

Next, we examined the effect varying the amine concentration had on the current through both pathways. This was done by performing rate deconvolution experiments at 1.52 V vs RHE in pH 13 solutions with propylamine and benzylamine concentrations ranging from 5 mM to 50 mM. The resulting deconvoluted current, $k_{obs,ind}$, and average Ni valence data are shown in **Figure 4.7**.

As can be seen in **Figure 4.7**, the PD current for benzylamine oxidation increases as the concentration increases from 5 mM to 20 mM, after which it plateaus. The reason for this plateau is that, as benzylamine concentration increases, the importance of the Ni^{4+} regeneration step for determining the overall current also increases. Since the increase in the benzylamine concentration does not increase the driving force for Ni^{4+} regeneration, the PD current is eventually limited by Ni^{4+} regeneration and becomes independent of concentration, which appears to occur at 20 mM

when the applied potential is 1.52 V vs RHE. (If a more positive potential is used, the plateau would be achieved at a higher concentration.) The increased importance of the Ni^{4+} regeneration step as benzylamine concentration increases is well demonstrated by the trend in the average Ni valence. As the concentration of benzyl amine increases, Ni^{4+} is consumed more rapidly and the steady-state average Ni valence declines considerably. Thus, further increasing the rate of PD oxidation would require application of a more positive potential to enhance rate of Ni^{4+} regeneration.

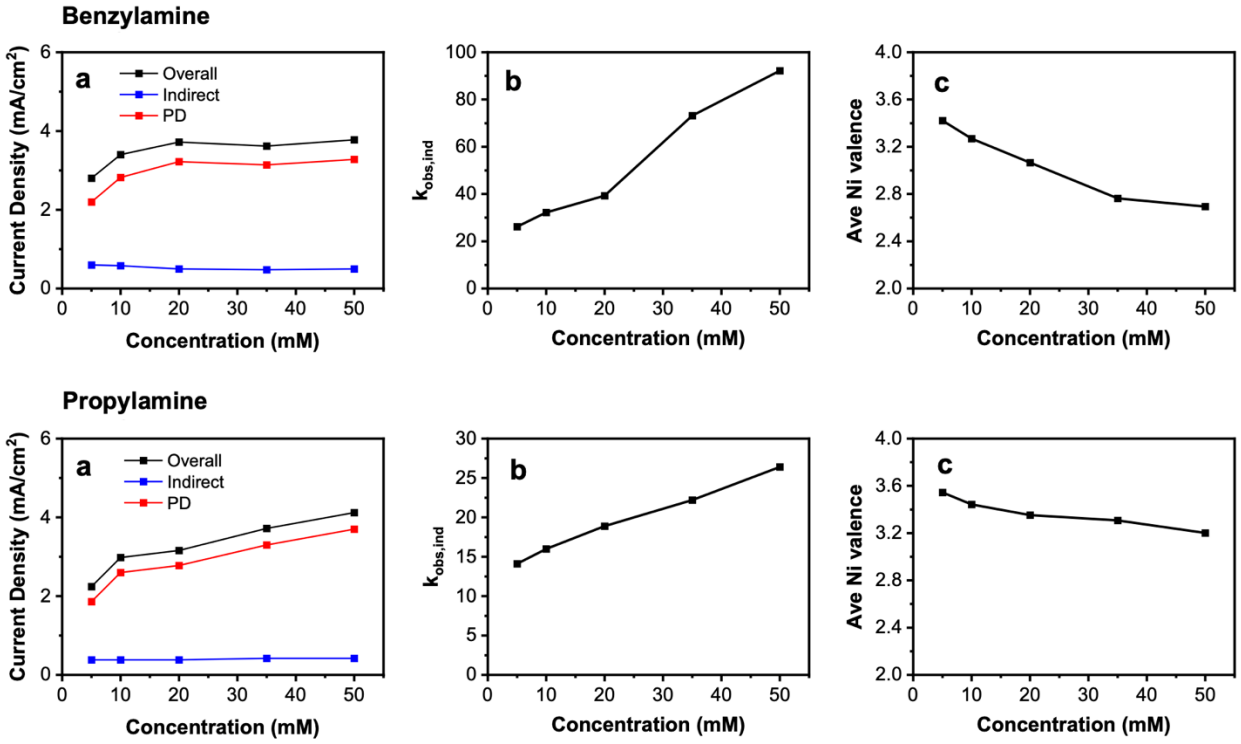

Figure 4.7. Plots displaying (a) the deconvoluted indirect and PD current, (b) $k_{obs,ind}$, and (c) the average Ni valence at 1.52V vs RHE in pH 13 solutions of various benzylamine (top) and propylamine (bottom) concentrations. For reference, the average Ni valence at 1.52 V vs RHE without the presence of an organic substrate is +3.68.

For the PD oxidation of propylamine, a gradual increase in current is observed as the concentration increases and no plateau is reached in the concentration range studied here. This is

because propylamine is significantly less reactive than benzylamine, which means the effective rate constant for the consumption of Ni^{4+} sites through PD oxidation, k_{PD} is significantly lower for propylamine than for benzylamine. As a consequence, at a given amine concentration the relative importance of the regeneration step for determining the PD oxidation rate will be smaller for propylamine than it is for benzylamine and the concentration at which PD oxidation becomes concentration independent will be significantly higher for propylamine. The smaller relative importance of the regeneration step on determining the PD oxidation current for propylamine as compared to benzylamine is well supported by comparing the changes in average Ni valence as concentration increase. For propylamine the decrease is gradual and even at 50 mM the average Ni valence is still +3.2 while for benzylamine the decline is precipitous, with the average Ni valence dropping to only +2.6 at 50 mM benzylamine, which means only a small portion of the total Ni sites are in the active Ni^{4+} state at any given moment.

For the indirect pathway, $k_{obs,ind}$, which includes an amine concentration term (equation 2), increases along with concentration for both benzylamine and propylamine. Since it is the amount of adsorbed amine (rather than the solution amine concentration) that matters for the indirect process, this increase in $k_{obs,ind}$ as the solution amine concentration increases means that, across the concentration range studied here, the active higher valent Ni sites are not fully covered with amines and the coverage of those sites by amines increases along with concentration. Despite the increase in $k_{obs,ind}$, the actual rate for indirect oxidation does not increase along with concentration. This is because, as shown in equation 1, the rate of indirect oxidation depends not only on $k_{obs,ind}$ but also on the positive charge stored in the NiOOH film and, as shown in **Figure 4.5c**, the Ni valence decreases as the concentration increases, offsetting the increase in $k_{obs,ind}$. In other words,

as is the case for PD oxidation, regeneration can also become a key limiting step for indirect oxidation when $k_{obs,ind}$ is enhanced by a high amine concentration.

The discussion above does beg the question why, for propylamine, the PD rate increases with concentration while the indirect rate does not. This difference likely stems from the difference in primary active site of indirect and PD oxidation. PD oxidation must occur at Ni^{4+} sites, and adsorption on these is likely to be more difficult as it necessitates outcompeting hydroxide and OER intermediates for adsorption on those sites.[21] Conversely, amine adsorption on the Ni^{3+} sites that are primarily responsible for indirect oxidation does not face this competition with OER intermediates.[21] Consequently, the coverage of the Ni^{3+} sites with adsorbed propylamine is likely to be higher than that of the Ni^{4+} sites, meaning increasing the solution concentration of propylamine would enhance the PD pathway more than the indirect one. The trend in $k_{obs,ind}$ as propylamine concentration increases reflects this. While it does increase, this increase is modest (and is much smaller than for the more reactive benzylamine), indicating that while the coverage of the Ni^{3+} sites with propylamine does increase along with concentration, this increase is fairly modest.

4.2.5 Potential Dependence Study

The results from the concentration dependence study discussed above make it clear that for both the indirect and PD pathways the rate of regeneration of higher valent Ni sites plays an important role in determining the current. As the regeneration of these Ni sites is a potential dependent process, this means that to have a more complete understanding of how amine oxidation occurs on NiOOH it is also necessary to understand how these two pathways are affected by changes in applied potential. (The choice of potentials used in this section may look unusual but

this is because the actual experiments were performed using potentials (0.55, 0.60, 0.65, 0.70 V) vs Ag/AgCl while they are reported here vs RHE.)

We found that NiOOH is more catalytic toward amine oxidation than toward water oxidation; even when we apply a potential that can enable water oxidation such as 1.67 V vs RHE (the onset potential for water oxidation is ~1.55V vs RHE at pH 13), the FE toward amine oxidation remains high (**Figure S4.8**). This enabled us to apply our rate deconvolution technique to separate out the contributions of the indirect and PD pathways to the current at higher bias conditions. We did so using pH 13, 10 mM solutions of propylamine and benzylamine with applied potentials ranging from 1.52 V RHE to 1.67 V vs RHE. The resulting deconvoluted current, $k_{obs,ind}$, and average Ni valence data are shown in **Figure 4.9**.

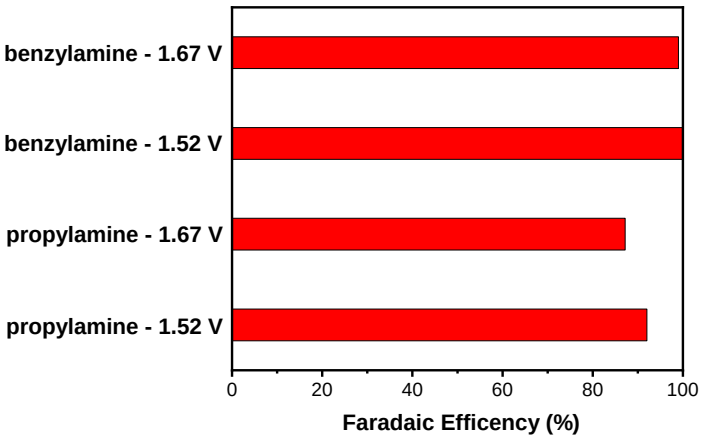

Figure 4.8. Faradaic efficiencies for benzylamine and propylamine oxidation to the corresponding nitriles at two different potentials vs RHE. The constant-potential electrolyses were conducted in rapidly stirred pH 13 solutions with 10 mM propylamine or benzylamine. The FEs were calculated after passing 25% of the stoichiometric charge required for full conversion. In all cases the nitrile was the only product detected.

The rate of the PD process increases significantly as the applied potential increases. This is as expected, since the applied bias affects not only Ni^{4+} regeneration but also the rate constant

for hydride transfer. The strong enhancement in the rate of PD oxidation also means that the proportion of the current occurring through the PD pathway increases along with potential.

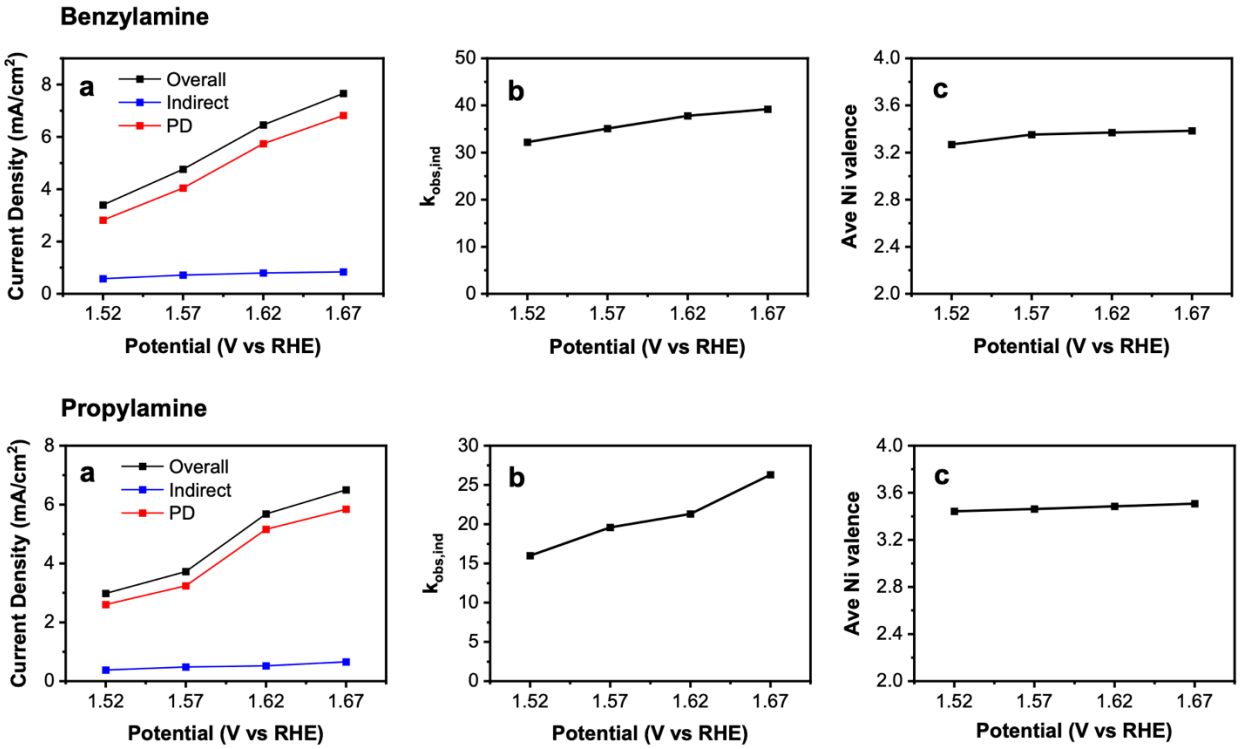

Figure 4.9. Plots depicting (a) the partial current for oxidation through the indirect and PD pathways, (b) $k_{obs,ind}$, and (c) the average steady state Ni valence at various applied potentials in a rapidly stirred pH 13 solution with a 10 mM concentration of benzylamine (top) and propylamine (bottom).

We found that the indirect rate also increased with the applied potential, although the increase was not as significant (**Figure 4.9a**). Surprisingly, this increase is primarily caused by an increase in $k_{obs,ind}$ (**Figure 4.9b**), which should theoretically be potential independent, rather than by an increase in the average Ni valence (**Figure 4.9c**). We believe that this is caused by the fact that not all the Ni sites in the NiOOH used in our experiments are perfectly identical. Instead, the local environments of the Ni sites vary and so do their catalytic activities toward amine oxidation. When we consider the steady state balance of sites that will be oxidized vs reduced at a given applied bias, the least reactive sites toward amine oxidation are the ones most likely to be in the

oxidized state (since they would be slowest to react with amine and be reduced) while the most active sites toward amine oxidation are the most likely to be in the reduced state. Accordingly, when the applied bias is increased (increasing the driving force for Ni oxidation), the accompanying increase in the steady state average Ni valence is primarily caused by an increased number of these most reactive sites being in the oxidized state rather than the reduced state. This in turn means the average reactivity of the oxidized sites toward amine oxidation will be higher (i.e. $k_{obs,ind}$ will be higher). This occurs not because the higher applied bias has done anything to make any individual site more reactive, but rather because applying a higher bias means the most active sites toward amine oxidation will comprise a greater proportion of the Ni sites in the oxidized (rather than reduced) state. This appears to have had a greater relative effect on propylamine than the more reactive benzylamine, perhaps because benzylamine is sufficiently reactive that even the less active Ni sites are already enough to ensure rapid benzylamine oxidation.

4.2.6 KIE experiments

To gain further insight into what steps are important for determining the rate of PD and indirect oxidation of primary amines, we performed experiments comparing the results of oxidation of normal propylamine and benzylamine with oxidation of propyl-d_7-amine and benzyl-α,α-d_2-amine to test whether substituting the hydrogens at the alpha position for deuterium results in a primary KIE effect. We did this first by comparing CVs taken at pH 13 with 10 mM solutions of the normal and deuterium substituted amines. The results are shown in **Figure 4.10** and reveal that, for both propylamine and benzylamine, deuterium substitution does anodically shift the peak corresponding to amine oxidation, though the effect on the peak current achieved is minimal. These results qualitatively indicate there is at least a modest kinetic isotope effect (KIE) caused by deuterium substitution.

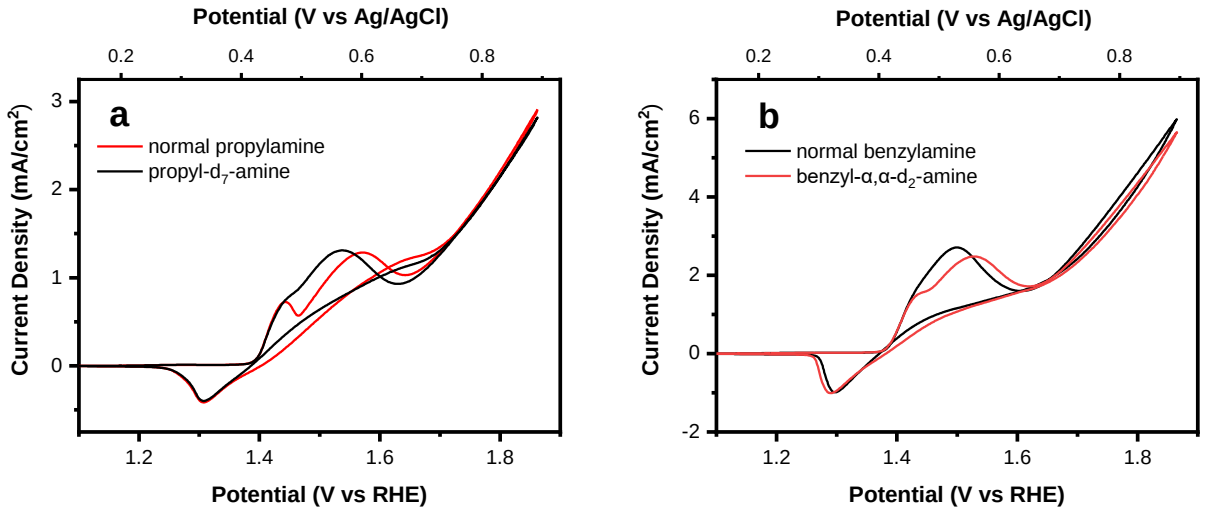

Figure 4.10. CVs collected using a $Ni(OH)_2$ working electrode in pH 13 solutions with 10 mM normal (black) and deuterated (red) solutions of (a) propylamine and (b) benzylamine (scan rate, 10 mV/s).

To gain more detailed information into the extent of this KIE and whether it differs for PD and indirect oxidation, we also compared the results of rate deconvolution experiments for normal and deuterium substituted amines taken with pH 13, 10 mM solutions at 1.52V vs RHE. The resulting 1/charge plots are shown in **Figure 4.11** while the comparison of the partial currents is shown in **Figure 4.12**.

These results show that, for the indirect process, there is a modest kinetic isotope effect evident for both propylamine (I_H/I_D = 1.3) and benzylamine (I_H/I_D = 1.4). Notably, these measured KIE values are much lower than the KIE of ~7 reported by Fleischmann *et al.* for methanol oxidation.[17] Instead, the more modest values found here are consistent with the other results reported throughout our pH, concentration, and potential dependence sections which highlight that both amine adsorption and regeneration of oxidized Ni sites play a meaningful role in determining the rate of the indirect process. All told, then, our data suggests that rather than being determined solely by the rate of the HAT step as implied by Fleischmann *et al.'s* proposed mechanism

(**Scheme 4.2**), the rate of the indirect process is actually controlled by a more complex interplay between several steps, with the HAT step being but one.

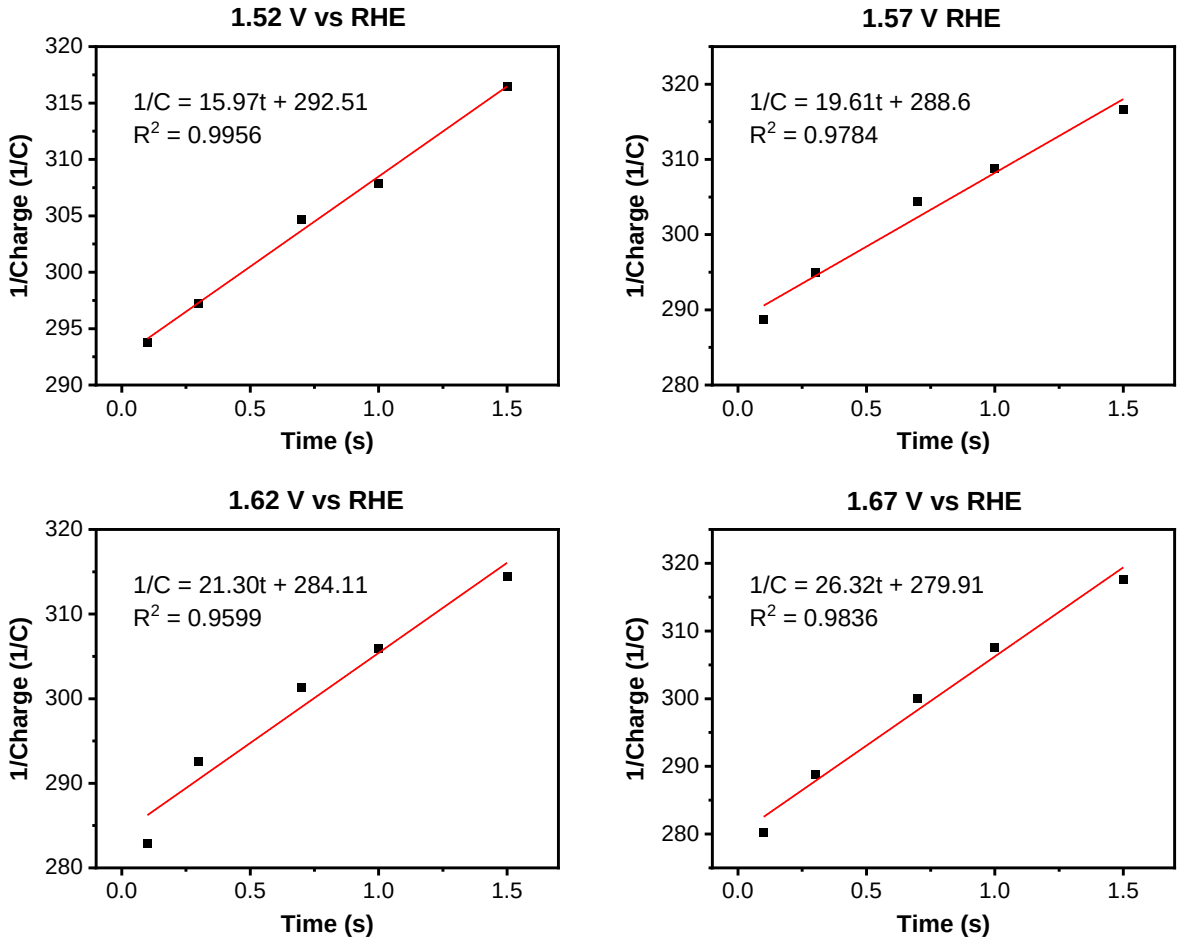

Figure 4.11. 1/Charge vs time plots measuring the disappearance of positive charge from NiOOH films pre-oxidized at different potentials as a function of time immersed at open circuit in rapidly stirred pH 13 solutions with 10 mM propylamine.

The KIE observed for the PD pathway is also quite small. For propylamine there is a modest KIE observed for the PD pathway (I_H/I_D = 1.3) while for benzylamine the KIE is negligible. As was the case for the indirect pathway, the data discussed above indicates that amine adsorption and regeneration of Ni^{4+} play an important role in determining the rate of PD oxidation, which explains the small/negligible effects observed here. Furthermore, as was mentioned in the pH

dependence section, the fairly strong effect of pH on the rate of the PD process indicates that the deprotonation step that accompanies hydride transfer likely has an important effect on the rate. When paired with the modest/negligible KIE observed here, this suggests that (at least in pH 13 solutions) this deprotonation step might play a greater role in controlling the rate than does the hydride transfer step, particularly for benzylamine which shows the greater pH dependence and a negligible KIE for PD oxidation.

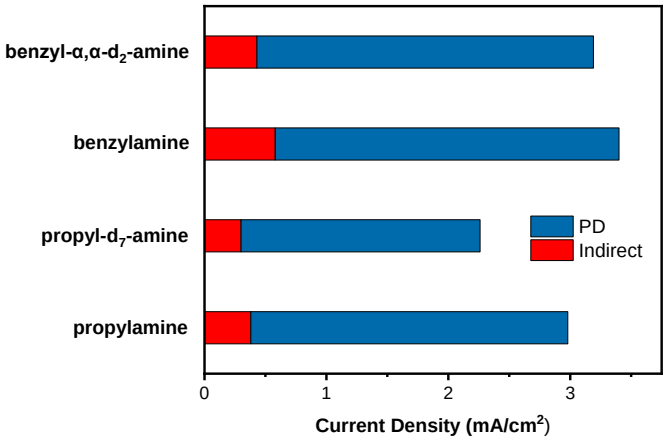

Figure 4.12. The component of the current due to indirect (red) and PD (blue) oxidation of pH 13 solutions with 10mM concentrations of normal and deuterated benzylamine or propylamine at 1.52 V vs RHE.

4.3 Conclusion

The present work offers a comprehensive look at the mechanism for oxidation of primary amines to nitriles on NiOOH electrocatalysts. It demonstrates that, as is the case for alcohol and aldehyde oxidation on NiOOH, primary amine oxidation occurs through two concurrent mechanisms, indirect oxidation and PD oxidation. In fact, as is the case for alcohol oxidation, amine oxidation on NiOOH occurs predominantly through the PD pathway. We also investigated how the rates of PD and indirect oxidation are influenced by a variety of factors including pH, concentration, applied potential, and deuterium substitution. The results reveal that, for both

pathways, the rate is determined by a complex interplay between several steps including adsorption of the amines, the hydrogen atom/hydride transfer step, regeneration of higher valent Ni sites, and (for PD oxidation) deprotonation of the amine. The kinetics cannot be reduced to a single controlling step for either pathway and indeed the relative impact of each of the steps mentioned varies with changes to the solution conditions, applied potential, and the nature of the amine being oxidized. There are, however, a few general statements that can be made. Across the concentration range examined in this work (5 mM to 50 mM) the coverage of the active sites with adsorbed amine is not complete and can be increased by increasing the amine concentration in solution. Moreover, for all the conditions examined here the average Ni valence is substantially lower in the presence of the amines than when no amine is present and decreases further if the amine concentration increases. This effect is more pronounced when a more reactive amine is used. This demonstrates that the kinetics for $Ni(OH)_2$ oxidation are not sufficient to keep all the Ni sites fully oxidized in the presence of the amine solution and means the regeneration of oxidized Ni sites plays an important role in determining the rate of amine oxidation through both pathways. Accordingly, properly understanding the effect each reaction condition (pH, potential, amine reactivity and concentration) has on the consumption and regeneration of higher valent Ni sites is critical to accurately interpreting results and to being able to predict what effect varying those conditions will have.

Overall, this work provides a comprehensive examination of the mechanism of primary amine oxidation on NiOOH. Moreover, the strong similarity between the results found here for amine oxidation and the results we have previously reported for alcohol and aldehyde oxidation indicates that this mechanistic framework provides a good foundation to understand a much broader set of dehydrogenation reaction on MOOH electrocatalysts.

4.4 Experimental Section

4.4.1 Materials.

The chemicals employed were all acquired from commercial sources and used without further purification. Benzylamine (99%, Sigma Aldrich), propylamine (≥99%, Sigma Aldrich), n-propyl-d_7-amine (CDN isotopes, 99.4%-d_7), benzyl-α,α-d_2 alcohol (CDN isotopes, 99.4%-d_2), potassium hydroxide (≥85%, Sigma Aldrich), $Ni(NO_3)_2 \cdot 6H_2O$ (99%, Acros), KNO_3 (99%, Alfa Aesar), $KClO_4$ (≥99%, Sigma Aldrich), boric acid (≥99.5%, Sigma Aldrich). All solutions were prepared using deionized water (Barnstead E-pure water purification system, resistivity >18 MΩ cm).

4.4.2 $Ni(OH)_2$ Electrode Preparation.

α-$Ni(OH)_2$ films were prepared using an established technique in which nitrate is electrochemically reduced.[22] This produces hydroxide and raises the local pH at the working electrode (WE), causing $Ni(OH)_2$ to precipitate out and form a $Ni(OH)_2$ film. This process was controlled using an SP-200 potentiostat/EIS (BioLogic Science Instrument) and conducted with a 3-electrode setup in a single compartment glass cell. The WE was fluorine doped tin oxide (FTO), the counter electrode (CE) was Pt, and the reference electrode (RE) was Ag/AgCl (4 M KCl). To prepare the FTO WE, larger FTO plates were cut into 2.5 cm x 1 cm strips after which Cu tape was affixed to the top to provide electrical contact and the FTO with masked with electroplating tape (3M Company) with a 0.5 cm^2 hole punched in it to ensure a well-defined conductive surface area was exposed. The Pt counter electrodes were prepared by sputter coating a 20 nm Ti adhesion layer followed by 100 nm of Pt onto clean glass slides. The $Ni(OH)_2$ films were deposited by galvanostatically maintaining a current of -0.25 mA/cm^2 for 45 s in an aqueous plating solution

consisting of 10 mM $Ni(NO_3)_2 \cdot 6H_2O$ and 30 mM KNO_3. The resulting $Ni(OH)_2$ films were rinsed with >18 MΩ cm water and then dried with an air stream.

4.4.3 Electrochemical Experiments.

CVs and electrolyses were performed using a 3-electrode setup in a sealed glass cell. For CVs, the cell was undivided while for the electrolyses the cell used had a glass frit separating the WE and CE compartments. $Ni(OH)_2$ films were used as the WE, Ag/AgCl as the RE and Pt mesh as the CE. CVs were performed starting from open circuit and the potential was swept at a scan rate of 10mV/s in the positive direction first. For all CVs the potential was cycled at least twice and the curves shown are from the second cycle. For the stirred CVs, the solution was rapidly stirred using a magnetic stir bar throughout the time the potential was being scanned.

Electrolyses were performed at a constant potential in a rapidly stirred amine solution until the stochiometric charge required for 25% (pH 13, 14) or 12.5% (pH 12) conversion of the initial amine to nitrile had been passed. A lower charge passed was used for the least reactive case (pH 12) to allow for more rapid completion of the electrolyses. In all cases, we chose to pass only part of the charge required for full conversion to ensure that the results would accurately reflect the selectivities and Faradic efficiencies of the rate deconvolution experiments, as these were conducted with amine concentrations equal to the concentrations at the beginning of the electrolyses. The pH of all solutions used for our electrochemical experiments was adjusted using KOH. For the CV and rate deconvolution experiments the pH 12 solutions could be used unbuffered as the minimal amount of charge passed meant pH drift would not be an issue even without a buffer. In these cases 90mM $KClO_4$ was added to the pH 12 solutions as supporting electrolyte to ensure they had sufficient solution conductivity. For the electrolyses, the pH 12 solutions were instead buffered using 0.5 M borate.

4.4.4 Product Analysis.

The electrolysis products were quantified by ^{1}H NMR spectroscopy using a Bruker Avance III 400 MHz NMR spectrometer. Samples were prepared by adding 0.450 mL of the electrolysis solution and 0.050 mL of D_2O to an NMR tube and shaking vigorously. The analyses were conducted with a relaxation delay of 30 s and used a WATERGATE method with excitation sculpting to remove the background signal from the water solvent. Product quantification was performed by comparing the integrations of the product peaks of the post electrolysis solutions to those of standards of known concentration.

4.4.5 Rate Deconvolution Procedure.

A detailed explanation of our three-step rate deconvolution procedure can be found in Chapter 2; so only a briefer overview and description of the specific experimental parameters used in this study will be outlined here. The process was performed using a rapidly stirred, 30mL amine solution in a single-cell glass sealed cell with a 3-electrode setup. A thin $Ni(OH)_2$ film deposited using the methods described above was used as the WE, Ag/AgCl as the RE, and Pt mesh as the CE. Before being used for the rate deconvolution experiments each $Ni(OH)_2$ film was tested by CV (2 cycles with switching potentials of 1 V vs Ag/AgCl and 0 V vs Ag/AgCl (pH 12), 0.9V vs Ag/AgCl and 0 vs Ag/AgCl (pH 13), or 0.8V vs Ag/AgCl and 0V vs Ag/AgCl (pH 14)) to confirm the $Ni(OH)_2$/NiOOH peak and water oxidation behavior of each film was consistent.

In the first step of the three-step procedure, a fixed potential was applied to the WE in a rapidly stirred solution long enough for the current to reach a steady state value (typical 30 s). This converts the film into the steady state condition it would be in during a potentiostatic electrolysis at the applied potential. During this step both the indirect and PD oxidation pathways are active. For the second step, the potential is no longer applied, leaving the film to sit in the stirred solution

under open circuit conditions. During this time neither the PD pathway nor reoxidation of $Ni(OH)_2$ can occur (since both require applied bias); however, the indirect pathway, which proceeds through a chemical (rather than electrochemical) HAT step still occurs. This reduces a portion of the higher valent Ni sites generated during the first step back to $Ni(OH)_2$. During the third step, the higher valent Ni sites that still remain after step 2 are rapidly reduced back to $Ni(OH)_2$ by sweeping the potential from open circuit to 0 V vs Ag/AgCl at a scan rate of 1V/s and then holding the potential at 0V for 20 s. The magnitude of the charge passed during this third, reductive step corresponds to the amount of charge that was still stored in the film after a portion of it was used in step 2 to oxidize the amine through the indirect pathway. By repeating the whole 3-step process with different times stirring at open circuit in step 2, we could construct plots showing the disappearance of charge from the film as a function of time at open circuit. This was used to generate kinetics equations and determine the rate of charge loss from the NiOOH film at 0s at open circuit, which corresponds to the rate of the indirect pathway under electrolysis conditions at the potential applied in step 1.

When conducting the rate deconvolution trials for a given amine and condition, each data point in the 1/charge vs time points was obtained by averaging the results from four separate measurements obtained with four different $Ni(OH)_2$ films. During these trials, each $Ni(OH)_2$ film was replaced after being used to measure data for 4 different times at open circuit. Additionally, whenever the $Ni(OH)_2$ film was replaced the amine solution was replaced with a fresh solution. Finally, to compensate for small variations in the active Ni content from film to film and trial to trial, after the measurement was collected for each data point an additional instance of the 3-step procedure was performed immediately with 0.1 s as the time at open circuit in step 2. This was

used to adjust the measured charge stored in the NiOOH film during the previous trial using an adjustment described in Chapter 2.4.8.

4.4.6 Conversion from Ag/AgCl to the reversible hydrogen electrode (RHE)

All potentials were measured using a Ag/AgCl (4 M KCl) reference electrode (RE). To allow for easier comparison of results across pH values, in most cases these potentials have been converted to the RHE scale. This was done according to equation 5 where E_{RHE} is the potential on the RHE scale, $E_{Ag/AgCl}$ is the potential against the Ag/AgCl RE and pH is the solution pH.

$$E_{RHE} = E_{Ag/AgCl} + 0.197V + 0.0591V*pH \quad (5)$$

4.4.7 Calculation of Average Ni valence

The values reported for the average Ni valence in this work were calculated according to equation 6 below where Q_0 is the magnitude of the charge required to reduce the films from their steady state condition after step 1 of the rate deconvolution procedure back to $Ni(OH)_2$, n_{Ni} is moles of Ni in one of the $Ni(OH)_2$ films (previously determined by inductively coupled plasma mass spectrometry to be 23.6 ± 0.4 nmol for our films)[20], and F is Faraday's constant. Q_0 was obtained by taking the reciprocal of the y-intercept of the 1/charge vs time plots produced by the rate deconvolution trials.

$$\langle \text{Ni valence} \rangle = 2 + \frac{Q_0}{n_{Ni}F} \quad (6)$$

4.5 References

1. Yamaguchi, K.; Mizuno, N. Development of highly active heterogeneous oxidation catalysts based on the properties of metal hydroxides. *Top. Catal.* **2014**, *57*, 1196-1207.
2. Tseng, K.-N. T.; Szymczak, N. K. Dehydrogenative oxidation of primary amines to nitriles. *Synlett* **2014**, *25*, 2385–2389.
3. Schümperli, M. T.; Hammond, C.; Hermans, I. Developments in the aerobic oxidation of amines. *ACS Catal.* **2012**, *2*, 1108−1117.
4. Yan, G.; Zhang, Y.; Wang, J. Recent advances in the synthesis of aryl nitrile compounds. *Adv. Synth. Catal.* **2017**, *359*, 4068 – 4105.
5. Ray, R.; Hazari, A. S.; Lahiri, G. K.; Maiti, D. Ruthenium-catalyzed aerobic oxidation of amine. *Chem. Asian J.* **2018**, *13*, 2138 – 2148.
6. Xu, B.; Hartigan, E. M.; Feula, G.; Huang, Z. Lumb, J.-P.; Arndtsen, B. A. Simple copper catalysts for the aerobic oxidation of amines: selectivity control by the counterion *Angew. Chem. Int. Ed.* **2016**, *55*, 15802 –15806.
7. Kim, J.; Golime, G.; Kim, H. Y.; Oh, K. Copper(II)-catalyzed aerobic oxidation of amines: Divergent reaction pathways by solvent control to imines and nitriles. *Asian J. Org. Chem.* **2019**, *8*, 1674–1679.
8. Kim, J.; Stahl, S. S. Cu/nitroxyl-catalyzed aerobic oxidation of primary amines into nitriles at room temperature. *ACS Catal.* **2013**, *3*, 1652−1656.
9. Patil, R. D.; Gupta, M. K. Methods of nitriles synthesis from amines through oxidative dehydrogenation. *Adv. Synth.Catal.* **2020**, *362*, 3987–4009.
10. Hampson, N. A.; Lee, J. B.; Morley, J. R.; Scanlon B. Oxidations involving silver. V. The oxidation of primary aliphatic amines. *Can. J. Chem.* **1969**, *47*, 3729-3736.
11. Ye, J. Q.; Zhang, Z.-L.; Zha, Z.-G.; Wang, Z.-Y. A green and efficient access to aryl nitriles via an electrochemical anodic oxidation. *Chin. Chem. Lett.* **2014**, *25*, 1112-1114.
12. Xue, S.; Watzele, S.; Čolić, V.; Brandl, K.; Garlyyev, B.; Bandarenka, A. S. Reconsidering water electrolysis: Producing hydrogen at cathodes together with selective oxidation of n-butylamine at anodes. *ChemSusChem* **2017**, *10*, 4812 –4816.
13. Schäfer, H.-J. Oxidation of organic compounds at the nickel hydroxide electrode. *Top. Curr. Chem.* **1987**, *142*, 101–129.

14. Lyalin, B. V.; Petrosyan, V. A. Oxidation of organic compounds on NiOOH electrode. Russ. J. Electrochem. **2010**, *46*, 1199−1214.
15. Robertson, P. M. On the oxidation of alcohols and amines at nickel oxide electrodes: mechanistic aspects. *J. Electroanal. Chem. Interfacial Electrochem.* **1980**, *111*, 97−104.
16. Fleischmann, M.; Korinek, K.; Pletcher, D. The oxidation of organic compounds at a nickel anode in alkaline solution. *J. Electroanal. Chem. Interfacial Electrochem.* **1971**, *31*, 39−49.
17. Fleischmann, M.; Korinek, K.; Pletcher, D. The kinetics and mechanism of the oxidation of amines and alcohols at oxide-covered nickel, silver, copper, and cobalt electrodes. *J. Chem. Soc., Perkin Trans. 2* **1972**, *10*, 1396−1403.
18. Taitt, B. J.; Nam, D.-H.; Choi, K.-S. A comparative study of nickel, cobalt, and iron oxyhydroxide anodes for the electrochemical oxidation of 5-hydroxymethylfurfural to 2,5-furandicarboxylic acid. *ACS Catal.* **2019**, *9*, 660−670.
19. Miao, Y.; Ouyang, L.; Zhou, S.; Xu, L.; Yang, Z.; Xiao, M.; Ouyang, R. Electrocatalysis and electroanalysis of nickel, its oxides, hydroxides and oxyhydroxides toward small molecules. Biosens. Bioelectron. **2014**, *53*, 428−439
20. Bender, M. T.; Lam, Y. C.; Hammes-Schiffer, S.; Choi, K.-S. Unraveling two pathways for electrochemical alcohol and aldehyde oxidation on NiOOH. *J. Am. Chem. Soc.* **2020**, *142*, 21538–21547.
21. Bender, M. T.; Warburton, R. E.; Hammes-Schiffer, S.; Choi, K.-S. Understanding hydrogen atom and hydride transfer processes during electrochemical alcohol and aldehyde oxidation. *ACS Catal.* **2021**, *11*, 15110–15124.
22. Kang, D.; Kim, T. W.; Kubota, S. R.; Cardiel, A. C.; Cha, H. G.; Choi, K.-S. Electrochemical synthesis of photoelectrodes and catalysts for use in solar water splitting. *Chem. Rev.* **2015**, *115*, 12839−12887.

Chapter 5: Electrochemical Oxidation of HMF via Hydrogen Atom Transfer and Hydride Transfer on NiOOH and the Impact of NiOOH Composition on These Mechanisms

Portions of this chapter have been adapted from:

Bender, M. T.; Choi, K.-S. Electrochemical oxidation of HMF via hydrogen atom transfer and hydride transfer on NiOOH and the impact of NiOOH composition on these mechanisms. *ChemSusChem.* **2022**, e202200675. DOI: 10.1002/cssc.202200675

5.1 Introduction

Currently, production of a wide variety of chemicals relies upon nonrenewable precursors derived from fossil fuels, which raises environmental and sustainability related concerns.[1,2] One method to address these concerns is to replace the fossil fuel derived precursors with biomass derived ones, thereby opening up renewable and carbon neutral pathways to access a variety of chemicals.[3,4] One transformation in particular that has garnered a great deal of attention is the electrochemical oxidation of 5-hydroxymethylfurfural (HMF), which can be produced from biomass derived cellulose and hemicellulose, to 2,5-furandicarboxylic acid (FDCA), a molecule most notable for being a possible replacement for the petroleum derived terephthalic acid in the production of widely used polymers such as polyethylene terephthalate (PET).[5,6] The electrochemical route for upgrading HMF to FDCA is particularly appealing since it can occur effectively at ambient temperatures and pressure, does not require the addition of chemical oxidizing agents, can be catalyzed by inexpensive electrocatalysts (both homogeneous and heterogeneous), and can be driven by electricity produced from renewable sources.[5-9] Furthermore, HMF oxidation can be coupled with cathode reactions that produce valuable fuels and chemicals, further enhancing the economic appeal of the approach.[10-12]

A variety of materials have been investigated as potential electrocatalysts for oxidation of HMF to FDCA and NiOOH based ones have emerged as among the most promising, able to convert HMF to FDCA with near quantitative yields and Faradic efficiency (FE). [5,9,13-17] Despite these impressive results, however, there are still many questions remining about the mechanism of this oxidation. Most works have assumed this reaction proceeds though the long-established indirect mechanism proposed by Fleischmann *et al*. for oxidation of alcohols and amines on NiOOH (and later extended to include aldehyde as they are oxidized after undergoing an initial hydration to form a 1,1-geminal diol) (**Scheme 5.1**).[6,9,18-21] In this mechanism, $Ni(OH)_2$ is first

oxidized to NiOOH by the applied bias. This NiOOH then acts as a chemical oxidizing agent, reacting with alcohols through a non-electrochemical and rate limiting hydrogen atom transfer (HAT) from the carbon at the alpha position of the alcohol (or geminal diol in the case of aldehyde oxidation) to a Ni^{3+} site in the NiOOH, thereby reducing the NiOOH back to $Ni(OH)_2$.[18,19] In such a mechanism, the applied bias does not directly drive the oxidation of HMF but instead is simply important for continuously regenerating the chemical oxidizing agent NiOOH, which is therefore needed only in a catalytic amount rather than a stochiometric amount.

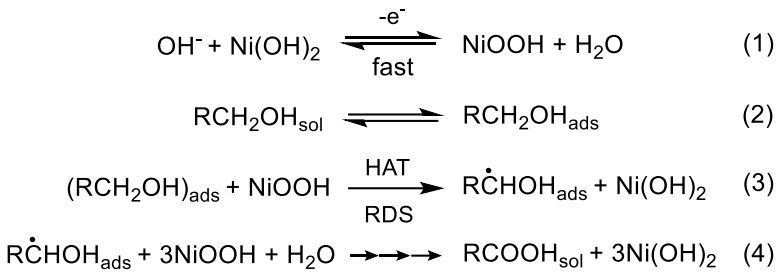

Scheme 5.1. Literature mechanism proposed by Fleischmann *et al.* for the indirect oxidation of alcohols at NiOOH electrodes in alkaline aqueous media.[19] Aldehyde oxidation is proposed to occur after an initial hydration to form the 1,1-geminal diol (an alcohol), after which it undergoes an equivalent oxidation mechanism to form the carboxylic acid.

In our previous work on the use of transition metal oxyhydroxides as electrocatalysts for HMF oxidation, we reported that in addition to the well-known indirect mechanism, there is also a second, potential dependent oxidation mechanism enabled at potentials more positive than those needed for the $Ni(OH)_2$/NiOOH transition.[9] Since this second mechanism should be different from the indirect mechanism which involves the conversion of NiOOH to $Ni(OH)_2$, we speculated that in this second mechanism NiOOH may remain as NiOOH throughout the oxidation and referred to it as direct oxidation to give a contrast to indirect oxidation.[9] We did not, however, closely probe this second mechanism in our earlier HMF oxidation study because HMF possesses both an

alcohol and aldehyde functional group, which can complicate the mechanistic analysis, and therefore HMF is not the best model system to study for elucidating this second mechanism.

In order to investigate the second mechanism, we developed an electroanalytical technique that allowed us to deconvolute the rates of the two oxidation mechanisms and applied it to study the oxidation of a variety of simple alcohols and aldehydes first.[22,23] The results revealed that our initial speculation that this second pathway involved oxidation on NiOOH with no change in the oxidation state of Ni^{3+} was incorrect. Instead, using a combination of experimental and computational results we showed that this second pathway is only active when Ni^{4+} is present and that it involves hydride transfer from the carbon at the alpha position of the alcohol (or geminal diol) to those Ni^{4+} sites (**Scheme 5.2**).[22,23] This hydride transfer is coupled with proton transfer from the alcohol group to a base in solution, which can occur either concurrently with or prior to (likely before adsorption in alkaline conditions) hydride transfer. Because this hydride transfer reduces the Ni^{4+} sites back to Ni^{2+}, this pathway cannot be called a direct pathway. Another critical difference between indirect oxidation and this second pathway is the role the applied bias plays. For the second pathway, the application of a positive bias is necessary not only to generate the active Ni^{4+} sites but also to drive the hydrogenation reaction. As a result, the rate of oxidation through this pathway is potential dependent and it drops to zero as soon as bias is no longer applied even if Ni^{4+} remains. As a result, we refer to this pathway as potential dependent (PD) oxidation (**Scheme 2**).

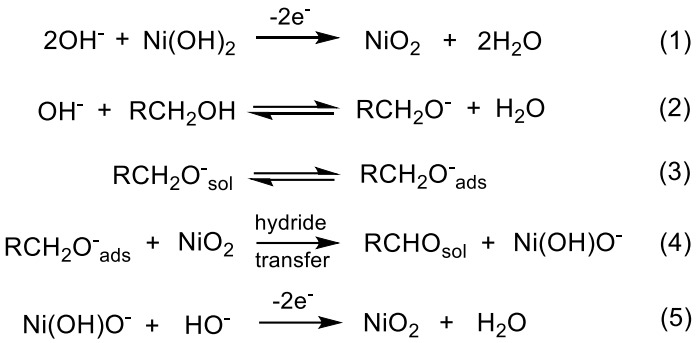

Scheme 2. Hydride transfer mechanism we have previously proposed for oxidation of alcohols to aldehydes through the PD oxidation pathway.[23] Aldehyde oxidation occurs though an equivalent mechanism as it exists in equilibrium with its hydrated form, the 1,1-geminal diol, a type of alcohol which can undergo the same oxidation mechanism to form the carboxylic acid.

From our studies investigating dehydrogenation mechanisms of simple alcohols and aldehydes, we established a general and comprehensive understanding of indirect and PD pathways and how they are affected by various factors.[22,23] Our new understanding includes that aldehyde oxidation occurs preferentially through indirect oxidation while alcohol oxidation favors PD oxidation. Using this new understanding and the electroanalytical method we developed to deconvolute the rates of the indirect and PD oxidation, we are now well positioned to return to the more complicated case of HMF oxidation. Accordingly, the purpose of this study is two-fold. The first goal is to develop an accurate understanding of the mechanism(s) for oxidation of HMF on NiOOH as well as the various intermediates along the way to FDCA. This includes understanding whether these oxidations occur though the indirect or PD pathway, what steps tend to limit the reaction rate, and whether HMF tends to first undergo aldehyde oxidation to form 5-hydroxymethyl-2-furancarboxylic acid (HMFCA) or alcohol oxidation to form 2,5-diformylfuran (DFF) (**Scheme 5.3**). The second goal is to use this understanding and our knowledge of the indirect and PD pathways to evaluate the effects of incorporating metal ions into NiOOH electrocatalysts to shift the potential of the $Ni(OH)_2$/NiOOH couple. Understanding the impact

NiOOH composition has on the two dehydrogenation mechanisms of NiOOH will be highly valuable to future studies trying to rationally design next generation catalysts for various electrochemical dehydrogenation reactions.

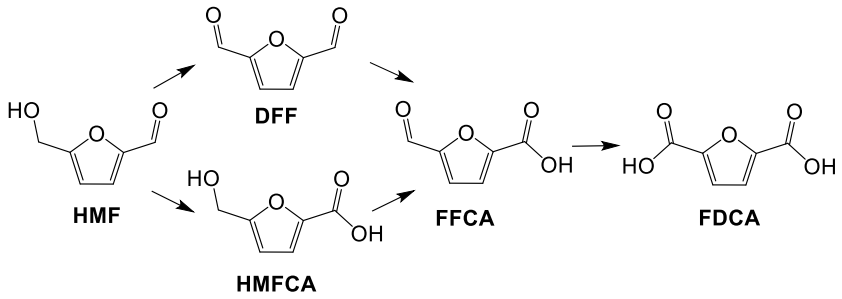

Scheme 5.3. Scheme depicting two possible routes for oxidation of HMF to FDCA. HMF can either undergo initial alcohol oxidation to form DFF or can instead undergo initial aldehyde oxidation to form HMFCA.

5.2 Results and Discussion

$Ni(OH)_2$ film on a flat, 2D fluorine doped tin oxide (FTO) substrate. The $Ni(OH)_2$ film is thin enough that the scanning electron microscopy (SEM) images of the FTO substrate with and without this film look comparable (**Figure 5.1**). The use of thin films in this study minimizes the heterogeneity in the local environments of Ni sites as well as any impacts that the porosity or depth of the electrocatalyst could have on the transport or adsorption of the organic species within the electrocatalysts. This is critical to obtaining results that accurately reflect the intrinsic oxidation mechanisms of NiOOH.

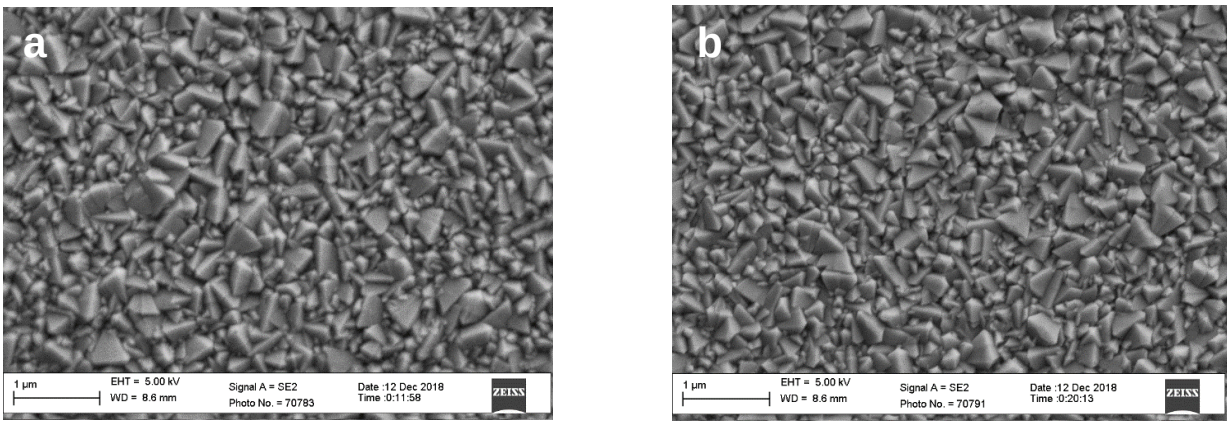

Figure 5.1. Scanning electron microscope (SEM) images of (a) an as-deposited $Ni(OH)_2$ film deposited on an FTO substrate and (b) a bare FTO substrate. The images look comparable as the $Ni(OH)_2$ film is too thin to alter the surface morphology.

5.2.1 Qualitative assessment through CV.

To begin, we collected cyclic voltammograms (CVs) in pH 13 solutions using a $Ni(OH)_2$ working electrode (WE) in the presence and absence of 5 mM solutions of HMF, HMFCA, DFF, and 5-formyl-2-furancarboxylic acid (FFCA) (**Figure 5.2**). We chose to use pH 13 for this study as we have previously shown HMF is unstable in pH 14 solutions,[24] which would complicate mechanistic analysis. The CVs were collected in a rapidly stirred solution whose stirring speed was chosen such that further increasing the stirring speed no longer enhanced the oxidation current. This prevented depletion of the organic species (or hydroxide) around the electrode from having an effect on the current profiles associated with the indirect and PD pathways. Rapidly stirring the solution has the same effect of preventing depletion of species around the electrode surface as using a rotating disc electrode while allowing us to use the same NiOOH electrode in the same setup for all experiments performed in this study (CVs, rate deconvolution analysis, constant potential electrolysis).

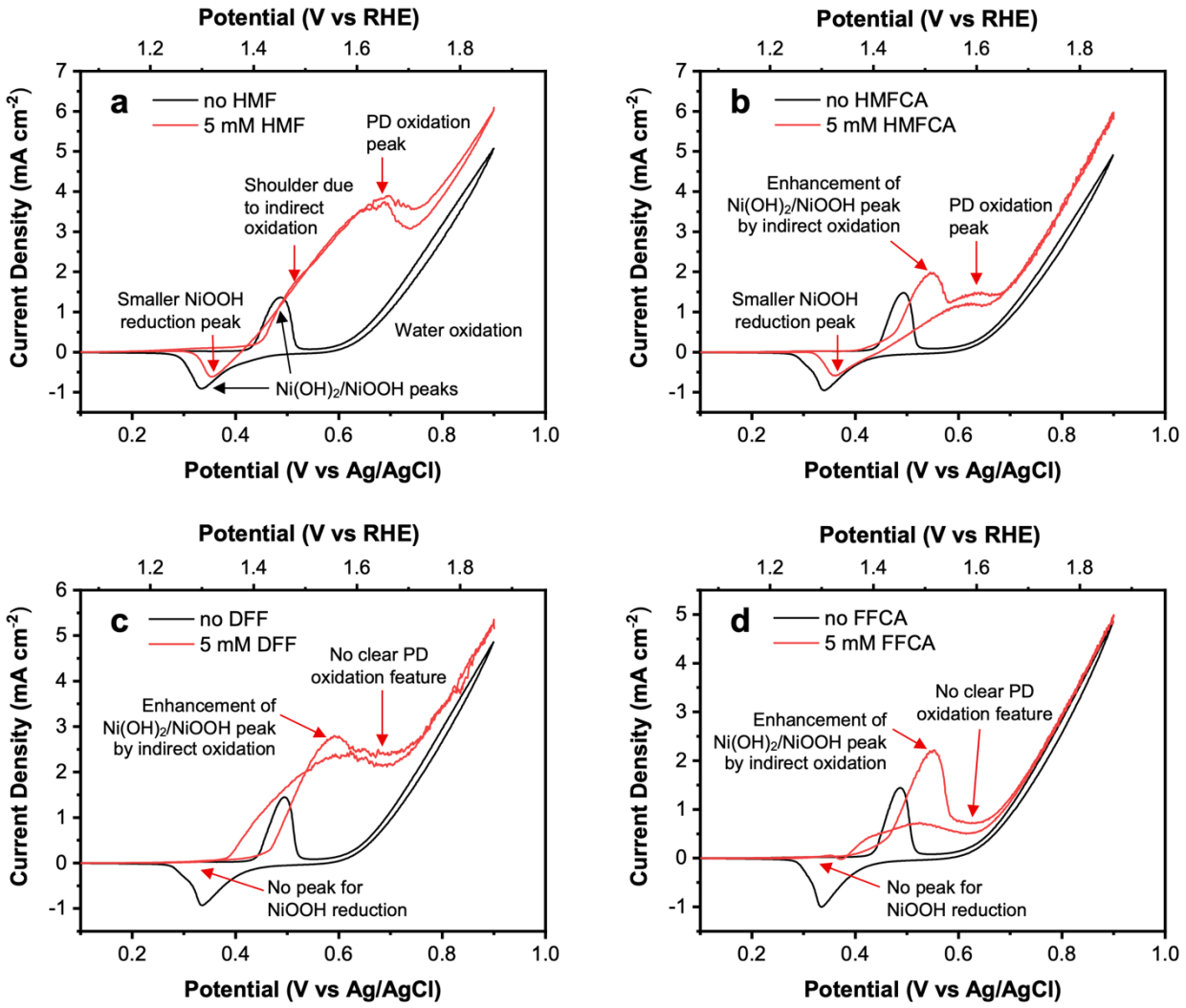

Figure 5.2. CVs collected using a $Ni(OH)_2$ working electrode in pH 13 solutions with (red) and without (black) 5mM solutions of (a) HMF and (b) HMFCA, (c) DFF, (d) FFCA (scan rate, 10 mV/s). The solutions were rapidly stirred to eliminate the effect of mass-transport limitations.

All CVs were recorded by first sweeping the potential from open circuit in the positive direction and then returning to the initial potential. In CVs collected in the presence of an organic species, the indirect oxidation of the organic species appears as an increase in the $Ni(OH)_2$ oxidation peak during the forward scan and a decrease in the NiOOH reduction peak during the reverse scan.[22,23] This is because when $Ni(OH)_2$ is oxidized to NiOOH during the forward scan, the concurrent indirect oxidation of organic species by NiOOH converts NiOOH back to $Ni(OH)_2$.

As a result, more charge is passed oxidizing $Ni(OH)_2$ to NiOOH during the forward scan. During the reverse scan, since some of the NiOOH is reduced back to $Ni(OH)_2$ by the indirect oxidation of organic species, less charge is required to reduce NiOOH to $Ni(OH)_2$, diminishing the reduction peak.[22,23] In the presence of each of the organic species tested here some degree of both enhancement in the $Ni(OH)_2$ oxidation peak and a diminishment in the NiOOH reduction peak are evident, suggesting that all are oxidized at least in part through the indirect pathway. Also, in the presence of all the organic species the position of the $Ni(OH)_2$ oxidation peak has been shifted anodically, though in the case of HMF the shift is less pronounced. The most likely explanation for the delayed onset of $Ni(OH)_2$ oxidation is that HMF, HMFCA, DFF, and FDCA adsorb on the Ni^{2+} sites, which stabilizes Ni in the 2+ state and makes its oxidation difficult. This observation will be revisited in a discussion further below as it turned out to be important for understanding the oxidation mechanisms of HMFCA, DFF, and FDCA.

Unlike indirect oxidation, PD oxidation typically appears in CVs as a second oxidation feature occurring at more anodic potentials than the $Ni(OH)_2$/NiOOH redox couple. Additionally, as the name implies, this feature typically shows a clear potential dependence as, unlike indirect oxidation, its rate is driven by the applied bias and not by the oxidizing power of the NiOOH couple.[22,23] We note that the species containing only an aldehyde (DFF, FFCA) do not show any clear indication of a PD oxidation feature, instead showing only the enhancement of the $Ni(OH)_2$ oxidation peak characteristic of indirect oxidation. Additionally, the cathodic peak corresponding to the reduction of NiOOH to $Ni(OH)_2$ is entirely absent from the reverse scan. This indicates that DFF and FFCA are oxidized predominantly though the indirect mechanism and that this process is fast enough to consume all the Ni^{3+} before it can be electrochemically reduced during the reverse scan. In contrast, for the species containing an alcohol (HMF, HMFCA), the current profiles are

different. For HMFCA, in addition to the enhancement of the $Ni(OH)_2$ oxidation peak at ~0.55 V vs Ag/AgCl indicative of indirect oxidation there is a clear second feature that occurs at ~0.64 V vs Ag/AgCl, well after the $Ni(OH)_2$ oxidation peak. Similarly, HMF also shows two features, though they do overlap. The first is a shoulder at ~0.5 V vs Ag/AgCl, which corresponds to the position of $Ni(OH)_2$ oxidation and thus is related to indirect oxidation while the second feature, attributable to PD oxidation, peaks at the more anodic potential of ~0.69 V vs Ag/AgCl. Additionally, unlike with DFF and FFCA, CVs of HMF and HMFCA show a notable reductive wave corresponding to NiOOH reduction during the reverse scan, meaning the indirect process is not fast enough to fully consume Ni^{3+}. Together, these results suggest HMF and HMFCA are primarily oxidized through the PD process. Finally, we note that as these CVs were obtained in rapidly stirred solutions, any decrease in oxidation current when the potential is swept in the positive direction is not due to the depletion of the organic species. Instead, it is evidence that the electrocatalyst becomes less active for oxidation of the organic species as the potential is swept to values closer to triggering the onset of the oxygen evolution reaction (OER). Using a combination of experimental and theoretical results, we have shown in a prior work that the most likely cause for this deactivation of NiOOH toward oxidation of alcohols and aldehydes at more anodic potential is an increase in the competition with hydroxide for adsorption on Ni^{4+}.[23] Moreover, in that work we showed that this competition affects aldehyde adsorption on Ni^{4+} more considerably than it does alcohol adsorption and therefore causes the current decay to initiate at less positive potentials for aldehyde oxidation than for alcohol oxidation.[23]

5.2.2 Quantitative assessment through rate deconvolution.

While the CVs discussed above can give a qualitative guide to which oxidation pathway is preferred, to achieve a quantitative measurement it is necessary to use the rate deconvolution

procedure we developed to separate the rates of the two pathways. A detailed description of this procedure and the principles behind can be found in Chapter 2, so only an overview will be provided here. In brief, the procedure is a method to first isolate and measure the rate of the chemical reaction between NiOOH and an organic species, a measurement which is equivalent to the rate of the indirect process. Then, assuming the potential being examined is one where only oxidation of the organic species is possible, we can note that the overall current (I_{tot}) will simply be the sum of the partial currents for PD (I_{PD}) and indirect (I_{ind}) oxidation (equation 1). Since I_{tot} can be measured easily, once I_{ind} is known equation 1 can be used to calculate $I_{PD.}$

$$I_{tot} = I_{PD} + I_{ind} \quad (1)$$

In order to isolate and measure I_{ind}, we perform a series of short, 3-step procedures. In the first step, a constant potential is applied at the $Ni(OH)_2$ WE in a solution containing the organic species and being stirred rapidly with the same speed used for the CV experiments. This ensures that the concentrations of solution species at the electrode surface do not change over time and thus are effectively "flooded". During this first, constant potential step the NiOOH film is converted into the same state it would be in during a constant potential electrolysis at the chosen potential in the tested solution. In the second step the potential is no longer applied and the NiOOH electrode is instead left to sit in the rapidly stirred solution at open circuit for a specific length of time. During this step, neither oxidation of $Ni(OH)_2$ nor PD oxidation can occur, since both require applied bias. NiOOH can, however, still react with the organic species as a chemical oxidizing agent like it does in the indirect pathway, oxidizing the organic species while being reduced back to $Ni(OH)_2$. In the third step, a reducing potential is applied to rapidly convert the NiOOH that still remains after the second step back into $Ni(OH)_2$. The charge passed during this step represents how much of the NiOOH "reactant" generated by the bias applied in the first step remained after

chemically reacting with the organic substrate in the second step with a reaction time equivalent to the time left at open circuit. By repeating this whole 3 step process for a variety of different times at open circuit in the second step, a data set can be obtained showing the disappearance of charge from the NiOOH film due to chemical reaction with the organic species as a function of time at open circuit. By examining whether [charge] vs *t*, ln[charge] vs *t*, or 1/[charge] vs *t* plots give a good linear fit for the data, we can determine whether this reaction follows 0^{th}, 1^{st}, or 2^{nd} order kinetics with respect to charge in the NiOOH film and the observed rate constant for indirect oxidation ($k_{obs,ind}$) can be determined from the slope of the linear plot. We note that this is an observed rate constant ($k_{obs,ind}$) rather than a true rate constant (k_{ind}) because, as noted above, the rapid stir speed means the concentrations of solution species at the electrode surface are constant and can be incorporated into the rate constant according to equation 2 where *a* and *b* are the reaction order with respect to the organic species and hydroxide respectively.

$$k_{obs,ind} = k_{ind}[\text{organic species}]^{a}[OH^{-}]^{b} \quad (2)$$

By using $k_{obs,ind}$ and the kinetics equations we can solve for the rate of the chemical reaction at 0 seconds at open circuit which is when the NiOOH electrocatalyst is in the same state as it is in during a constant potential electrolysis at the potential applied in step 1 (see the experimental section for more details regarding these calculations). This is a measure of the partial current for the indirect process (I_{ind}) which, along with the steady state current observed in step 1 (I_{tot}), can be used to calculate I_{PD} using equation 1.

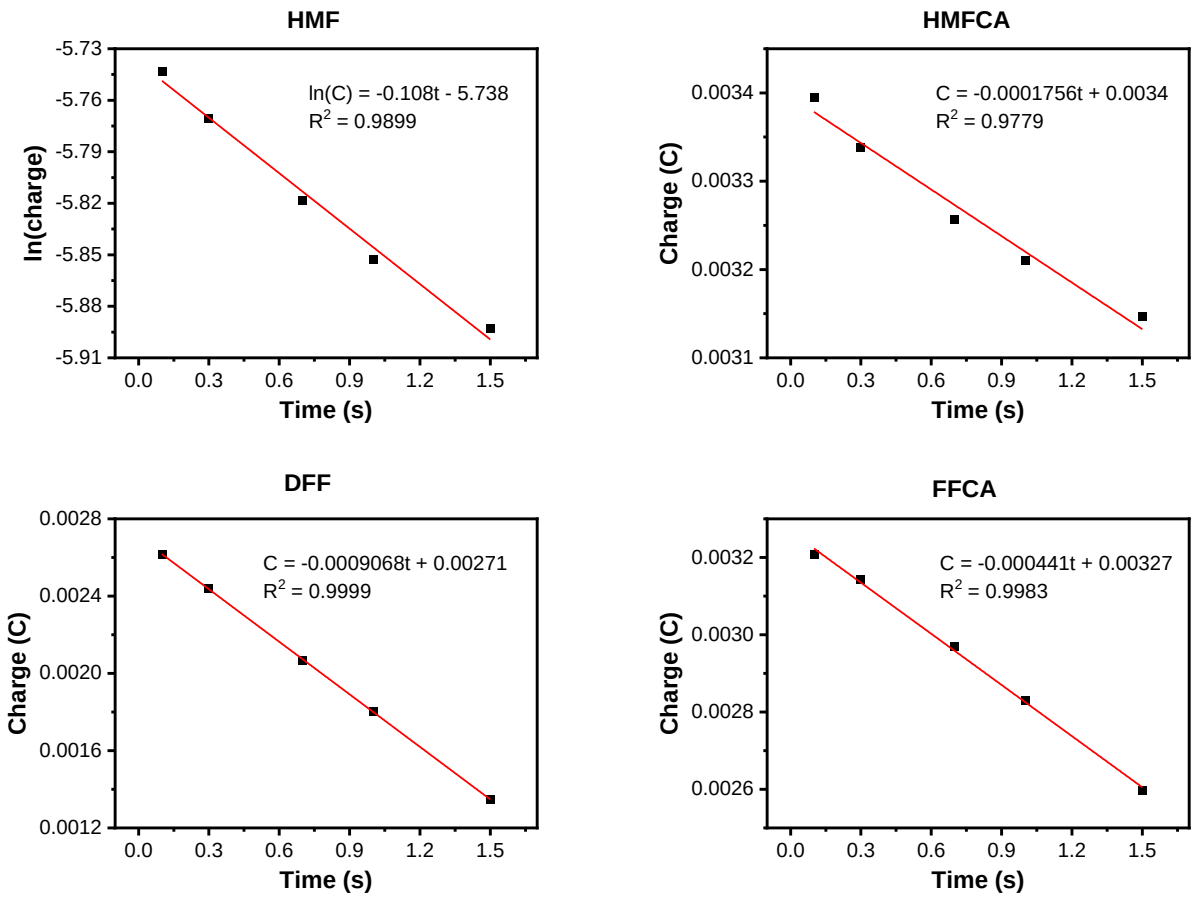

Figure 5.3. Plots showing the disappearance of positive charge as a function of time from NiOOH films due to indirect oxidation of 5 mM HMF, HMFCA, DFF, or FFCA in a rapidly stirred pH 13 solution. The linearity of the ln(charge) vs time plot for HMF indicates that the indirect oxidation of HMF can be modeled as a reaction with 1st order kinetics with respect to charge in the film. Conversely, the linearity of the charge vs time plots for HMFCA, DFF, and FFCA indicate that their indirect oxidation follows 0th order kinetics with respect to charge in the NiOOH films. In all cases the NiOOH used for these measurements was pre-oxidized at 0.55 V vs Ag/AgCl in the given solution.

The rate deconvolution experiments described above were performed for 5 mM solutions of HMF, DFF, HMFCA, and FFCA at pH 13 and 1.52 V vs RHE. The linear kinetics plots this resulted in (ln(charge) vs time for HMF and charge vs time for HMFCA, DFF, and FFCA) are shown in **Figure 5.3** while the deconvoluted partial current densities for indirect and PD oxidation

calculated form these are shown in **Figure 5.4**. The quantitative rate deconvolution results shown in Figure 5.4 agree well with the qualitative picture given by CVs in stirred solutions. HMF and its oxidation products all have an indirect component to their current; however, for HMF and HMFCA the PD pathway dominates, representing 72% and 73% of the overall current respectively. Conversely, for the species with only an aldehyde, the indirect process dominates instead, representing 67% of the current for DFF and 100% of the current for FFCA. The comparison between FFCA and DFF is also interesting in that DFF, which possesses 2 aldehyde groups, shows almost exactly double the indirect rate as FFCA, which has only one. Indeed, and perhaps unsurprisingly, the molecules with two active functional groups (HMF, DFF) are both substantially more reactive than those with only one (FFCA, HMFCA). This is likely because the presence of two reactive functional groups increases the probability that a collision between the molecule and the NiOOH surface will result in adsorption that can subsequently lead to oxidation.

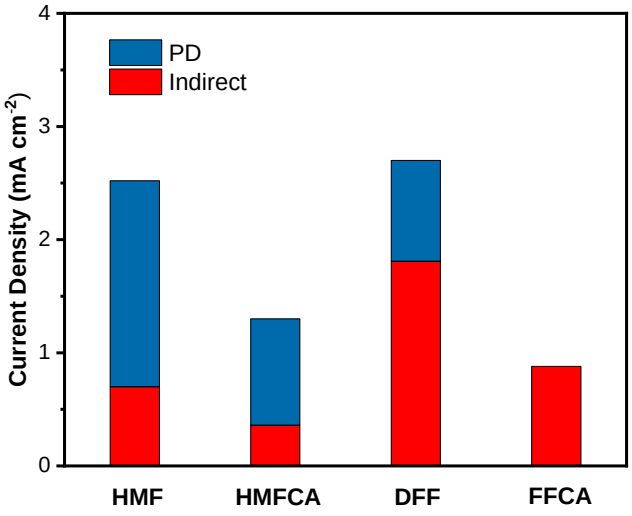

Figure 5.4. The component of the current due to indirect (red) and PD (blue) oxidation of 5 mM HMF, HMFCA, DFF, or FFCA in a pH 13 solution at 0.55 V vs Ag/AgCl.

5.2.3 Constant Potential Oxidation.

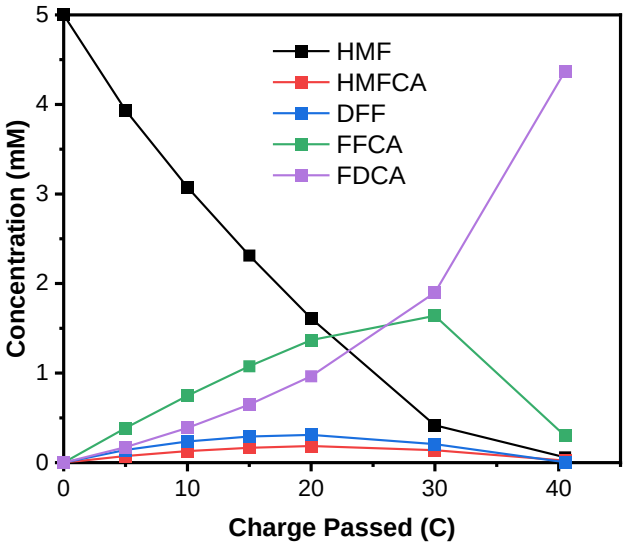

Figure 5.5. Change in concentration of HMF and its oxidation products over charge passed at 0.55 V vs Ag/AgCl in a pH 13 solution containing 5 mM HMF.

To further examine the process of HMF oxidation, we also performed a constant potential electrolysis at 0.55 V vs Ag/AgCl (1.52 V vs. RHE) in a pH 13 solution containing 5 mM HMF and analyzed the changes in solution composition as the electrolysis proceeded (**Figure 5.5**). FFCA is the dominant product observed until more than half the stoichiometric charge is passed, indicating the relatively slow FFCA oxidation step does play an important role in limiting the rate of FDCA formation. Looking at this result, one may think that the application of a more positive bias is needed to expedite the oxidation of FFCA to FDCA. However, an important new insight we obtained from the rate deconvolution analysis is that at this pH and concentration FFCA oxidation occurs entirely through the indirect pathway and therefore is not expected to be enhanced by applying more positive potentials. In fact, our previous study showed that the rate of aldehyde oxidation can actually decrease when a more positive bias is applied and more of the Ni^{3+} is converted to Ni^{4+}.[23] This is because unlike the Ni^{3+} sites, the Ni^{4+} sites are active for OER and thus

hydroxide ions will compete with aldehydes for adsorption on them. Because hydroxide adsorption tends to outcompete the aldehyde adsorption,[23] this can limit the current for aldehyde oxidation when increases to the applied potential increases the amount of Ni^{4+} sites and therefore limits the amount of aldehyde that is adsorbed on the NiOOH. Indeed, we confirmed that the steady state current for FFCA oxidation actually decreases as the applied potential increases (**Figure 5.6**). This counterintuitive result that the fastest FFCA oxidation on NiOOH can be achieved at a less positive bias can be understood only when the two dehydrogenation mechanisms of aldehyde on NiOOH are recognized and comprehensively understood.

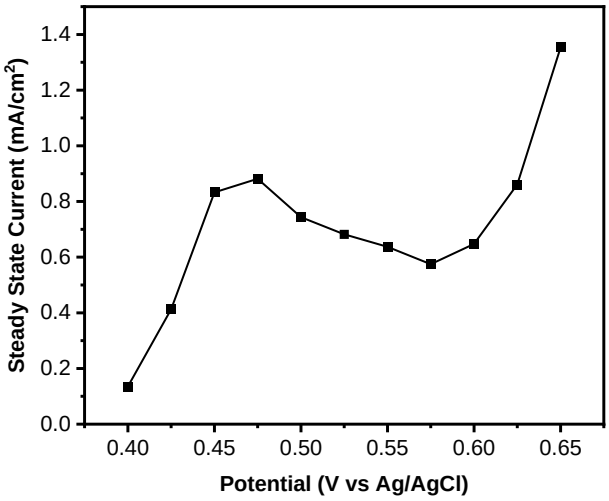

Figure 5.6. Plot depicting the steady state current achieved when different potentials are applied to a $Ni(OH)_2$ WE in a rapidly stirred pH 13 solution containing 5 mM FFCA. The exponential increase in the current density as the potential increases above 0.575 V vs Ag/AgCl is due to the onset of water oxidation.

Another interesting result shown in **Figure 5.5** is that DFF accumulates to almost twice the extent as HMFCA (0.31 mM vs 0.19 mM) despite the fact that DFF is more reactive, which suggests that HMF is converted to FFCA predominantly through the DFF route with the HMFCA route occurring as a minor pathway under our conditions. We reasoned that the preference toward

the DFF route could be because PD oxidation (which we showed in **Figure 5.4** dominates for HMF oxidation at our condition) would selectively oxidize the alcohol in HMF over the aldehyde. This is suggested by our prior studies showing alcohols are primarily oxidized through the PD pathway while aldehydes are primarily oxidized though the indirect pathway.[22,23] Our reasoning is further supported by the results we obtained by oxidizing HMF using NiOOH with no bias applied (meaning only the indirect pathway can occur). This experiment was carried out by repeatedly applying 0.55 V vs Ag/AgCl to a $Ni(OH)_2$ film in a pH 13 KOH solution without any organic species, then moving the oxidized NiOOH electrode to a solution containing HMF and allowing it to chemically oxidize the HMF under open circuit condition. After this process was repeated 20 times the HMF solution was sampled and the products tested by HPLC.

The results of this experiment are shown in **Figure 5.7** and reveal that when only the indirect oxidation pathway is allowed, the selectivity between HMFCA and DFF is reversed, with roughly twice as much HMFCA produced as DFF. This demonstrates that oxidation through the indirect pathway preferentially oxidizes the aldehyde to produce HMFCA which in turn confirms that the greater amount of DFF observed in **Figure 5.5** must be because the PD pathway preferentially oxidizes the alcohol in HMF to produce DFF. This finding means that that HMF oxidation on NiOOH can occur through either the DFF route or the HMFCA route and that which one dominates will depend on the chosen oxidation conditions (i.e. the DFF route if PD oxidation is favored and the HMFCA route if indirect oxidation is favored). Our previous study showed that conditions such as a more positive potential, higher pH, and higher concentration of the organic species tend to promote PD oxidation and thus are likely to increase the preference toward the DFF route.[23]

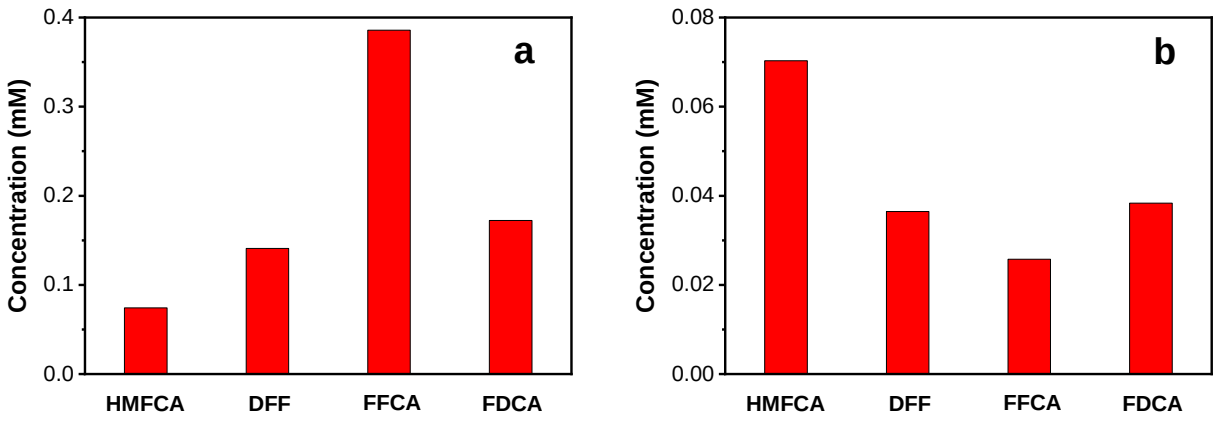

Figure 5.7. Product distribution (a) after 5 C was passed at 0.55 V vs Ag/AgCl (72% PD and 28% indirect) and (b) after using NiOOH pre-oxidized at 0.55V as a chemical oxidant (100% indirect). A pH 13 solution containing 5 mM HMF was used for both cases. To obtain the results shown in (b) we repeated 20 cycles of pre-oxidizing the $Ni(OH)_2$ film in a pH 13 KOH solution without any HMF and then transferring it to the aforementioned rapidly stirred HMF solution to chemically react at open circuit condition before sampling the HMF solution for analysis by HPLC. The overall product concentrations in (b) are lower because the charge we could conveniently pass for chemical oxidation was limited (~0.65 C instead of 5 C) and a larger volume of the HMF solution (25 mL instead of 14 mL) was used for the chemical oxidation.

5.2.4 Comparison to prior literature.

We note that most prior studies, which were performed without knowledge of the presence of two different oxidation pathways on NiOOH, have reported that HMF oxidation on NiOOH proceeds though the HMFCA route.[14,21,25-31] While it is difficult to be certain without performing the rate deconvolution experiments, these studies were often conducted under conditions we would expect to favor PD oxidation as much as or more than those used in this study (0.55 V vs Ag/AgCl in a pH 13 solution containing 5 mM HMF) where the PD pathway (and thus DFF formation) dominates. Therefore, we believe it is unlikely that the reason they all observed HMFCA instead of DFF is because they all were using conditions that heavily favored the indirect pathway. Instead,

we think it is most likely because they used high surface area NiOOH often deposited on three-dimensional, porous substrates such as Ni foam to maximize the surface area and the rate of HMF oxidation, which can distort the accumulation profile of the intermediates due to the reasons explained below.

For a high surface area, three-dimensional electrode, if a molecule is oxidized to one of the intermediates (HMFCA, DFF, FFCA) at a more interior site in the electrocatalyst and then desorbs, it would be almost surrounded by other catalyst sites. This would make it much more likely to reabsorb onto one of those sites and be further oxidize before it can make its way out into the bulk solution as would be necessary for it to be detected using ex situ analysis methods. While this is good when designing a fast and effective electrocatalyst, it is not ideal when analyzing the mechanism or attempting to ascertain what intermediates form. Moreover, we might expect this to be particularly problematic if the intermediates differ in activities for adsorption or oxidation. For example, DFF, which is more reactive than HMFCA, might more readily undergo further oxidation before making its way out of a three-dimensional catalyst's interior, meaning its amount will be more severely underestimated than that of HMFCA when using a thicker, porous catalyst. By contrast, the thin, flat electrodes used in our study do not have this issue, and so the intermediate profile we observed is more representative of what actually is produced during the reaction.

To test whether differences in the thickness of the $Ni(OH)_2$ electrode could substantially impact the detected intermediate profile, we also conducted an electrolysis of a pH 13 solution containing 5 mM HMF at 0.55 V vs Ag/AgCl using a much thicker $Ni(OH)_2$ electrode. Our results show that simply increasing the deposition time from 45 s to 12 min to deposit a thicker $Ni(OH)_2$ electrode on the 2D flat FTO substrate (which is still significantly thinner than those deposited on 3D Ni foam substrates used in previous studies) significantly alters the accumulation of

intermediates during the course of an electrolysis. As can be seen in **Figure 5.8**, the accumulation of DFF and HMFCA became negligible and even the accumulation of FFCA was diminished considerably, resulting in an almost linear increase of the terminal product FDCA over the coulombs passed. This result clearly demonstrates how the thickness of the film can alter the intermediate accumulation not by changing the actual oxidation mechanisms but rather by promoting the re-adsorption and further oxidation of intermediates before they escape the catalyst layer. This explains why prior studies using 3D electrodes could not detect the more reactive DFF intermediate during HMF oxidation and concluded that HMF oxidation occurs through the HMFCA route. This result also highlights the necessity of using a flat, thin electrocatalyst for an accurate mechanistic study.

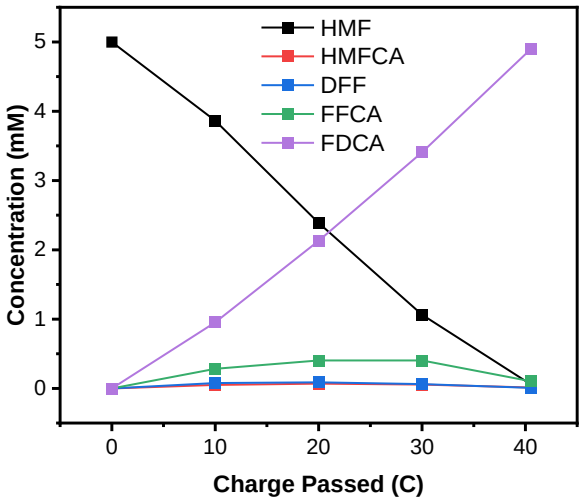

Figure 5.8. Change in concentration of HMF and its oxidation products over charged passed at 0.55 V vs Ag/AgCl in a pH 13 solution containing 5 mM HMF using a thick NiOOH electrode. The plot shows that using a thick film results in detection of far fewer intermediates than were seen when using a thin film.

5.2.5 Understanding 0th order behavior.

For the simple alcohols and aldehydes we studied previously, a pseudo second order relationship between the indirect reaction rate and charge stored in the NiOOH film was observed

(i.e. the best linear fit was obtained when 1/charge was plotted against *t*).[22,23] We note that this does not necessarily mean the reaction is truly "second order" with respect to charge stored in the NiOOH film. In fact, we expect that the true rate law is probably more complicated and we do not give any chemical meaning to this "second order" relationship. Instead, we simply use this mathematical relationship as it accurately models the disappearance of charge from the NiOOH across the timeframe of interest, which allows us to determine $k_{obs,ind}$ and I_{ind}.

In this study, we found that HMF instead shows a first order relationship with charge stored in the NiOOH film (i.e. the best linear fit was obtained when ln (charge) was plotted against *t*) while for HMFCA, DFF, and FFCA the relationship is 0^{th} order (i.e. the best linear fit was obtained when *Q* was plotted against *t*) (**Figure 5.3**). Again, we do not give any serious chemical meaning to the first order relationship observed for HMF and just use this relationship to obtain the best fitting of our experimental data to most accurately determine the indirect rate. The 0^{th} order behavior of HMFCA, DFF, and FFCA, however, is bizarre in that it means the concentration of Ni^{3+} has no effect on the indirect rate of HMFCA, DFF, and FFCA oxidation. This would seem to be impossible because (at least according to how the indirect mechanism has traditionally been described) Ni^{3+} is not only a reactant consumed in the indirect reaction but also comprises the active sites where the organic species must first adsorb before undergoing further reaction (Step 2 in **Scheme 5.2**).

To have a 0^{th} order relationship it must be the case that the oxidized Ni sites are not involved in the rate determining step. The only scenario that we believe is consistent with this is if DFF, HMFCA, and FFCA are able to adsorb on Ni^{2+} sites as well as on Ni^{3+} and Ni^{4+} sites and that the organic species adsorbed on Ni^{2+} sites can rapidly undergo HAT to adjacent oxidized sites in a step that is fast relative to the adsorption step. Since the slow, rate determining adsorption step

would then depend on the total number of Ni sites rather than on the number of oxidized Ni sites, a 0^{th} order relationship to charge stored in the Ni film would result.

If the above explanation is correct, we would expect to see a deviation from 0^{th} order behavior at some point as charge leaves the film as eventually the HAT step would no longer be fast relative to adsorption, since the HAT step will depend on the charge in the film. Similarly, if adsorption is truly the rate limiting step and subsequent reaction of the adsorbed species is fast we would expect the indirect rate to increase as the concentration increases since the adsorption step is the one that has a direct kinetic dependence on the concentration of the unbound organic species (rather than the adsorbed species).

To test whether these predictions are accurate, we performed rate deconvolution experiments with time points collected up to almost full conversion of the film in a 10 mM FFCA solution and compared those to the results from a 5 mM solution. As can be seen in **Figure 5.9**, the 0^{th} order behavior holds well throughout the first 2 seconds of reactivity, corresponding to roughly 80% conversion of the NiOOH back to $Ni(OH)_2$. After this, however, the 0^{th} order behavior breaks down and the same 1^{st} order behavior seen for HMF emerges and describes the reaction well from 2 seconds onward to the final point collected at 3.5 seconds corresponding to ~99% conversion of the NiOOH. Moreover, when comparing the indirect current for 5 mM FFCA to that of 10 mM FFCA, we can see the expected doubling of the rate, with the current increasing from 0.88 mA/cm^2 to 2.01 mA/cm^2. These results support our proposed mechanism that FFCA can adsorb on any Ni site, including ones in $Ni(OH)_2$ and then undergo a HAT step to adjacent oxidized sites that is rapid unless almost all the Ni sites are in the reduced Ni^{2+} state (which will not occur under applied bias unless substantially higher concentrations are used and the potential remains at 0.55 V vs Ag/AgCl).

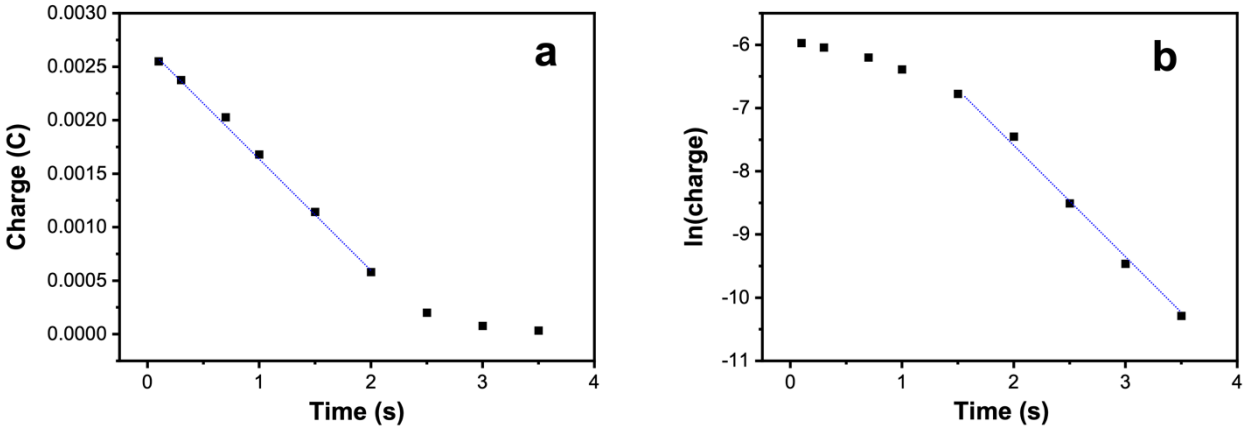

Figure 5.9. (a) Charge vs time and (b) ln(charge) vs time plots showing the consumption of positive charge stored in a NiOOH film for indirect oxidation of 10 mM FFCA in a rapidly stirred pH 13 solution at open circuit condition. The NiOOH film used in this experiment was pre-oxidized at 0.55 V vs Ag/AgCl in the FFCA solution.

The ability of these molecules to adsorb on $Ni(OH)_2$ sites also provides an explanation for the delayed onset of the $Ni(OH)_2$/NiOOH conversion in the presence of the organic species mentioned when discussing **Figure 5.2**. Adsorption of these molecules on the $Ni(OH)_2$ would change the energetics of those sites, likely having a stabilizing effect. Moreover, oxidizing a $Ni(OH)_2$ site with a bound organic molecule may necessitate breaking bonds or interactions involving the organic molecule, further adding to the barrier. As such, we would expect adsorption of these molecules on $Ni(OH)_2$ to delay the onset of its oxidation, which is exactly what is observed. Moreover, this delay is much more substantial for the molecules which follow 0^{th} order kinetics (HMFCA, DFF, and FFCA) with respect to charge in the NiOOH film rather than for HMF. This suggests HMF adsorbs less readily on Ni^{2+} sites and explains why the indirect oxidation of HMF has a different relationship with charge in the NiOOH film than does the oxidation of HMFCA, DFF, and FFCA. This also highlights that the ability to adsorb readily on $Ni(OH)_2$ and then undergo further oxidation is likely a property fairly unique to HMFCA, DFF, and FFCA rather

than one shared more broadly by alcohols and aldehydes as none of the other organic species we've tested have shown either a comparable shift in the $Ni(OH)_2$ oxidation peak nor 0^{th} order kinetics with respect to charge stored in the NiOOH film.[22,23] Finally, this ability to adsorb onto and react at $Ni(OH)_2$ sites also provides an explanation for the small amount of current observed in the presence of the organic species before the onset of $Ni(OH)_2$ oxidation that can be seen in **Figure 5.2** and which has been reported previously.[9] This current has previously been speculated to be due to oxidation of organic species on $Ni(OH)_2$.[9] Unlike both the indirect and PD mechanisms discussed above and which involve the reduction of Ni sites as part of oxidizing the organic species, an oxidation at $Ni(OH)_2$ sites would likely be a direct electrochemical oxidation and involve no change in the Ni oxidation state. While the current for this process which occurs before the onset of $Ni(OH)_2$ oxidation is very low in all cases (perhaps due to the poor conductivity of $Ni(OH)_2$) it is much more pronounced for HMFCA, DFF, and FFCA than it is for HMF, further confirming that these molecules adsorb more readily on $Ni(OH)_2$ sites and that this current is due to oxidation occurring at $Ni(OH)_2$ sites.

5.2.6 The impact of NiOOH Composition.

There are various metal ions that are known to shift the potential of the $Ni(OH)_2$/NiOOH peak when incorporated into the $Ni(OH)_2$ structure.[31-34] In this section, we investigated how such shifts of the $Ni(OH)_2$/NiOOH peak affects the indirect and PD oxidation rates and their contributions to the total anodic current. We chose to incorporate Co and Ga to shift the $Ni(OH)_2$/NiOOH peak cathodically and anodically, respectively. This was done by adding small amounts of $Co(NO_3)_2$ or $Ga(NO_3)_3$ to the deposition solutions (see methods section). Co was chosen because it has been one of the most common metals mixed with Ni in previous studies.[29,31,32,35] Ga was chosen to shift the $Ni(OH)_2$/NiOOH peak anodically instead of the more

commonly used Fe because, unlike Fe,[33,34] Ga does not significantly improve the performance of NiOOH for OER. Improved activity for OER could lower the Faradaic efficiency for HMF oxidation and create potential complications in our rate deconvolution experiments.

The samples we prepared and investigated are summarized in **Table 5.1**. These films were prepared such that they all contain comparable absolute amounts of Ni regardless of the different % amount of Co and Ga present in each film. The film compositions were determined by dissolving these films in 1 vol% nitric acid and analyzing the resulting solutions by inductively coupled plasma-mass spectrometry (ICP-MS). We note that the amounts of Co and Ga incorporated and the deposition conditions we used here were not chosen to achieve the best possible performance for HMF oxidation. Instead, they were chosen to provide a set of samples with clear differences in the position of the $Ni(OH)_2$ peak while maintaining the same morphology and thickness of the pristine NiOOH. This allows us to best identify the impact that shifts in the $Ni(OH)_2$/NiOOH couple have on indirect and PD oxidation. Therefore, the following data should not be used to judge the overall value of Co or Ga incorporation for improving HMF oxidation. The effect of the composition tuning on the $Ni(OH)_2$/NiOOH peak is shown in **Figure 5.10** and is also summarized in **Table 5.1**.

Table 5.1. NiOOH films with various compositions investigated in this study.

Modification of the plating solution	Film composition	Ni content in the film (nmol)	Co or Ga content in the film (nmol)	$Ni(OH)_2$/NiOOH peak position
w/ 2 mM Co	NiOOH w/ 31% Co	27	12	0.41 V vs Ag/AgCl
w/ 1 mM Co	NiOOH w/ 19% Co	30	7	0.46 V vs Ag/AgCl
No alteration	NiOOH	29	N/A	0.49 V vs Ag/AgCl
w/ 0.5 mM Ga	NiOOH w/ 3.4% Ga	28	1	0.51 V vs Ag/AgCl
w/ 1 mM Ga	NiOOH w/ 6.7% Ga	28	2	0.56 V vs Ag/AgCl

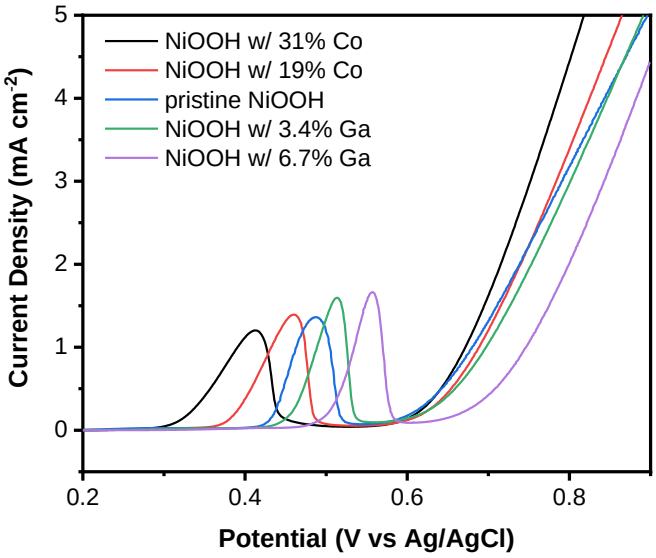

Figure 5.10. LSVs of NiOOH with various compositions taken in a pH 13 KOH solution (scan rate, 10 mV/s).

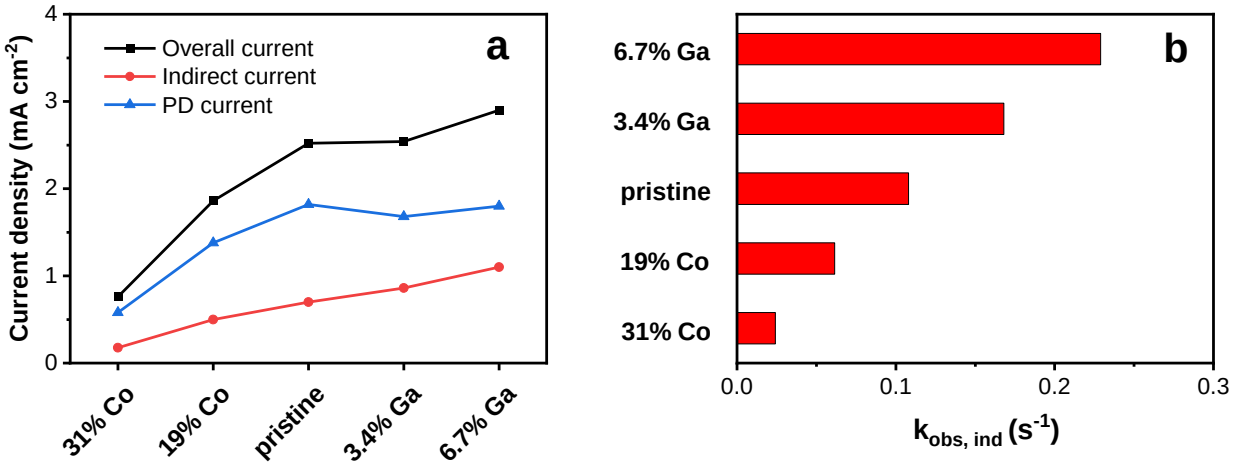

Figure 5.11. Plots displaying (a) the deconvoluted indirect and PD current and (b) $k_{obs,ind}$ when 0.55 V vs Ag/AgCl is applied to a rapidly stirred pH 13 solution containing 5 mM HMF using NiOOH electrodes with various compositions.

The effects of the film composition on the indirect and PD oxidation pathways were also investigated through rate deconvolution analysis performed at 0.55 V vs Ag/AgCl using 5 mM HMF solutions at pH 13. The deconvoluted currents and $k_{obs,ind}$ values are shown in **Figure 5.11**. For all films, the charge disappearance due to indirect oxidation gave the best linear fit when

ln(charge) was plotted against time **(Figure 5.12**). We note that the $k_{obs,ind}$ obtained from the slope of the ln(charge) vs time plots is the overall observed rate constant for the indirect process as performed by the film (rather than only the Ni sites in the film). Since $Co(OH)_2$ can also be oxidized to CoOOH, which is capable of HMF oxidation, for the Co-containing films some of the current and contribution to $k_{obs,ind}$ may come from activity of Co sites. However, we expect the degree of HMF oxidation at Co^{3+} sites to be fairly small as CoOOH has previously been shown to be significantly less active toward HMF oxidation than NiOOH.[9]

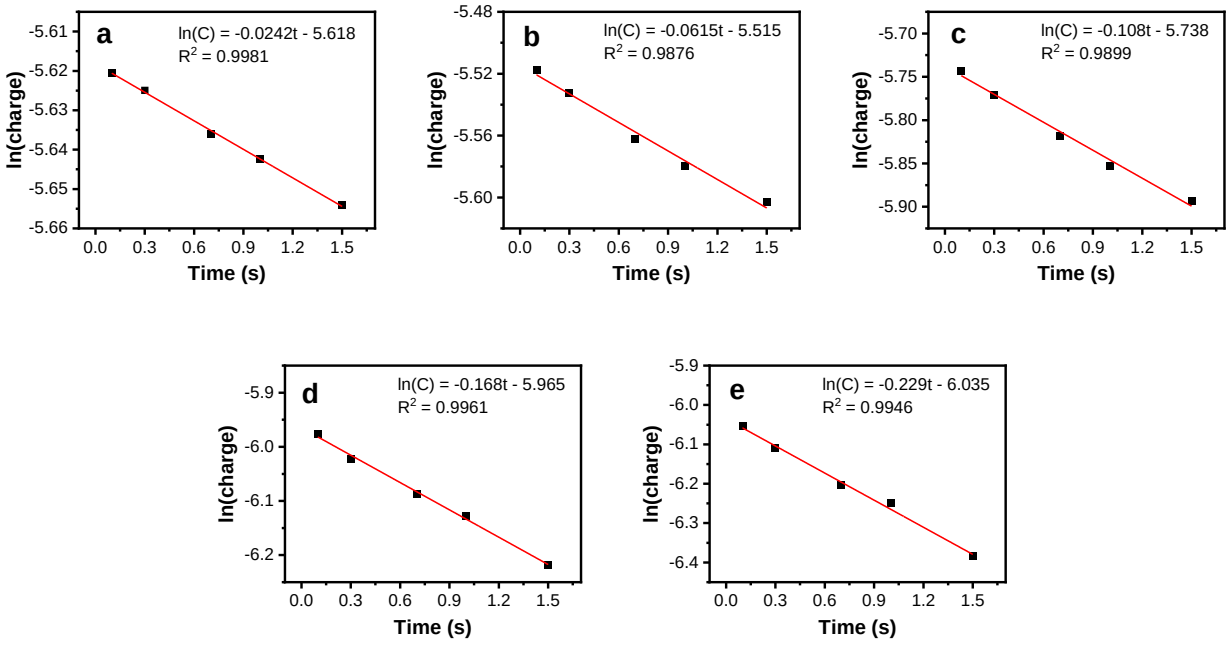

Figure 5.12. Plots of ln(charge) vs time showing the disappearance of positive charge from (a) NiOOH with 31% Co, (b) NiOOH with 19% Co, (c) pristine NiOOH, (d) NiOOH with 3.4% Ga, and (e) NiOOH with 6.7% Ga electrodes due to indirect oxidation of HMF as a function of time immersed in a rapidly stirred 5 mM HMF solution at pH 13. The NiOOH used for these measurements was pre-oxidized at 0.55 V vs Ag/AgCl in the HMF solution.

The results in **Figure 5.11** reveal that there is a clear trend between activity toward indirect oxidation and the potential of the $Ni(OH)_2$/NiOOH couple. As the couple shifts anodically, there is an accompanying increase in the partial current for the indirect pathway, going from 0.18 mA/cm^2 in the case of the NiOOH containing 31% Co up to 1.1 mA/cm^2 for the NiOOH containing 6.7% Ga. This results in an increase in the percentage of the current occurring through the indirect pathway as the potential of the $Ni(OH)_2$/NiOOH couple shifts anodically, increasing from a minimum of 23% for the NiOOH containing 31% Co to a maximum of 38% in the NiOOH containing 6.7% Ga. This increase in the indirect current is driven by the increase in $k_{obs,ind}$ as the $Ni(OH)_2$/NiOOH couple is shifted anodically, meaning individual Ni sites are more active toward indirect HMF oxidation. This trend is as expected and can be best explained using the diagrams shown in **Figure 5.13**.

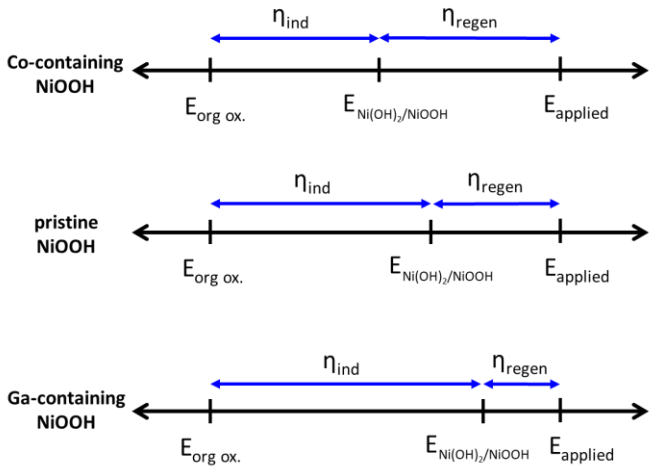

Figure 5.13. Scheme illustrating how shifting the potential of the $Ni(OH)_2$/NiOOH couple affects the overpotential for indirect oxidation of HMF, η_{ind}, and the overpotential for regeneration of NiOOH from $Ni(OH)_2$, η_{regen}. $E_{org.ox}$ is the thermodynamic potential for oxidation of the organic species (e.g. alcohol or aldehyde), $E_{Ni(OH)_2/NiOOH}$ is the thermodynamic potential of the $Ni(OH)_2$/NiOOH redox couple, and $E_{applied}$ is the potential applied at the electrode.

The definition for overpotential (η) is the difference between the thermodynamic potential for a given reaction and the potential available to perform the given reaction. Since NiOOH serves as a chemical oxidant for indirect oxidation, the overpotential for indirect alcohol or aldehyde oxidation (shown as η_{ind} in **Figure 5.13**) is always the difference between the thermodynamic potential for alcohol or aldehyde oxidation ($E_{org\ ox.}$) and the redox potential of $Ni(OH)_2$/NiOOH ($E_{Ni(OH)_2/NiOOH}$) regardless of the potential applied. Therefore, when the $Ni(OH)_2$/NiOOH couple shifts anodically, it increases η_{ind} and this change results in an increase in $k_{obs,ind}$. The shift of the $Ni(OH)_2$/NiOOH couple also has the effect of decreasing the overpotential for NiOOH generation (shown as η_{regen} in **Figure 5.13**), which is the difference between the applied potential ($E_{applied}$) and the redox potential of $Ni(OH)_2$/NiOOH. Under our conditions, however, the kinetics of the HAT step is more rate-determining than those for regeneration of NOOH when determining the rate of HMF oxidation, so the anodic shift of the Ni(OH)2/NiOOH couple results in an overall increase in the oxidation current for indirect oxidation.

We note that the prediction that η_{ind} will affect I_{ind} is valid only when HAT is the rate determining step for indirect oxidation. As mentioned above, unlike for HMF, the indirect oxidation of FFCA, HMFCA, and DFF were limited by the adsorption step. In such cases, anodically shifting the $Ni(OH)_2$/NiOOH peak would not be expected to increase the rate of indirect oxidation since increasing the oxidizing power of NiOOH would only speed up steps which are already rapid. The effect of cathodically shifting the peak would depend on how much slower the HAT steps become with the less oxidizing NiOOH. If the HAT steps are still rapid relative to adsorption despite the decrease in the oxidizing power of the NiOOH then we would not expect to see any effect from the cathodic shift of the $Ni(OH)_2$/NiOOH peak. Conversely, if the decrease is enough that the HAT steps are no longer much faster than adsorption then we would expect that

the indirect reaction would not follow 0th order kinetics with respect to charge in the film because then the oxidized Ni sites would be involved in rate affecting steps.

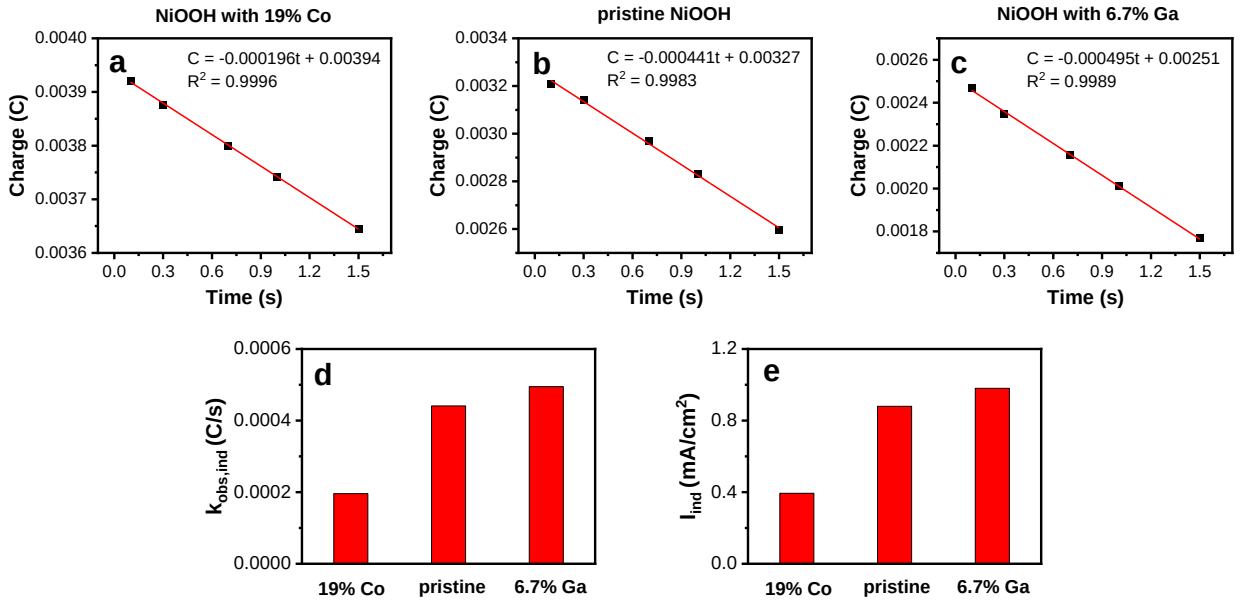

Figure 5.14. Plots showing the disappearance of positive charge from (a) NiOOH with 19% Co, (b) pristine NiOOH, and (c) NiOOH with 6.7% Ga electrodes as a function of time immersed in a rapidly stirred 5 mM FFCA solution at pH 13. The NiOOH used for these measurements was pre-oxidized at 0.55 V vs Ag/AgCl in the FFCA solution. (d) $k_{obs,ind}$ obtained from the slopes of the plots in (a-c) and (e) I_{ind} as calculated from $k_{obs,ind}$. The conversion of $k_{obs,ind}$ to I_{ind} was achieved by multiplying $k_{obs,ind}$ by 1000 to convert from C/s to mA then dividing by the electrode area of 0.5 cm^2 to yield the current density in mA/cm^2.

To illustrate this point, we performed rate deconvolution experiments comparing pristine, 19% Co-containing, and 6.7% Ga-containing NiOOH films for oxidation of 5 mM FFCA in a pH 13 solution. The resulting charge vs time plots along with the values of $k_{obs,ind}$ and I_{ind} are shown in **Figure 5.14**. As was expected, anodically shifting the $Ni(OH)_2$/NiOOH peak through Ga incorporation did not meaningfully change $k_{obs,ind}$ or I_{ind}. For the Co-containing films, FFCA oxidation also follows 0th order kinetics with respect to the charge in the NiOOH film, meaning FFCA adsorption is still rate determining. We also note that, with the Co-containing films, I_{ind} for

FFCA oxidation is only 0.39 mA/cm^2 which is substantially lower than the I_{ind} of 0.88 mA/cm^2 for the pristine films and 0.98 mA/cm^2 for the Ga-containing films. Given that the 0th order behavior with respect to charge in the film is still observed for the Co-containing films, this lower I_{ind} cannot be explained by the decreased η_{ind}. Instead, it is most likely because the presence of Co has the additional effect of interfering with the adsorption of FFCA. Further evidence for this can be seen when comparing LSVs taken with pristine, Co-containing, and Ga-containing NiOOH films in solutions with and without 5 mM FFCA (**Figure 5.15**). As can be seen, while the LSVs taken with pristine and Ga-containing films show a significant anodic shift of the $Ni(OH)_2$/NiOOH peak upon addition of FFCA (evidence of a strong interaction between FFCA and the $Ni(OH)_2$ in those films) no shift is observed with the Co-containing films. This supports that the addition of Co interferes with the ability of FFCA to interact with and adsorb on the electrocatalyst.

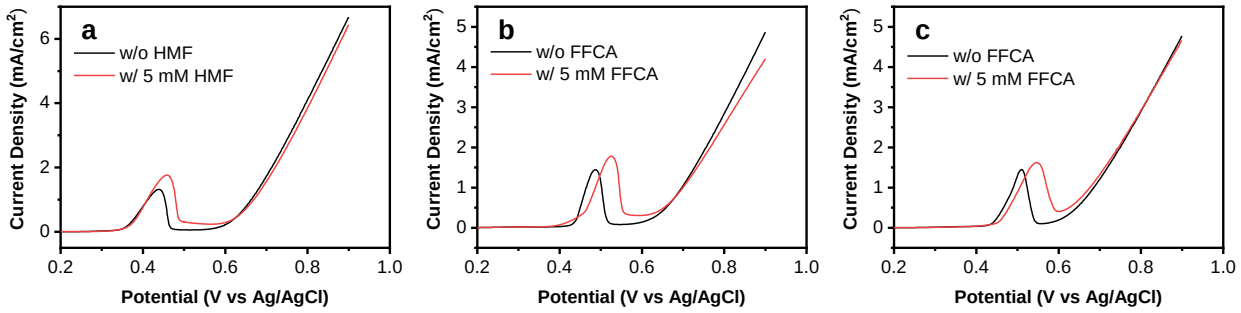

Figure 5.15. LSVs collected in an unstirred pH 13 solution with (red) and without (black) 5 mM FFCA using (a) NiOOH containing 19% Co, (b) pristine NiOOH, and (c) NiOOH containing 6.7% Ga (scan rate, 10 mV/s).

We now examine the effect of NiOOH composition tuning on the rate of PD oxidation. Ideally, PD oxidation, whose rate depends on the applied potential rather than the chemical potential of oxidized Ni, should not be directly affected by shifts of the $Ni(OH)_2$/NiOOH peak. Indeed, the Ga-containing samples in which the $Ni(OH)_2$/NiOOH peak has been shifted anodically show I_{PD} values comparable to those of pristine NiOOH (**Figure 5.11a**). On the other hand, I_{PD}

was decreased by Co incorporation. Given that no change in I_{PD} resulted from the anodic shift induced by Ga incorporation, we do not think the decrease in I_{PD} caused by Co incorporation is due to the cathodic shift of the $Ni(OH)_2$/NiOOH peak. Instead, we believe that it is most likely due to the additional effect Co incorporation has of unfavorably affecting HMF adsorption on catalytic sites. This is related to our discussion above showing that Co incorporation weakened FFCA adsorption.

5.2.7 Electrolyses using NiOOH of various compositions.

To further study how shifting the $Ni(OH)_2$/NiOOH peak affects the activity for HMF oxidation, we performed constant potential electrolyses at 0.55 V vs Ag/AgCl of 5 mM HMF in pH 13 solutions using pristine, 31% Co-containing, and 6.7% Ga-containing films. The resulting j-t plots are shown in **Figure 5.16** while the products detected by HPLC at various values of charge passed are shown in **Figure 5.17**.

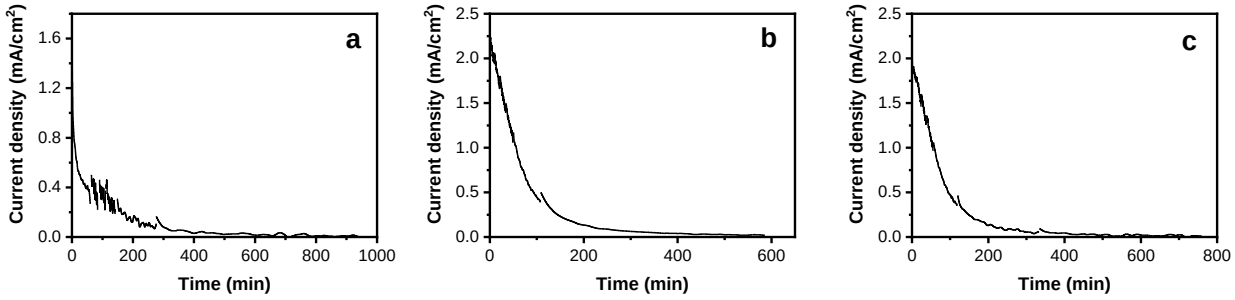

Figure 5.16. J-t plots obtained during oxidation of 5 mM in a pH 13 solution at 0.55 V vs Ag/AgCl using (a) NiOOH with 31% Co, (b) pristine NiOOH, and (c) NiOOH with 6.7% Ga. The breaks in the current profiles correspond to where the anolyte solution was sampled to allow for HPLC analysis. All electrolyses passed 40.52 C, which is the amount required for full stoichiometric conversion of HMF to FDCA.

The data in **Figure 5.17** shows there is very little difference between the electrolysis results using the pristine and the Ga-containing films. The current densities generated by these films

during the electrolysis were also comparable (**Figure 5.16**). The overall similarity between these results is unsurprising based on the rate deconvolution data reported above; while the Ga incorporation did shift the preferred pathway to favor indirect oxidation of HMF a bit more (38% indirect versus 28% indirect) the overall current density was similar. Moreover, as shown above, Ga incorporation would not have much effect on the conversion of FFCA to FDCA (which appears to be the slowest step) because the oxidation of FFCA is controlled by the adsorption step and not η_{ind}.

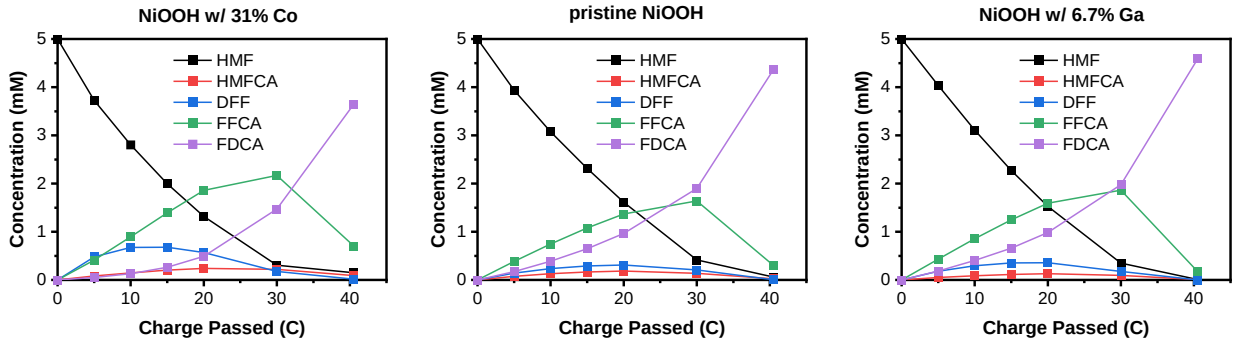

Figure 5.16. The change in concentration of HMF and its oxidation products over charge passed at 0.55 V vs Ag/AgCl in pH 13 solutions containing 5 mM HMF using Co-containing, pristine, and Ga-containing NiOOH.

Incorporation of Co into the films did produce more substantial changes in the electrolysis results, though the overall intermediate profile is still similar. The biggest change is in the current density. This is as expected based on the rate deconvolution experiments which show the Co-containing films are less active for both HMF and FFCA oxidation, likely due primarily to weaker adsorption, though the lower oxidizing power of the Co-containing NiOOH also likely played a role in suppressing HMF oxidation through the indirect pathway. The changes to the intermediate profile, while still fairly minor, are more noticeable than the differences between the pristine and Ga-containing cases. DFF accumulates to roughly twice the level as it does in the pristine and Ga-containing cases, likely due to the shift toward PD oxidation (which favors DFF formation)

induced by the inclusion of Co in the films. Additionally, at earlier amounts of charge passed more FFCA accumulates relative to the FDCA formed, likely due to the suppressed kinetics for FFCA oxidation causing more of the molecules to get "stuck" at this least reactive intermediate before eventually being oxidized to FDCA. Additionally, there is less FDCA formed after the stoichiometric amount of charge has been passed and more of the initial HMF has gone missing and isn't found either as unreacted HMF or as any of the detectible oxidation products. This is because the less reactive Co-containing films took longer to pass the set charge and HMF and its oxidation intermediates, which are not completely stable in pH 13, degraded over time before being converted into FDCA.

5.3 Conclusion

In this study, we have provided a comprehensive mechanistic understanding of HMF oxidation on NiOOH using our rate deconvolution method. We showed that DFF and FFCA (which contain only an aldehyde group) are primarily oxidized through the indirect pathway while HMFCA (which contains only an alcohol) is oxidized primarily through the PD pathway. For HMF (which contains both an aldehyde and an alcohol), which oxidation pathway dominates (and thus which group tends to be oxidized first) depends on the oxidation conditions. Under the open circuit condition where only indirect oxidation is allowed, the aldehyde group was preferentially oxidized first, resulting in more formation of HMFCA than DFF. However, when 0.55 V vs Ag/AgCl was applied and caused PD oxidation to be dominant, the alcohol group was instead preferentially oxidized first to form DFF. Moreover, the 0^{th} order dependence with respect to charge in the NiOOH film observed for HMFCA, DFF, and FFCA oxidation allowed us to conclude that those molecules can adsorb on Ni^{2+} sites in addition to the oxidized Ni sites and can be oxidized through HAT to adjacent oxidized Ni sites, meaning the adsorption site and the site where HAT occurs

need not be the same for these molecules. Also, for indirect oxidation of these molecules, the adsorption step appears to be rate limiting, with the subsequent HAT steps being fast unless the percentage of Ni sites in the oxidized state is very low.

We also examined the effect on HMF oxidation of shifting the $Ni(OH)_2$/NiOOH peak through composition tuning of NiOOH. The $Ni(OH)_2$/NiOOH peak position had a direct impact on the rate of indirect oxidation of HMF because it affected the overpotential for HAT, a step important for determining the rate of HMF oxidation. It did not, however, have much impact on the indirect oxidation of FFCA because for FFCA oxidation adsorption is the rate determining step. Co incorporation does significantly decrease the rate of FFCA oxidation, however, this is not due to shifting the $Ni(OH)_2$/NiOOH peak position but rather by hindering FFCA adsorption. Anodically shifting the $Ni(OH)_2$/NiOOH peak through Ga incorporation did not have a noticeable impact on PD oxidation as the $Ni(OH)_2$/NiOOH peak position does not have a direct impact on the rate of PD oxidation. As with indirect oxidation of FFCA, Co incorporation did considerably decrease the rate of PD oxidation but this was due to hindering adsorption and not because of the cathodic shift of the $Ni(OH)_2$/NiOOH peak.

The results presented here reveal that the direct effect of shifting the potential of the $Ni(OH)_2$/NiOOH couple on the performance for HMF oxidation is modest. This insight suggests those seeking to make catalyst modifications to further improve the performance of NiOOH electrocatalysts toward HMF oxidation should focus on optimizing other catalyst properties (such as adsorption energy and morphology) rather than on tuning the potential of the $Ni(OH)_2$/NiOOH couple. However, for other organic species where indirect vs PD oxidation can lead to different products, tuning the potential of the $Ni(OH)_2$/NiOOH couple could be an important tool for altering the selectivity of the reaction.

5.4 Experimental Section.

5.4.1 Materials.

The chemicals employed were all acquired from commercial sources and used without further purification. HMF (97%, Alfa Aesar), HMFCA (98%, Astra Tech), DFF (97%, Sigma Aldrich), FFCA (>98.0% TCI), FDCA (>98.0%, TCI), potassium hydroxide (≥85%, Sigma Aldrich), $Ni(NO_3)_2 \cdot 6H_2O$ (99%, Acros), KNO_3 (99%, Alfa Aesar), $Ga(NO_3)_3$ (99.9%, Alfa Aesar), $Co(NO_3)_2$ (98%, Sigma Aldrich), HNO_3, 70% (≥99.999%, Sigma Aldrich), Ni standard for ICP (1000 mg/L ± 2 mg/L, Sigma Aldrich), Ga standard for ICP (1000 mg/L ± 2 mg/L, Sigma Aldrich), Co standard for ICP (1000 mg/L ± 2 mg/L, Sigma Aldrich). All solutions were prepared using deionized water (Barnstead E-pure water purification system, resistivity >18 MΩ cm).

5.4.2 $Ni(OH)_2$ Electrode Preparation.

Amorphous α-$Ni(OH)_2$ films were prepared using an established technique featuring electrochemical nitrate reduction.[36] This produces hydroxide, raising the local pH at the working electrode (WE) and causing $Ni(OH)_2$ to deposit on the WE to form a $Ni(OH)_2$ film. This process was controlled with a SP-200 potentiostat/EIS (BioLogic Science Instrument) and conducted with a 3-electrode setup in a single compartment glass cell. The WE was fluorine doped tin oxide (FTO), the counter electrode (CE) was Pt, and the reference electrode (RE) was Ag/AgCl (4 M KCl). The FTO WEs were prepared by cutting larger FTO plates into 2.5 cm x 1 cm strips after which Cu tape was attached to the top to provide electrical contact. The FTO was then masked with electroplating tape (3M Company) with a 0.5 cm^2 hole punched in it so that a well-defined conductive surface area was exposed. For the films that would be used in electrolyses, two 0.5 cm^2 holes were punched in the tape instead of one to increase the electrode surface area without

changing the nature of the electrode. The Pt CE were prepared by sputter coating a 20 nm Ti adhesion layer followed by 100 nm of Pt onto clean glass slides. To prepare the thin and pristine $Ni(OH)_2$ films used for most experiments in this work a current density of -0.25 mA/cm^2 was maintained for 45 s in an aqueous plating solution consisting of 10 mM $Ni(NO_3)_2 \cdot 6H_2O$ and 30 mM KNO_3. The thicker $Ni(OH)_2$ film used for one electrolysis was prepared using a larger FTO WE with 4 cm^2 exposed to the solution. The deposition solution was 50 mM $Ni(NO_3)_2$ and a current of -0.5 mA/cm^2 was maintained for 6 minutes. The $Ni(OH)_2$ films containing Co and Ga were prepared by adding an amount of $Co(NO_3)_2$ (1 mM or 2 mM) or $Ga(NO_3)_3$ (0.5 mM or 1 mM) to the deposition solution used for the thin pristine $Ni(OH)_2$ deposition (10 mM $Ni(NO_3)_2$ and 30 mM KNO_3). The current density and deposition time were optimized for each deposition solution to give a uniform $Ni(OH)_2$ film with a comparable amount of Ni as in the pristine case and were as follows: 1mM Co (-0.25 mA/cm^2, 54.5 s), 2 mM Co (-0.25 mA/cm^2, 57 s), 0.5 mM Ga (-1.2 mA/cm^2, 14 s), 1 mM Ga (-1.2 mA/cm^2, 18 s). After deposition, all of the $Ni(OH)_2$ films were rinsed with >18 MΩ cm water and then dried with an air stream.

5.4.3 Electrochemical Experiments.

CVs and LSVs were performed using a 3-electrode setup in a glass single glass compartment. $Ni(OH)_2$ films were used as the WE, Ag/AgCl as the RE and Pt as the CE. CVs and LSVs were performed by starting at open circuit and sweeping the potential first in the positive direction at a scan rate of 10 mV/s. For all CVs the potential was cycled at least twice and the curves shown are from the second cycle. For the stirred CVs, the solution was rapidly stirred by a magnetic stir bar while the potential was being scanned.

Electrolyses were performed with the same 3 electrode setup described above but in a glass divided cell rather than a single cell. The two compartments were separated by a glass frit and each

was filled with 14 mL of solution. The anolyte was a pH 13 solution of 5 mM HMF unless specified otherwise while the catholyte was just a pH 13 KOH solution. The anode compartment was equipped with a stir bar and was rapidly stirred throughout the electrolysis. To allow the electrolyses to be completed more quickly despite using thin $Ni(OH)_2$ WEs that were only 0.5 cm^2 in surface area multiple $Ni(OH)_2$ electrodes were immersed and used simultaneously. To do this, as mentioned above, when depositing the $Ni(OH)_2$ to be used for an electrolysis two 0.5 cm^2 holes were punched in the masking tape to allow two $Ni(OH)_2$ to be deposited onto the same FTO plate. For the electrolyses using pristine and Ga-containing films four of these FTO plates were arranged together (two plates back to back then one more on each side so the faces with the $Ni(OH)_2$ were all 90° apart). These were then joined together and brought into electrical contact with one another by wrapping more Cu tape around the Cu tape "handles" affixed to the FTO plates. This allowed all 4 FTO plates (for a total of eight 0.5 cm^2 $Ni(OH)_2$ electrodes) to be immersed and polarized simultaneously. For the Co-containing case, to allow the electrolyses to be completed in a comparable amount of time despite the lower current density, two of these four FTO plate arrangements were taped together side by side for a total of sixteen 0.5 cm^2 Co-containing electrodes immersed in solution. In all cases, the Cu tape was well above the solution level so only the immersed $Ni(OH)_2$ electrodes could participate in HMF oxidation.

The electrolyses were performed at 0.55 V vs Ag/AgCl unless specified otherwise and proceeded until the stoichiometric amount of charge was passed for full conversion of the HMF to FDCA (40.52 C). The applied bias was paused after specified amounts of charge passed (generally, 5, 10, 15, 20, and 30 C) so an aliquot (0.15 mL) could be drawn from the anolyte solution for analysis by HPLC, after which the potential was applied once more. The remaining charge to be

passed was adjusted to account for the slightly lower solution volume after removal of the aliquots, so the true charge passed for each electrolysis was a bit less than 40.52 C.

5.4.4 Product Analysis.

Product analysis for the aliquots drawn from the electrolysis solutions was achieved by HPLC performed using a Shimadzu Prominence-i LC-2030C 3D HPLC system equipped with an internal UV−Vis detector. The mobile phase was an aqueous solution of 0.1% sulfuric acid at a flow rate of 0.5 mL/min in isocratic mode. Ten microliters of the sample aliquots were injected into a 300 mm × 7.8 mm ICSep ICE-Coregel 87H3 column (Transgenomic) and the column oven temperature was maintained at 65 °C. Product concentration was determined by comparing the peak position and intensity to those of standard solutions of known concentration. Retention times of 20, 23, 27, 32, and 39 min corresponded to FDCA, HMFCA, FFCA, HMF, and DFF respectively. The UV−Vis signal whose intensity was used for quantification was analyzed at the λ_{max} for each compound with wavelength of 262, 258, 281, 283, and 288 nm corresponding to FDCA, HMFCA, FFCA, HMF, and DFF, respectively.

5.4.5 ICP-MS.

The Ni and Co/Ga amount in our deposited films was analyzed by first dissolving the films in 10 mL solutions of 1 vol% nitric acid (70%, Trace Metal grade) in polypropylene centrifuge tubes. For each of the NiOOH conditions, 3 separate samples were prepared and analyzed by inductively coupled plasma mass spectrometry (ICP-MS) and their results averaged to give the amount of Ni and Co/Ga in a film displayed in **Table 5.1**. Prior to being dissolved these films were used to conduct 2 CV cycles in a pH 13 solution to ensure they were in the same state films would be in prior to rate deconvolution analysis. The solutions were analyzed using a triple quadrupole

inductively coupled plasma mass spectrometer (Agilent 8900 ICP-QQQ). For each sample, intensity data was collected in triplicate and averaged for ^{59}Co, ^{58}Ni, ^{60}Ni, ^{69}Ga, ^{71}Ga in the He gas mode. This intensity data was converted to concentrations by comparison with calibration curves collected just prior to sample measurement by analyzing freshly prepared standard solutions. For elements where more than one isotope was analyzed (Ni, Ga) the concentrations produced by both were averaged to give the concentration of the sample.

5.4.6 SEM.

SEM images of the as-deposited thin $Ni(OH)_2$ films were obtained using a LEO Supra 55 VP (Zeiss) scanning electron microscope at an accelerating voltage of 5 kV.

5.4.7 Rate Deconvolution Procedure.

Our three-step rate deconvolution procedure has been described in detail in Chapter 2 so only a more brief description with mention of experimental parameters specific to this study will be provided here. The process was performed using a rapidly stirred, 30 mL aqueous solution containing the organic species in a sealed single-cell glass compartment with a 3-electrode setup. A thin $Ni(OH)_2$ film deposited according to the procedure outlined above was used as the WE, Ag/AgCl as the RE, and Pt mesh as the CE. Prior to its use in rate deconvolution experiments, each $Ni(OH)_2$ film was used to collect a CV in a pH 13 aqueous KOH solution (2 cycles with switching potentials of 0.9V vs Ag/AgCl and 0 vs Ag/AgCl). This was to confirm the $Ni(OH)_2$/NiOOH peak and water oxidation behavior of each film was consistent.

In the first step of the three-step procedure, a fixed potential (generally 0.55 V vs Ag/AgCl) was applied to the WE in a rapidly stirred solution until the current reached a steady state value (typical 45 s). This converts the film into the steady state condition it would be in during a

potentiostatic electrolysis at the applied potential. Both the indirect and PD oxidation pathways are active during this step. In the second step, potential is no longer applied and the film is left to sit in the stirred solution at open circuit condition. During this time neither PD oxidation nor reoxidation of $Ni(OH)_2$ can occur since both require applied bias; however, the indirect pathway can still occur as it proceeds through chemical (rather than electrochemical) HAT steps. This reduces a portion of the higher valent Ni sites generated during the first step back to $Ni(OH)_2$. During the third step, the higher valent Ni sites still remaining after step 2 are rapidly reduced back to $Ni(OH)_2$ by sweeping the potential from open circuit to 0 V vs Ag/AgCl at a scan rate of 1 V/s and then holding the potential at 0 V for 20 s. The magnitude of the charge passed during this third, reductive step corresponds to the amount of charge still stored in the film after some of it was used in step 2 to oxidize the organic species through the indirect pathway. Repeating this whole 3-step process with different times stirring at open circuit in step 2 allowed us to construct plots showing the disappearance of charge from the film as a function of time at open circuit. This was used to generate kinetics equations and determine the rate of charge loss from the NiOOH film at 0 s at open circuit, which corresponds to the rate of the indirect pathway under electrolysis conditions at the potential applied in step 1.

The specific kinetics equations used to determine I_{ind} from the rate deconvolution plots depends on the observed relationship between charge stored in the film and the rate of charge loss from the film (**Table 5.2**). For FFCA, HMFCA, and DFF, plots of charge vs time were highly linear across the timeframe of interest, indicating oxidation of those species follows 0^{th} order kinetics with respect to charge in the NiOOH film across this time span. As such, the rate of charge loss from the film at time t, $\frac{\mathrm{d}Q_{film}(t)}{\mathrm{d}t}$, can be described using a pseudo-0^{th} order kinetics expression (equation 3) where $k_{obs,ind}$ (in units of C/s) is the magnitude of the slope of the charge vs time plot.

Reaction order	Differential rate law	Integrated rate law	Linear plot	Slope of linear plot	Units of rate constant
Zero	$-\frac{dQ}{dt} = k$	$Q = Q_0 - kt$	Q vs t	-k	C/s
First	$-\frac{dQ}{dt} = kQ$	$\ln Q = \ln Q_0 - kt$	lnQ vs t	-k	s^{-1}
Second	$-\frac{dQ}{dt} = kQ^2$	$1/Q = 1/Q_0 + kt$	1/Q vs t	k	$C^{-1} \cdot s^{-1}$

Table 5.2. A summary of differential and integrated rate laws for the determination of reaction order in Q where Q is the positive charge stored in NiOOH. These expressions are available in any general chemistry textbook where these rate laws are expressed in terms of [A] where A represents a reactant in a solution expressed in terms of molarity.

$$-\frac{dQ_{film}(t)}{dt} = k_{obs,ind} \quad (3)$$

When the NiOOH film is in the same state as it is in during a constant potential electrolysis (i.e. after 0 seconds at open circuit in the stirred solution after the initial constant potential step) the rate of charge loss from the film due to chemical oxidation will be equal to the rate of the indirect process during a constant potential electrolysis at the potential applied in step one (equation 4). For the 0^{th} order case, because the rate of charge loss is independent of time and determined only by $k_{obs,ind}$ (in units of C/s), I_{ind} (in mA/cm^2) can be obtained by simply multiplying $k_{obs,ind}$ by 1000 and dividing by the electrode area (0.5 cm^2).

$$-\frac{dQ_{film}(t=0)}{dt} = I_{ind} \quad (4)$$

For HMF, while charge vs time plots are not linear, ln(charge) vs time plots are which means the loss of charge due to chemical oxidation is best modeled as being 1^{st} order in charge in the NiOOH films (**Table 5.2**). This means that for HMF, the rate of charge loss from the film can be described using a pseudo first order rate equation (equation 5) instead of the pseudo 0^{th} order rate equation shown in equation 3. Here $k_{obs,ind}$ (in units s^{-1}) is obtained from the magnitude of the

slope of the ln(charge) vs time plots and Q_t is the charge stored in the NiOOH film at time t as measured by the magnitude of charge that must be passed to reduce the film from the state it is in at time t to the $Ni(OH)_2$ resting state.

$$-\frac{dQ_{\text{film}}(t)}{dt} = k_{\text{obs,ind}} Q_t \quad (5)$$

As shown in equation 4, solving equation 5 for when $t = 0$ will yield I_{ind}. This can be done as long as we known the charge stored in the film when $t = 0$, Q_0. The value of Q_0 can be found from the y-intercept of the ln(charge) vs time plot since this will be equal to $\ln(Q_0)$. In either case, once I_{ind} is known it can be compared to the steady state current observed in step 1 of the rate deconvolution process (I_{tot}) to calculate the value of I_{PD} according to eq. 1.

When conducting the rate deconvolution analyses for a given condition (organic species, concentration, NiOOH composition) each data point in the kinetics plots (ln(charge) vs time or charge vs time) was obtained by averaging results from four different measurements obtained with four different $Ni(OH)_2$ films. When obtaining this data, each $Ni(OH)_2$ film was used to collect no more than four data points. This is because the rapid reduction in the third step of the rate deconvolution process can cause the films to gradually become deactivated upon repeated use for deconvolution trials (i.e., the amount of positive charge stored for a given condition can decrease for successive trials). Additionally, whenever a new $Ni(OH)_2$ film was used, the solution containing the organic species was also replaced with a fresh solution. Furthermore, we developed a calibration procedure to monitor and correct for any differences in initial active Ni content between films as well as any slight film deactivation that occurs from repeated use that involved immediately performing a sperate instance of the 3-step rate deconvolution procedure with 0.1 s as the time at open circuit in step 2 immediately performing each measurement used to collect data points. This calibration procedure allowed us to adjust the data in such a way that any variation in

active Ni sites from film to film or trial to trial were accounted for and did not interfere with the measurement. A detailed description of how this was done experimentally and the principles behind it are provided in Chapter 2.4.7 and 2.4.8. For this work; however, while the experimental methods were identically, the fact that the best liner fits for the rate deconvolution data was obtained for 1st order or 0th order kinetics with respect to charge stored in the Ni film instead of 2nd order kinetics necessitated a change in how the mathematical adjustment was performed using the calibration data.

For the indirect oxidation of HMF, which is best modeled as being 1st order in charge in the NiOOH film, the adjustment was made according to equation 6 where $Q_{obs}(t)$ is the magnitude of the measured charge required to reduce the film after *t* seconds at open circuit, $Q_{cal}(t=0.1)$ is the charge required to reduce the film in the calibration measurement collected immediately after the trial in which $Q_{obs}(t)$ was obtained, $Q_{ave}(t=0.1)$ is the average of the first $Q_{cal}(t=0.1)$ value collected from each film for a given reaction condition,, and $Q_{adj}(t)$ is the adjusted (i.e. calibrated) value for the charge required to reduce the film after *t* seconds at open circuit after accounting for any deviation between Q_{ave} (t = 0.1) and Q_{cal} (t = 0.1). The resulting $Q_{adj}(t)$ values are what was used to construct all the ln(charge) vs time plots presented in this study.

$$Q_{adj}(t) = \frac{Q_{obs}(t) * Q_{ave}(t=0.1)}{Q_{cal}(t=0.1)} \quad (6)$$

The derivation for equation 1 can be obtained by noting that, over the timeframe of interest, the charge in the NiOOH film follows equation 7, which is the pseudo first order integrated rate law expressed in terms of coulombs (**Table 5.2**).

$$\ln\left(Q_{obs}(t)\right) = \ln(Q_0) - k_{obs}t \quad (7)$$

Based on this, we can note that the difference between the actual charge required to reduce the film after *t* seconds at open circuit ($Q_{obs}(t)$) and the charge that would have been required had

the film started with the average amount of active Ni in the steady state condition in step 1 ($Q_{adj}(t)$) is given by equation 8. This equation can then be rearranged and simplified to yield equation 6 above.

$$\ln\left(\mathrm{Q_{adj}}(t)\right) - \ln\left(\mathrm{Q_{obs}}(t)\right) = \ln\left(\mathrm{Q_{ave}}(t = 0.1)\right) - \ln\left(\mathrm{Q_{cal}}(t = 0.1)\right) \quad (8)$$

Unlike indirect HMF oxidation which follows 1st order kinetics, indirect oxidation of HMFCA, DFF, and FFCA is best modeled as being 0th order in the charge in the NiOOH film. As a result, equation 6 cannot be used for the adjustment for the data obtained from them. Instead, those data sets were adjusted using eq. 9. This equation can be derived using an equivalent process as the one shown above for the 1st order adjustment, but starts from the 0th order integrated rate law (**Table 5.2**) rather than the 1st order one.

$$\mathrm{Q_{adj}}(t) = \mathrm{Q_{obs}}(\mathrm{t}) - \left(\mathrm{Q_{cal}}(t = 0.1) - \mathrm{Q_{ave}}(t = 0.1)\right) \quad (9)$$

5.5 References

1. Chu, S.; Cui, Y.; Liu, N. The path towards sustainable energy. *Nat. Mater.* **2016**, *16*, 16–22.
2. Mika, L. T.; Csefalvay, E.; Nemeth, A. Catalytic conversion of carbohydrates to initial platform chemicals: chemistry and custainability. *Chem. Rev.* **2018**, *118*, 505–613.
3. Sudarsanam, P.; Zhong, R.; Bosch, S. V.; Coman, S. M.; Parvulescu, V. M.; Sels, B. F. Functionalised heterogeneous catalysts for sustainable biomass valorisation. *Chem. Soc. Rev.* **2018**, *47*, 8349–8402.
4. Dai, L.; Wang, Y.; Liu, Y.; Ruan, R.; He, C.; Yu, Z.; Jiang, L.; Zeng, Z.; Tian, X. Integrated process of lignocellulosic biomass torrefaction and pyrolysis for upgrading bio-oil production: A state-of-the-art review. *Renew. Sust. Energ. Rev.* **2019**, *107*, 20–36.
5. Yang, Y.; Mu, T. Electrochemical oxidation of biomass derived 5-hydroxymethylfurfural (HMF): pathway, mechanism, catalysts and coupling reactions. *Green Chem.* **2021**, *23*, 4228–4254.
6. Giannakoudakis, A. D.; Colmenares, J. C.; Tsiplakides, D.; Triantafyllidis, K. S. Nanoengineered electrodes for biomass-derived 5-hydroxymethylfurfural electrocatalytic oxidation to 2,5-furandicarboxylic acid. *ACS Sustainable Chem. Eng*. **2021**, *9*, 1970−1993.
7. Liu, W.-J.; Dang, L.; Xu, Z.; Yu, H.-Q.; Jin, S.; Huber, G. W. Electrochemical oxidation of 5-hydroxymethylfurfural with NiFe layered double hydroxide (LDH) nanosheet catalysts. *ACS Catal.* **2018**, *8*, 5533−5541.
8. Cardiel, A. C.; Taitt, B. J.; Choi, K.-S. Stabilities, regeneration pathways, and electrocatalytic properties of nitroxyl radicals for the electrochemical oxidation of 5-hydroxymethylfurfural. *ACS Sustainable Chem. Eng.* **2019**, *7*, 11138−11149.
9. Taitt, B. J.; Nam, D.-H.; Choi, K.-S. A comparative study of nickel, cobalt, and iron oxyhydroxide anodes for the electrochemical oxidation of 5-hydroxymethylfurfural to 2,5-furandicarboxylic acid. *ACS Catal.* **2019**, *9*, 660−670.
10. Bender, M.; Yuan, X.; Choi, K.-S. Alcohol oxidation as alternative anode reactions paired with (photo)electrochemical fuel production reactions. *Nat. Commun.* **2020**, *11*, 4594.
11. Jiang, N.; You, B.; Boonstra, R,; Terrero Rodriguez, I. M.; Sun, Y. Integrating electrocatalytic 5-hydroxymethylfurfural oxidation and hydrogen production via Co–P-derived electrocatalysts. *ACS Energy Lett.* **2016**, *1*, 386−390.

12. Cha, H. G.; Choi, K.-S. Combined biomass valorization and hydrogen production in a photoelectrochemical cell. *Nat. Chem.* **2015**, *7*, 328−333.
13. Grabowski, G.; Lewkowski, J.; Skowronski, R. The electrochemical oxidation of 5-hydroxymethylfurfural with the nickel oxide/hydroxide electrode. *Electrochim. Acta* **1991**, *36*, 1995.
14. Barwe, S.; Weidner, J.; Cychy, S.; Morales, D. M.; Dieckhofer, S.; Hiltrop, D.; Masa, J.; Muhler, M.; Schuhmann, W. Electrocatalytic oxidation of 5-(hydroxymethyl)furfural using high-surface-area nickel boride. *Angew. Chem., Int. Ed.* **2018**, *57*, 11460–11464.
15. Woo, J.; Moon, B. C.; Lee, U.; Oh, H.-S.; Chae, K. H.; Jun, Y.; Min, B. K.; Lee, D. K. Collaborative electrochemical oxidation of the alcohol and aldehyde groups of 5-hydroxymethylfurfural by NiOOH and Cu(OH)2 for superior 2,5-furandicarboxylic acid production. *ACS Catal.* **2022**, *12*, 4078−4091.
16. You, B.; Jiang, N.; Liu, X.; Sun, Y. Simultaneous H_2 generation and biomass upgrading in water by an efficient noble-metal-free bifunctional electrocatalyst. *Angew. Chem. Int. Ed.* **2016**, *55*, 9913–9917.
17. Latsuzbaia, R.; Bisselink, R.; Anastasopol, A.; van der Meer, H.; van Heck, R.; Yagüe, M. S.; Zijlstra, M.; Roelands, M.; Crockatt, M.; Goetheer, E.; Giling, E. Continuous electrochemical oxidation of biomass derived 5-(hydroxymethyl)furfural into 2,5-furandicarboxylic acid. *J. Appl. Electrochem.* **2018**, *48*, 611–626.
18. Fleischmann, M.; Korinek, K.; Pletcher, D. The oxidation of organic compounds at a nickel anode in alkaline solution *J. Electroanal. Chem. Interfacial Electrochem.* **1971**, *31*, 39−49.
19. Fleischmann, M.; Korinek, K.; Pletcher, D. The kinetics and mechanism of the oxidation of amines and alcohols at oxide-covered nickel, silver, copper, and cobalt electrodes. *J. Chem. Soc., Perkin Trans. 2* **1972**, *10*, 1396−1403.
20. Zhang, P.; Sheng, X.; Chen, X.; Fang, Z.; Jiang, J.; Wang, M.; Li, F.; Fan, L.; Ren, Y.; Zhang, B.; Timmer, B. J. J.; Ahlquist, M. S. G.; Sun, L. Paired electrocatalytic oxygenation and hydrogenation of organic substrates with water as the oxygen and hydrogen source. *Angew. Chem. Int. Ed.* **2019**, 58, 9155 –9159.
21. Delparish, A.; Uslu, A.; Cao, Y.; Groot, T.; van der Schaaf, J.; Noel, T.; d'Angelo, M. F. N. Boosting the valorization of biomass and green electrons to chemical building blocks: A study

on the kinetics and mass transfer during the electrochemical conversion of HMF to FDCA in a microreactor. *Chem. Eng. J.*, **2022**, *438*, 135393.

22. Bender, M. T.; Lam, Y. C.; Hammes-Schiffer, S.; Choi, K.-S. Unraveling two pathways for electrochemical alcohol and aldehyde oxidation on NiOOH. *J. Am. Chem. Soc.* **2020**, *142*, 21538–21547.
23. Bender, M. T.; Warburton, R. E.; Hammes-Schiffer, S.; Choi, K.-S. Understanding hydrogen atom and hydride transfer processes during electrochemical alcohol and aldehyde oxidation. *ACS Catal.* **2021**, *11*, 15110–15124.
24. Nam, D. H.; Taitt, B. J.; Choi, K.-S. Copper-based catalytic anodes to produce 2,5-furandicarboxylic acid, a biomass-derived alternative to terephthalic acid. *ACS Catal.* **2018**, *8*, 1197−1206.
25. Zhang, N.; Zou, Y.; Tao, L.; Chen, W.; Zhou, L.; Liu, Z.; Zhou, B.; Huang, G.; Lin, H.; Wang, S. Electrochemical oxidation of 5-hydroxymethylfurfural on nickel nitride/carbon nanosheets: Reaction pathway determined by in situ sum frequency generation vibrational spectroscopy. *Angew. Chem.* **2019**, *131*, 16042 – 16050.
26. You, B.; Liu, X.; Jiang, N.; Sun, Y. A general strategy for decoupled hydrogen production from water splitting by integrating oxidative biomass valorization. *J. Am. Chem. Soc.* **2016**, *138*, 13639−13646.
27. You, B.; Liu, X.; Liu, X.; Sun, Y. Efficient H_2 evolution coupled with oxidative refining of alcohols via a hierarchically porous nickel bifunctional electrocatalyst. *ACS Catal.* **2017**, *7*, 4564−4570.
28. Gao, L.; Liu, Z.; Ma, J.; Zhong, L.; Song, Z.; Xu, J.; Gan, S.; Han, D.; Niu, L. NiSe@NiOx core-shell nanowires as a non-precious electrocatalyst for upgrading 5-hydroxymethylfurfural into 2,5-furandicarboxylic acid. *Appl. Catal. B* **2020**, *261*, 118235.
29. Deng, X.; Kang, X.; Li, M; Xiang, K.; Wang, C.; Guo, Z.; Zhang, J.; Fu, X.-Z.; Luo, J.-L. Coupling efficient biomass upgrading with H_2 production via bifunctional Cu_xS@NiCo-LDH core–shell nanoarray electrocatalysts. *J. Mater. Chem. A* **2020**, *8*, 1138–1146.
30. Heidary, N.; Kornienko, N. Operando vibrational spectroscopy for electrochemical biomass valorization. *Chem. Sci.* **2020**, *11*, 1798–1806.

31. Gao, L.; Bao, Y.; Gan, S.; Sun, Z.; Song, Z.; Han, D.; Li, F.; Niu, L. Hierarchical nickel–cobalt-based transition metal oxide catalysts for the electrochemical conversion of biomass into valuable chemicals. *ChemSusChem* **2018**, *11*, 2547 – 2553.
32. Chen, W.; Xie, C.; Wang, Y.; Zou, Y.; Dong, C.-L.; Huang, Xiao, Z.; Wei, Z.; Du, S.; Chen, C.; Zhou, B.; Ma, J.; Wang, S. Activity origins and design principles of nickel-based catalysts for nucleophile electrooxidation. *Chem*. **2020**, *6*, 2974–2993.
33. Görlin, M.; Chernev, P.; Araújo, J. F.; Reier, T.; Dresp, S.; Paul, B.; Krähnert, R.; Dau, H.; Strasser, P. Oxygen evolution reaction dynamics, faradaic charge efficiency, and the active metal redox states of Ni–Fe oxide water splitting electrocatalysts. *J. Am. Chem. Soc.* **2016**, *138*, 5603–5614.
34. Enman, L. J.; Burke, M. S.; Batchellor, A. S.; Boettcher, S. W. Effects of intentionally incorporated metal cations on the oxygen evolution electrocatalytic activity of nickel (oxy)hydroxide in alkaline media. *ACS Catal*. **2016**, *6*, 2416−2423.
35. Kang, M. J.; Park, H.; Jegal,J.; Hwang, S. Y.; Kang, Y. S.; Cha, H. G. Electrocatalysis of 5-hydroxymethylfurfural at cobalt based spinel catalysts with filamentous nanoarchitecture in alkaline media. *Appl. Catal. B* **2019**, *242*, 85–91.
36. Kang, D.; Kim, T. W.; Kubota, S. R.; Cardiel, A. C.; Cha, H. G.; Choi, K.-S. Electrochemical synthesis of photoelectrodes and catalysts for use in solar water splitting. *Chem. Rev.* **2015**, *115*, 12839−12887.